On diversity improvements for ultra wideband communication systems

Keni Popovski
University of Wollongong

On Diversity Improvements for Ultra Wideband Communication Systems

A thesis submitted in fulfilment of the
requirements for the award of the degree

Doctor of Philosophy

from

The University of Wollongong

by

Keni Popovski
Bachelor of Engineering (Telecommunications - Honors 1st Class)

School of Electrical, Computer
and Telecommunications Engineering
2008

To my beloved wife Kristina,
my parents, my sister, and my loving family.

Abstract

The wireless communications arena consists of a wide range of products and services, each with a specific target market and approach. Having characteristic advantages and disadvantages, all attempt to increase their market share through diversification and innovation. Ultra wideband (UWB) is a recent entry into the commercial short-range communications world, differentiated by its sparse spectral profile and low peak power emissions. Being unlicensed and capable of operating simultaneously with conventional communication systems, it has seen considerable attention by both industry and academia.

This thesis explores diversification improvements available for UWB systems, explicitly through orthogonal user multiplexing schemes, channel equalization, and forward error correction. A review of this communication method is presented, considering its technical evolution and standardization.

Multi-user sequencing is researched with regard to a time hopped UWB architecture. The successful adoption of UWB into commercial devices greatly depends upon the development of efficient user access mechanisms. A comparative analysis of varied time, frequency, and direct sequence hopping codes is presented in terms of their performance, diversity, and computational requirements. It is shown that for low user utilization levels, short periodicity deterministic codes attain a similar performance to randomly generated sequences. However, within a fully utilized system deterministic codes slightly out-perform short length random sequences.

The application of multiplexing codes to UWB chip level interleaving is also

examined. Interleaver performance is compared when designed through long length random codes versus design through deterministic hopping sequences, exemplifying similarities between the approaches.

A unique approach to sequence analysis is introduced, developing a set of state probabilities for pulse separations generated by each multiplexing code. Providing insight into optimal code design procedures, this separation profile is employed in the closed-form derivation of intersymbol and multi-user interference expressions. These formulations adopt a transmitter-side equalization process, with comparisons against a receiver-side approach presented. Derivations are based upon an analysis of transmission overlaps, together with the probabilities of each overlap. A close alignment against a simulated UWB system is evident for varied system parameters, exemplifying numerous properties of each equalization measure.

Despite diversification efforts to improve communication procedures, data errors are an unavoidable consequence of operation across a wireless medium. Forward error correction is researched within this dissertation for both binary and a non-binary encoding. Utilizing a transmitter-side equalization scheme, conventional binary turbo decoding is considered at the binary data level. Also, non-binary turbo decoding is applied to combine data encoding and user multiplexing stages. This latter method presents an innovative means of time hopping code generation. A comparative analysis of each technique against a simulated performance is given for both single- and multi-user scenarios, together with observations on the multi-user interference effects of signals employing forward error correction. A performance improvement for scarcely populated systems was evident, although a binary turbo scheme is shown to achieve optimal performance in high traffic systems. The mapping scheme required for non-binary encoding is evaluated in terms of random generation and design through deterministic coding schemes. Truncated orthogonal codes are shown to achieve a performance gain for higher turbo iteration levels, also having the advantage of simpler design.

Wireless communications are inherently subject to numerous signal degrada-

tions. With its revolutionary and unlicensed communication approach, UWB has emerged as a formidable contender in the wireless arena. Having an array of error mitigation techniques, including orthogonal user multiplexing, channel equalization, and advanced error correction, it prevails as a high rate and low power consuming system for the modern world of telecommunications.

Statement of Originality

This is to certify that the work described in this thesis is entirely my own, except where due reference is made in the text.

No work in this thesis has been submitted for a degree to any other university or institution.

Signed

Keni Popovski
23rd October, 2008

Acknowledgments

I would like to thank my supervisor Prof. Tadeusz Wysocki, for all of his help and guidance throughout my postgraduate studies. Thank you for sharing your time and experience, and challenging me to develop my skills. I would also like to express my sincerest gratitude for my co-supervisor Dr Beata Wysocki. Thank you for the support and guidance, and all of the great conversations.

Furthermore, my appreciation to all of the staff at the University of Wollongong for all of the help throughout the years. I would especially like to thank everyone in the SECTE workshop for their assistance and friendship, and the staff within the School of Mathematics who helped me through a crucial derivation in my studies.

A special thanks to all of my colleagues from House 114 and TITR. I will always remember the endless discussions, and great friendship.

To my family, my parents, and my sister, thank you for everything you have done for me throughout the years. You have always been there to give a helping hand, and allowed me to focus on my studies.

Finally, to my wife Kristina. Your unlimited support and encouragement means everything to me, and I would not be where I am today if it were not for you. I can only hope my studies will allow me to express my great appreciation for everything you have done for me.

Contents

List of Figures

List of Tables

List of Abbreviations

AC	Autocorrelation
ARake	All-RAKE
AWGN	Additive White Gaussian Noise
BEC	Backward Error Correction
CC	Cross-Correlation
CDMA	Code Division Multiple Access
DS	Direct Sequence
DS-CDMA	Direct Sequence Code Division Multiple Access
DS-UWB	Direct Sequence Ultra Wideband
EIRP	Effective Isotropic Radiated Power
FCC	Federal Communications Commission
FEC	Forward Error Correction
FR	Frame Repetition
GGA	Generalized Gaussian Approximation
ICM	Interleaved Coding-Modulation
ICTH	Interleaved Convolutional Time Hopping
IFFT	Inverse Fast Fourier Transform
ISI	Intersymbol Interference
LOS	Line Of Sight
LSE	Least Square Error
MAP	Maximum A Posteriori
MBOA	Multi-Band OFDM Alliance
MB-OFDM	Multi-Band Orthogonal Frequency Division Multiplexing
MHP	Modified Hermitian Pulses
ML	Maximum Likelihood

MSE	Mean Square Error
MUI	Multi-User Interference
NLOS	Non-Line Of Sight
OFDM	Orthogonal Frequency Division Multiplexing
PAM	Pulse Amplitude Modulation
PCTH	Pseudo Chaotic Time Hopping
PPM	Pulse Position Modulation
PRake	Partial-RAKE
PSD	Power Spectral Density
RF	Radio Frequency
RMS	Root Mean Squared
RSC	Recursive Systematic Convolutional
RX	Receiver
S-B-S	Symbol-By-Symbol
SGA	Standard Gaussian Approximation
SISO	Soft-Input-Soft-Output
SOVA	Soft-Output Viterbi Algorithm
SRake	Selective-RAKE
TCM	Trellis Coded Modulation
TH	Time Hopping
TH-UWB	Time Hopped Ultra Wideband
TR	Time Reversed
TTCM	Turbo Trellis Coded Modulation
TX	Transmitter
UWB	Ultra Wideband
WLAN	Wireless Local Area Network
ZCZ	Zero Correlation Zone

Chapter 1

Introduction

1.1 Background

The wireless transmission of information pioneered a new age of economic evolution and social development. Ultra wideband (UWB) is a communication technique designed for relatively short range data transfers. Although often viewed as a modern advancement in wireless communications, UWB has experienced several decades of technological growth [1]. Considering its impulsive nature and bandwidth occupancy, it may be argued UWB has its origins in the spark-gap transmissions by Marconi and Hertz near the turn of the 20th century [2]. These transmissions over the Atlantic Ocean marked the feasibility of wireless telecommunications, igniting over a century of research and development.

Ultra wideband operates at the physical layer of communications. Although defined primarily by its bandwidth usage, this technique is commonly implemented through the use of baseband pulses of very short duration [3]. These impulsive waveforms spread the energy of the radio signal from near DC to several gigahertz. Bandwidth inadequacy has consistently been a bottleneck for the advancement of wireless deployment. With its sparse spectral profile and low peak power emission level, UWB is capable of operating simultaneously with conventional communication systems.

There are two approaches to the measuring of UWB spectral characteristics [4]. These are referred to as the 'full-bandwidth' and the 'bandwidth-limited' measurements. The former considers a waveform's temporal characteristics, applying a Fourier transform for conversion to a frequency domain representation. The latter involves a direct frequency domain measurement of the spectral characteristics.

Wireless communications are inherently subject to numerous signal degradations. Multi-access interference is an inevitable consequence of multiple users operating in close proximity. The successful adoption of UWB into the commercial arena depends significantly on the development of efficient access techniques. Several dimensions exist over which user multiplexing may be achieved, these being:

- time slots;
- frequency bands;
- direct sequence codes;
- or a combination of the above.

The mode of multiplexing for each medium is illustrated in Fig. 1.1, notably indicating the multiplexing of direct sequence codes over both time and frequency.

Signal multipath is another source of energy loss within a wireless system. The large bandwidth of UWB implies resolvable multipath with path delays on the order of nanoseconds. Harnessing this dispersed energy, equalization techniques may be employed in either the receiver or the transmitter. Integration into the receiver-side is more common, although transmitter-side adoption utilizing the time reverse of the propagation impulse response has also emerged as a viable communication tool.

Ultimately, errors will arise in multi-user rich scattering environments. Numerous correction techniques exist, ranging from single parity bit additions and

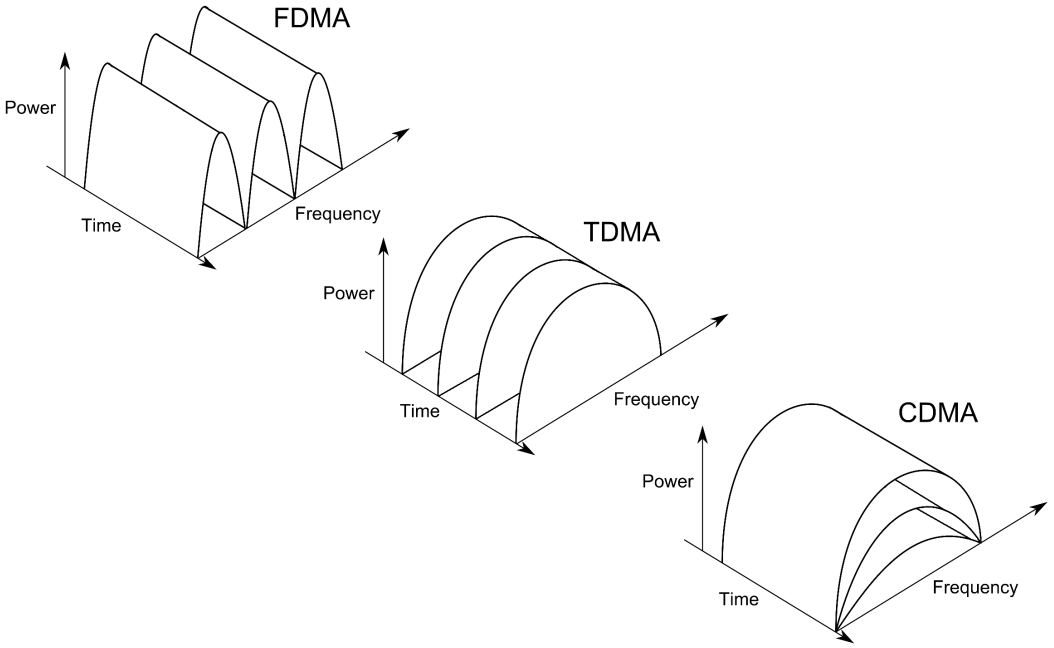

Figure 1.1 Channel use over frequency, time and code division multiple access

block based checksums, to complex iterative decoding algorithms. They are classified as either backward error correction (BEC), involving receiver-side error detection and subsequent data re-transmission; and forward error correction (FEC), requiring more intricate receiver-side detection and analysis methods, although eliminating the necessity of re-transmission.

With its revolutionary and unlicensed communication approach, UWB has emerged as a formidable contender in the wireless arena. Having an array of error mitigation techniques, it prevails as a high rate and low power consuming system for the modern world of telecommunications.

1.2 Aims of this Thesis

Significant commercial and academic research has been conducted into UWB, ultimately seeking to improve system performance. This dissertation explores varied diversity improvements in order to increase the capacity of UWB systems. The three main techniques researched within this thesis are:

- orthogonal multiplexing;
- channel equalization;
- and forward error correction.

Orthogonal multiplexing is considered with regard to a time hopped UWB architecture. Time, frequency, and direct sequence hopping codes are studied in order to draw a comparative performance analysis. Through this analysis, the possibility of altering sequence constructions in order to achieve a performance improvement is considered. While taking to account traditional code correlation measures, this thesis proposes a unique approach to sequence analysis, through the development of a set of state probabilities for pulse separations.

Channel equalization is also studied, researching both receiver- and transmitter-side implementations. Although discussing both approaches, this dissertation seeks to derive closed-form expressions for self- and multi-user interference within a transmitter-side equalization system. With UWB dependent upon numerous parameters, closed-form representations of performance enable a quick analysis of system capability for varied factors. These factors include: the propagation channel; transmit energy; and user multiplexing codes.

Error correction is addressed in terms of binary and non-binary means. Forward error correction is a common addition to wireless systems, although its integration is generally only concerned with the data bit level. Discussed herein is a proposal to combine data encoding with time hopping. Although achieved through an increase in complexity, this approach may simplify the flow structure of a UWB system, while introducing a novel method of time hopping code generation.

Finally, diversity techniques are analyzed through both mathematical modeling and comparative simulations. Through this, system performances may be evaluated within a noise degraded, multipath scattering, multi-user architecture. All areas of study will be examined in the effort to improve the capacity of UWB systems, increasing the rate of data transfer, and reducing multi-user

interference. This may subsequently improve the commercial viability of UWB, and its assimilation into mainstream short range wireless communications.

1.3 Thesis Overview

This dissertation is structured as follows:

- **Chapter 2** begins with a discussion of the background and standardization of UWB. Encompassed under the IEEE 802.15.3a and 802.15.4a protocols, the standard UWB multipath channel model has been designed according to common propagation characteristics. Several varied implementation methods are examined, together with common modulation techniques. Bandwidth efficiencies and multipath resolution capabilities are addressed with regard to the standard propagation channel. This chapter also presents overviews to diversity methods utilized within this dissertation. Orthogonal hopping sequence design, existing channel equalization measures, and current forward error correction approaches are discussed. The latter mainly considers recently emerged turbo coding techniques, which iteratively converge to an estimate of transmitted codewords;

- **Chapter 3** analyzes multi-access systems, where the most dominant errors occur due to multi-user interference. Orthogonal sequencing of user transmissions aids in minimizing degradations, although complete elimination is not feasible within asynchronous systems. The design of existing hopping codes is discussed in terms of various code parameters, including range, periodicity, and correlation properties. Codes are constructed to achieve orthogonality over a 'family' of sequences. Time, frequency, and direct sequence code designs are presented, together with varied performance analysis measures. A unique approach to sequence characterization is introduced, based upon the separation probability of signal transmissions. Both short and long codes are employed, exhibiting varied correlation properties. Finally the effect of interleaving at the chip level

is examined, comparing interleaver performances when designed through long random codes or deterministic hopping sequences;

- **Chapter 4** presents a set of preliminary and closed-form expressions for the intersymbol interference present within a UWB system employing a transmitter-side equalization. Derivations are based upon an analysis of transmission overlaps, together with the probabilities of each overlap. Comparative analysis of derived performance levels against a simulated system is also given;

- **Chapter 5** adopts a similar derivation approach to the previous chapter in the development of multi-user interference expressions. These preliminary and closed-form equations for a transmitter-side equalization analyze signal overlaps, together with the introduced separation probability profile which characterizes time hopping codes. Derived formulae are compared against a simulated multi-user system performance;

- **Chapter 6** discusses the integration of forward error correction into a time reversed UWB architecture. Conventional binary turbo decoding is considered at the binary data level, and non-binary turbo decoding is applied to combine data encoding and user multiplexing stages. The latter method encodes information symbols onto an expanded modulation set, utilizing a unique memoryless mapper to generate a time hopping code. Random and deterministic mapping procedures are presented, applying short length sequences. Soft output decoding algorithms are adopted for both error correction methods. While binary encoding uses a conventional bit-based decoding algorithm, non-binary encoding applies a symbol-by-symbol (S-B-S) decoder. Encoder and decoder structures are comprised of 'component' sub-structures to achieve iterative properties. A comparative analysis of each method against a simulated performance is presented. Tests are conducted in single- and multi-user scenarios, also observing the multi-user interference effects of signals employing error correction;

- and **Chapter 7** concludes the thesis, giving suggestions for future research.

1.4 Contributions

The main contributions of this thesis are as follows:

1. A comparative analysis of existing orthogonal multiplexing sequences is presented, porting all code constructions to the time domain. These short codes are analysed in terms of their correlation properties, and also their transmission separation capabilities [5]. The application of long length deterministic codes for interleaved coding-modulation is also discussed with reference to randomly generated sequences [6, 7, 8]. This work provides an in-depth perspective to the multiplexing capabilities of common hopping code measures, including their application to foreign system architectures;

2. An innovative approach to user multiplexing code characterization is developed through the transmission separation probabilities achieved by each hopping sequence [9]. This allows further analysis of the waveform overlaps present between UWB transmissions;

3. A set of preliminary equations are developed for intersymbol interference within a transmitter-side equalization approach to UWB [9]. These are reduced into a closed-form solution, taking into consideration several system parameters [10, 11];

4. Preliminary expressions are also developed for the multi-user interference within a UWB system [9]. These are reduced to a closed-form solution in terms of the interference experienced by a single user, then scaled according to the number of active transmitters [10, 11];

5. A non-binary turbo encoding system is utilized to combine user multiplexing and data encoding stages [12]. This work is conducted with a random unique memoryless mapper to generate a time hopping sequence. The application of deterministic codes for the design of this mapper is also addressed, namely through the use of truncated hyperbolic congruence codes [13].

1.5 List of Publications

Contributions within this thesis have been presented on the following published or submitted conferences and journals:

K. Popovski, T. A. Wysocki & B. J. Wysocki, Truncated Hyperbolic Mapping for Non-binary Turbo Coding in UWB, Accepted in IEEE International Symposium on Personal, Indoor and Mobile Radio Communications (PIMRC), 2008.

K. Popovski, T. A. Wysocki & B. J. Wysocki, A Closed-Form Derivation of Self and Multi-User Interference for Time-Reversed UWB Communications, Accepted in Elsevier Special Issue of the Computers & Electrical Engineering Journal, 2008.

K. Popovski, T. A. Wysocki & B. J. Wysocki, Combined User Multiplexing and Data Modulation through Non-binary Turbo Codes for UWB, Accepted in IEEE Wireless Communications and Networking Conference, Las Vegas, 2008.

K. Popovski, T. A. Wysocki & B. J. Wysocki, Closed-Form Derivations of ISI and MUI for Time-Reversed Ultra Wideband, International Conference on Signal Processing and Communication Systems (9th International Symposium on DSP and Communication Systems, DSPCS2007, and 6th Workshop on the Internet, Telecommunications and Signal Processing, WITSP'2007), December, 2007.

K. Popovski, B. J. Wysocki & T.A.Wysocki, Modelling and Comparative Performance Analysis of a Time-Reversed UWB System, EURASIP Journal on Wireless Communications and Networking, Vol. 2007, Article ID 71610, 2007.

M. M. Pietrzyk, K. Popovski, T. A. Wysocki, B.J. Wysocki, & J. H. Weber, On the Performance of Scarcely Populated Coded UWB-IR Systems on Multipath Fading Channels, 27th Symposium on Information Theory in the Benelux, June, 2006, pp. 235-242.

M. M. Pietrzyk, K. Popovski, T. A. Wysocki, B. J. Wysocki & J. H. Weber, Scarcely Populated UWB-IR Systems with Interleaved Coding-Modulation on Multipath Fading Channels, The 2006 IEEE 2006 International Conference on Ultra-Wideband, September, 2006, pp: 55-60.

M. M. Pietrzyk, K. Popovski, T. A. Wysocki, B. J. Wysocki & J. H. Weber, Multi-User UWB-IR Systems with Interleaved Coding-Modulation on Multipath Fading Channels, The Institution of Engineering and Technology Forum on Waveform Diversity and Design in Communications, Radar and Sonar, November, 2006, pp: 91-98.

K. Popovski, B. J. Wysocki & T. A. Wysocki, Performance Comparison of UWB Hopping Codes in a Multi-User Rich Scattering Environment, IEEE 63rd Vehicular Technology Conference, Vol. 4, May, 2006, pp: 1864-1868.

D. Robinson, T. A. Wysocki, V. Smith & K. Popovski, Background Radio Frequency Interference Measurements for Wireless Devices in the Electricity Supply Industry, in 8th International Symposium on DSP and Communication Systems, DSPCS'2005 & 4th Workshop on the Internet, Telecommunications and Signal Processing, WITSP'2005, 2005, pp. 277 - 282.

Chapter 2

Literature Review - Ultra Wideband Communications

2.1 Introduction

Ultra wideband (UWB) communications is today seen as a viable candidate for short range data transfer. However, while its origins may be traced to the spark gap transmissions during the turn of the 20th century, technical limitations resulted in a movement away from wideband signals [14]. Narrowband communications were preferred as demultiplexing and effective recovery of wideband energy was difficult. However, Claude Shannon's discoveries in 1948 outlined the connection between spread bandwidth and information holding capacity [15]. The result of this was the Federal Communications Commission (FCC) allocating a block of spectrum over which coding, rather than traditional narrowband techniques, was used to multiplex multiple users.

In February, 2002, UWB emerged into the commercial arena on an unlicensed basis. This was subject to the modified Part 15.209 rules within the United States, with communication restricted to the 3.1 to 10.6 GHz band [16]. The 'FCC First Report and Order' established standards and restrictions for three types of UWB devices based on their potential to cause interference, these being:

1. imaging systems including Ground Penetrating Radars (GPRs), wall-

through-wall, surveillance, and medical imaging devices;

2. vehicular radar systems; and

3. communications and measurement systems.

UWB is characterized by having either a signal bandwidth greater than 500 MHz at a power level of -41.3 dBm/MHz, or a fractional bandwidth greater than 20% according to the definition [16, 17, 18]:

$$\text{Fractional Bandwidth} = \frac{(f_H - f_L)}{\left(\frac{f_H + f_L}{2}\right)}.$$

The parameters f_L and f_H represent the lower and upper frequencies of the -10 dB emission points respectively, as established by the FCC in 2002. These noise-like wideband communications hence produce similar power emission levels as general consumer goods, such as a laptop computer. The unilateral spectral mask imposed by the FCC for indoor UWB communications is shown in Fig. 2.1 [1]. Power limitations within this mask are imposed on the effective isotropic radiated power (EIRP), which occurs when impedances are matched between the transmitter circuitry and the antenna. As a reference, mobile phones may transmit up to +30 dBm, which is of order 10^7 times higher than the power spectral density permitted by UWB [18].

Ultra wideband is designed with low enough power emissions such that it may appear as noise to other communications operating in the same frequency band. However, studies have shown that in a non line-of-sight (NLOS) scenario, a UWB interferer operating at the peak allowable power density possible, may have significantly detrimental effects to data rates in 802.11a wireless local area network (WLAN) systems [19]. Thus, interference to and from RF equipment in close proximity is a concern for UWB radio.

UWB is currently standardized under IEEE 802.15.3a for short range (< 10 m) and high data rate (100 Mbit/s) communications, and under IEEE 802.15.4a for moderate range ($100 - 300$ m) and low data rates (less than a few Mbit/s) [14].

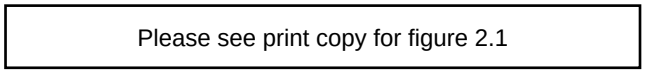

Figure 2.1 FCC spectral mask for UWB indoor applications

The two main proposals seeking to be the IEEE standardized UWB architecture are Multi-Band Orthogonal Frequency Division Multiplexing (MB-OFDM) and Direct-Sequence UWB (DS-UWB) [17].

MB-OFDM is supported by the 'WiMedia Alliance', which merged with the 'Multi-Band OFDM Alliance' (MBOA) in 2005 and is operating under the original name [20]. This technique combines frequency hopping with OFDM, interleaving symbols over sub-bands in the available frequency spectrum. Through this technique, an entire 528 MHz band appears to be simultaneously utilized [21, 22]. MB-OFDM requires complex inverse fast Fourier Transform (IFFT) operations, may have relatively higher peak to average ratio, and is susceptible to frequency selectivity of the channel. The alternate method, DS-UWB, is supported by the 'UWB Forum', and represents symbols by a series of pulses that are pulse amplitude modulated by a preset sequence [14, 23]. DS-UWB requires complex high speed analogue-to-digital converters (causing power consumption issues), and necessitates the use of complex receivers for significant energy capture [24, 25].

Unfortunately, the IEEE body responsible for the UWB 802.15.3a standard was disbanded in 2006. With continued debate over standardization, and competitors beginning to develop chip solutions for their UWB variations, the decision has been left to be made by market forces [26]. Developments include Freescale Semiconductor's high definition television chipset [27], and Focus Enhancements' 'Talaria' chipset, which integrates both MB-OFDM and DS-OFDM modulation methods into a single device [28].

2.2 System Architecture

2.2.1 UWB Transmitter Design

This dissertation considers time hopped UWB (TH-UWB), which is similar in implementation to DS-UWB. While DS-UWB uses constant intervals between pulses, TH-UWB adopts an additional time shifting for data encoding, and has a uniform pulse polarity. The data modulation applied is pulse position modulation (PPM), entailing an additional time shift for each pulse. An alternate form of modulation is pulse amplitude modulation (PAM), where the amplitudes of transmitted pulses are altered in accordance with the transmitted data [29]. This carrier-less transmission is potentially an inexpensive radio technique due to the subsequent low-cost design.

The signal $s^{(u)}(t)$ transmitted for the uth user in a time-hopped UWB system, with time hopping sequence $c_m^{(u)}$, and equiprobable data $b_m^{(u)} \in \{-1, 1\}$ mapped through binary PPM, is given by [30, 31]:

$$s^{(u)}(t) = \sqrt{E_{TX}(u)} \sum_{m=-\infty}^{\infty} w\left(t - mT_f - c_m^{(u)} T_c - \varepsilon b_m^{(u)}\right), \tag{2.1}$$

where $E_{TX}(u)$ is the user signal energy, $w(t)$ is the base transmitted waveform of width T_w seconds, the time shift ε is set to equal the pulse width, and m is the frame number. T_f is a single frame length, which is segmented into equally spaced intervals called 'chips' of duration T_c, such that $T_f = N_h T_c$. Transmissions are designed to only permit one pulse per user per frame. This

dissertation considers a perfectly power controlled system, where $E_{TX}(u)$ is constant for all u.

With the data shift ε, and the pulse duration T_w, the remaining duration of a chip is the guard time T_g, given as:

$$T_g = T_c - (\varepsilon + T_w). \tag{2.2}$$

This time may be chosen sufficiently larger than the duration of the channel impulse response, permitting a portion of the multipath components to pass before the transmission of the next pulse [32]. Defining the data rate as R, the symbol duration $T_s = 1/R$, and the number of transmissions per symbol N_s, the frame duration T_f and chip duration T_c are expressed as:

$$T_f = \frac{T_s}{N_s} = \frac{1}{N_s R}, \tag{2.3}$$

$$T_c = \frac{1}{N_h N_s R}. \tag{2.4}$$

The parameter $c_m^{(u)}$ denotes the position within the particular frame (the chip number) that is occupied by the uth user's signal in accordance with a time hopping sequence [33]. The characteristic parameters of these codes are the cardinality (N_h), which specifies the alphabet size; and the periodicity (N_p), which indicates the length of the code before it is repeated. Generally, the periodicity of the sequence is chosen to equal its cardinality. Codes are designed such that $c_m^{(u)} \in \Re$, $0 \leq c_m^{(u)} \leq N_h - 1$, and $c_m^{(u)} T_c + \varepsilon < T_f$. The latter restriction is imposed to contain each pulse within a single chip.

A signal transmitted through time hopped UWB, applying PPM, is illustrated in Fig. 2.2(a). In the example, 2 bits are sent, with a frame of $N_h = 5$ chips and $N_s = 2$. For the purpose of contrast, a data signal transmitted through a DS-UWB architecture is depicted in Fig. 2.2(b). It can be seen in DS-UWB that the hopping sequence is introduced through means of a bipolar pulse polarity multiplier, with the data modulation introduced by the same means [34]. Due to the compacted multiplexing employed, DS-UWB can operate in a relatively smaller time window, although TH-UWB outperforms DS-UWB by approximately 1 dB [29].

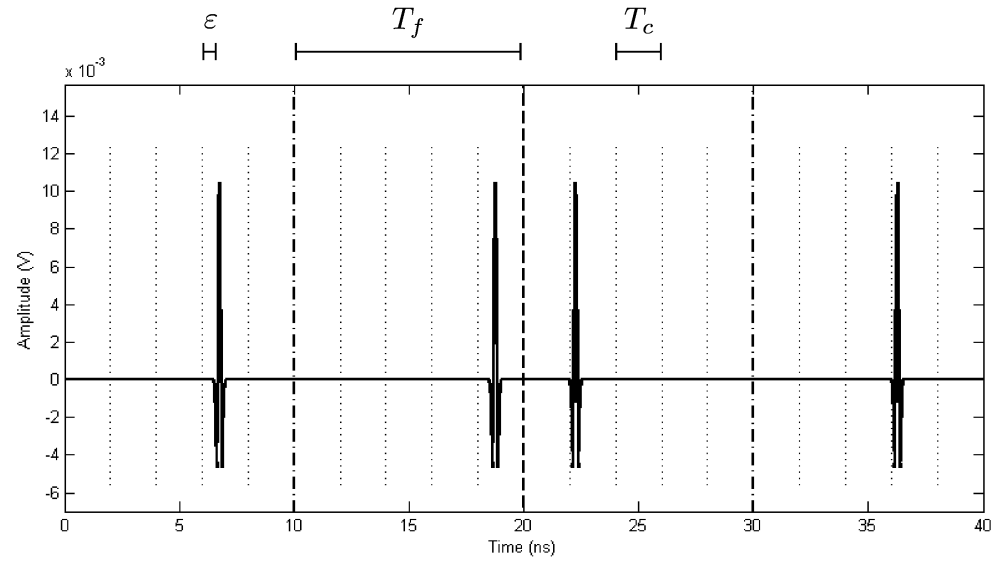

(a)

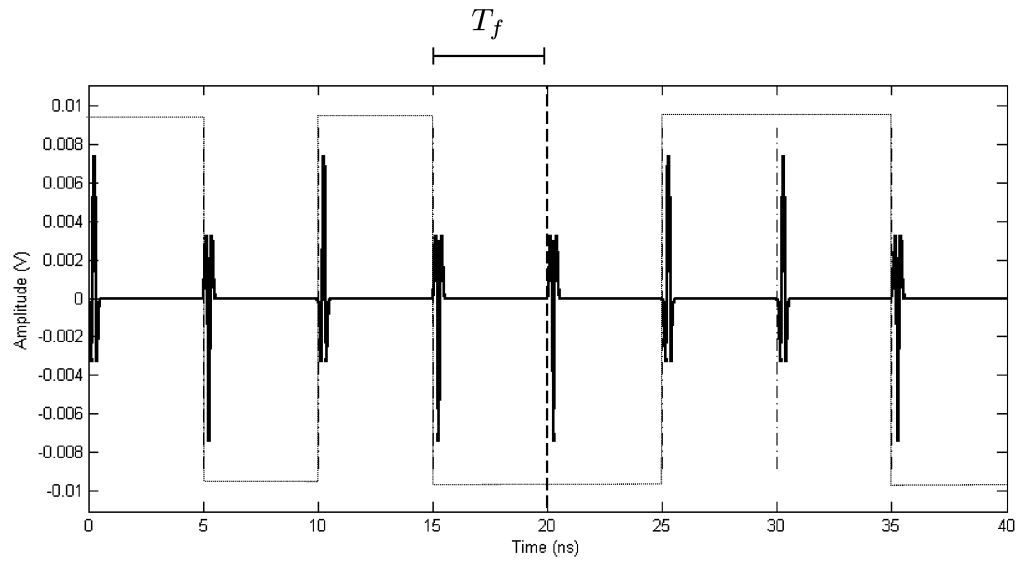

(b)

Figure 2.2 Transmitted signal structure for (a) TH-UWB with PPM and (b) DS-UWB

This thesis considers a chip synchronous, single-input-single-output system, where user transmissions are aligned with the chip time T_c. Chip synchronism, due to the resulting pessimistic pulse overlapping, leads to a worst-case performance for the system [35].

The base waveform $w(t)$ was set as the second derivative of the Gaussian pulse, with center frequency f_0, defined as [36]:

$$w(t) = \left[1 - 2(\pi t f_0)^2\right] \exp\left\{-(\pi t f_0)^2\right\}, \tag{2.5}$$

with energy:

$$E_{w(t)} = \frac{3}{\sqrt{32\pi \cdot f_o^2}}, \tag{2.6}$$

and energy normalized Fourier transform of:

$$\widetilde{W}(f) = \sqrt{\frac{\sqrt{32\pi \cdot f_o^2}}{3}} \frac{2}{\sqrt{\pi \cdot f_o^2}} \left(\frac{f}{f_0}\right)^2 \exp\left\{-\frac{f^2}{f_0^2}\right\}. \tag{2.7}$$

A center frequency of 3.9 GHz was used, which results in a monocycle width of $T_w = 0.5$ ns. The time domain representation of this energy normalized Gaussian derivation is shown in Fig. 2.3, together with the corresponding normalized power spectral density.

Transmitter and receiver antennas generally behave as pulse distorting filters, with a differentiation of the pulse occurring as the wave radiates [37]. This thesis considers that the combined effect of both transmit and receive antennas has no significant effect on the signal transmitted.

Considering the impulsive nature of the monocycle in Fig. 2.3, it can be deduced that its electrostatic discharge has a spectrum that is infinite. As such, it may have an infinitely sparse interference potential. The spectrum may be shaped by techniques including:

- altering the pulse width, with an inversive relationship existing between the time duration of the pulse and its corresponding spectral width [38];
- changing the pulse rate, as this adjusts the spectrum's magnitude since the input power is changed based upon the number of pulses transmitted;

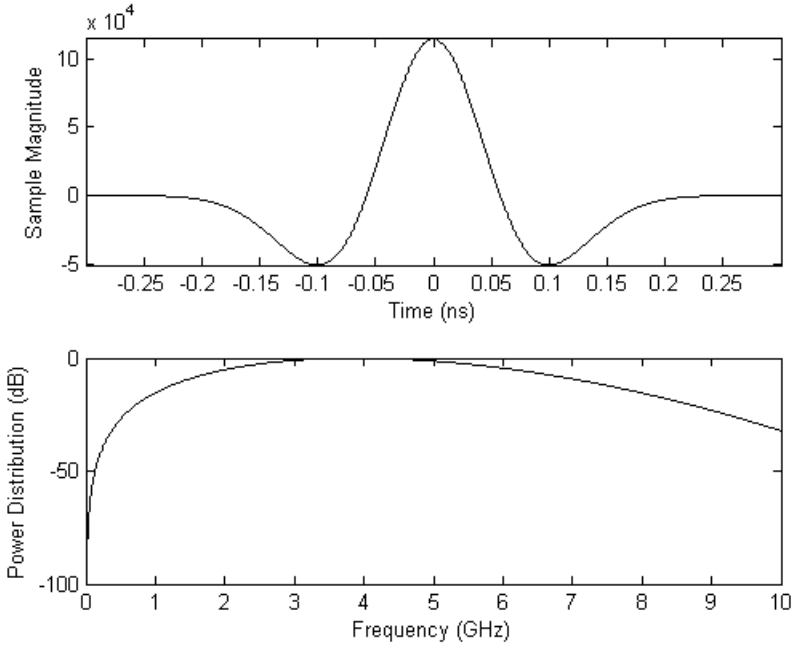

Figure 2.3 Time and frequency domain representations of a 2nd derivative Gaussian monocycle with center frequency of 3.9 GHz

- and differentiation of the base pulse, since Gaussian derivatives of higher order characteristically exhibit higher peak frequencies and also an increased signal bandwidth.

As an extension to this final technique, the base pulse may be designed through a combination of Gaussian derivative base functions. This can be done through a random selection of functions, or use of the Least Square Error (LSE) to minimize the error function between the transmitted and required signals [17]. Alternate waveform shape algorithms have been developed to reduce the pulse time duration [39,40], and pulse types such as modified Hermitian pulses (MHP) have been applied [34]. Each technique ultimately attempts to produce a power spectral density shaped according to the restrictive emission mask imposed by the FCC.

2.2.2 Multi Path Channel

Wireless communications are inherently predisposed to reflections and refractions of signal transmissions. Ultimately, this leads to multipath at the receiver, which may pose severe limitations on system performance. In February 2003, the IEEE 802.15.3a Study Group subcommittee released a 'Final Report' detailing a channel model specific for UWB signal propagation [41]. This model is based on the 'SV' channel outlined by Saleh and Valenzuela, where multipath components arrive in clusters [42].

Ignoring user referencing, the 802.15.3a UWB channel model is defined as [41]:

$$h(t) = X \sum_{l=0}^{L} \sum_{k=0}^{K} \alpha_{k,l} \delta(t - T_l - \tau_{k,l}), \tag{2.8}$$

where $\delta(t)$ represents the Dirac delta function. The parameter L denoted the number of clusters, K signifies the number of paths within each cluster, and $\alpha_{k,l}$ is the path magnitude for ray k within cluster l. The lth cluster arrives at time T_l, with the kth ray in this cluster arriving at time $\tau_{k,l}$, which is relative to the first path in the cluster ($\tau_{0,l} = 0$). The path magnitude $\alpha_{k,l}$ is modeled as having ± 1 Bernoulli mixed log-normal densities, giving a zero mean for each instance of the channel. Independent fading is assumed for each cluster and for each ray within the cluster, with mean cluster and ray powers decaying exponentially in time.

Shadowing, represented by the term X, is assumed to be a log-normal random variable, formulated as:

$$X = 10^{\frac{g}{20}}. \tag{2.9}$$

The term g is a characterized as a Gaussian random variable, with a mean of g_0 and a variance σ_g^2. The average g_0 is dependent upon the total multi-path gain G as:

$$g_0 = \frac{10 \log_e G}{\log_e 10} - \frac{\sigma_g^2 \log_e 10}{20}. \tag{2.10}$$

This total multipath gain is determined by the separation distance D between the transmitter and receiver, and may be estimated as [17]:

$$a = \frac{c_0}{D^{\gamma_p}}. \tag{2.11}$$

Target Channel Characteristics	**CM1**	**CM2**	**CM3**	**CM4**
Scenario	LOS	NLOS	NLOS	NLOS
TX-RX Separation	(0-4m)	(0-4m)	(4-10m)	(>10m)
τ_m [ns] (Mean excess delay)	5.0	9.9	15.9	30.1
τ_{rms} [ns] (rms delay spread)	5	8	15	25
NP10dB (number of paths that are within 10 dB of the strongest path)	12.5	15.3	24.9	41.2
NP (85%) (number of paths that capture 85% of channel energy	20.8	33.9	64.7	123.3
Λ [1/ns] (cluster arrival rate)	0.0233	0.4	0.0667	0.0667
λ [1/ns] (ray arrival rate)	2.5	0.5	2.1	2.1
Γ (cluster decay factor)	7.1	5.5	14	24
γ (ray decay factor)	4.3	6.7	7.9	12
σ_1 [dB] (stand. dev. of cluster lognormal fading)	3.3941	3.3941	3.3941	3.3941
σ_2 [dB] (stand. dev. of ray lognormal fading)	3.3941	3.3941	3.3941	3.3941
σ_x [dB] (stand. dev. of lognormal fading for total multipath)	3	3	3	3

Table 2.1 IEEE UWB channel model parameter settings

Here, γ_p is the power attenuation exponent, and c_0 is a 'tuning' constant manipulated to obtain a reference gain at a reference distance. Taking the reference attenuation at a separation distance of 1 m as $A_{dB} = 10 \cdot log_{10}(E_{TX}/E_{RX})$, with E_{RX} representing the receiver energy, c_0 may be calculated as:

$$c_0 = 10^{-A_{dB}/20}. \tag{2.12}$$

Within a LOS scenario, for instance, a reference attenuation of $A_{dB} = 47\ dB$ and attenuation exponent of $\gamma_p = 1.7$ are applied.

There are four channel scenarios defined by the IEEE for this highly dispersive channel structure (CM1 to CM4). These scenarios, together with the IEEE recommendations for common parameters, are shown in Table 2.1. Considering a root mean squared (RMS) delay spread of up to 25 ns, significant intersymbol interference may be caused for higher data rate transmissions, where lower pulse repetition intervals are evident.

Since defining parameters such as cluster/ray arrival rates (Λ, λ) and decay factors (Γ, γ) are known for each channel scenario, as are the mean and variance of the channel, it can be said that the random variables defining the path amplitudes and arrival times are independent. Also, when the variance is given, the set of random variables defining the consecutive gains for a single cluster are mutually independent.

For the purpose of simulation and closed-form derivations, the discrete-time channel impulse response is modeled as:

$$h(u; x_{pos}, t) = X \sum_{k=0}^{L-1} \alpha_k \delta(t - \tau_k). \tag{2.13}$$

It constitutes a segmentation of the original model into 'bins' of time width τ seconds. The term τ_k is formed by a multiplication of the bin width τ by the number of paths k, such that $\tau_k = \tau \cdot k$. The channel consists of L paths, each representing the energy within the bin width. Thus the total channel width is equivalent to $L\tau$ seconds. The channel model argument $(u; x_{pos}, t)$ is adopted for succinct terminology between equalization methods applied in subsequent chapters. The parameter x_{pos} represents the position of the intended receiver. The gain of the α_k coefficients is normalized to unity for each channel realization, such that:

$$\sum_{k=0}^{L-1} |\alpha_k|^2 = 1.$$

A quasi-stationary channel is assumed, remaining time-invariant for the transmission of a block of data, and independent between blocks.

The characteristic power delay profile of this channel is illustrated in Fig. 2.4(a) [42], showing the typical time of arrival of multipath components against the received power. For clarity, non-overlapping clusters are shown, although this generally is not the case. A sample profile within a LOS scenario is depicted in Fig. 2.4(b).

Please see print copy for figure 2.4(a)

(a)

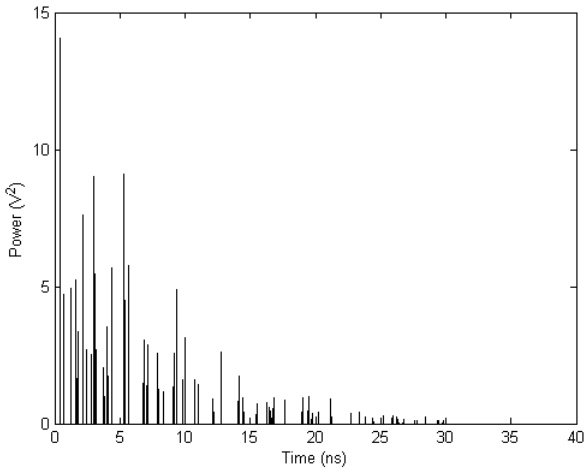

(b)

Figure 2.4 Power delay profiles for the IEEE UWB channel model (a) characteristic and (b) LOS sample

2.2.3 UWB Receiver Design

The large bandwidth of UWB waveforms has both advantages and disadvantages to system architecture. The simplistic transmitter design was outlined in Sec. 2.2.1, benefiting from the removal of the signal modulation stage. For a UWB receiver, larger bandwidth provides the advantage of increasing the capacity to resolve multipath caused by the transmission channel [18]. However, pulse overlapping and per-path pulse distortion increases receiver design complexity [14]. Considering the short pulse duration in time hopped UWB systems, sampling rates in the multi-GHz range are required. This also has a significant

impact on receiver performance in terms of sensitivity to synchronization errors.

The received signal is comprised of the transmitted signal, after manipulation by channel attenuation and delay, superimposed with noise interference. This noise is modeled as a random additive white Gaussian noise (AWGN) process with a two-sided power spectral density of $\sigma^2 = N_0/2$. Ignoring multipath and noise components, the received signal may be represented as:

$$r^{(u)}(t) = a \cdot s^{(u)}(t - t_\Delta), \tag{2.14}$$

where t_Δ is the transmitter/receiver time displacement. The parameter 'a' is the channel attenuation, defined as the square of the total multipath gain G.

Applying the definition for the propagation channel, the signal received is defined as:

$$r(t) = \left(\sum_{u=1}^{N_u} s^{(u)}(t) \otimes h(u; x_{pos}, t) \right) + n(t) \tag{2.15}$$

$$= \sum_{u=1}^{N_u} \sum_{k=0}^{L-1} \alpha_k(u; x_{pos}) p(t - \tau_k) + n(t), \tag{2.16}$$

where $\otimes$ represents convolution, $n(t)$ is the AWGN, and a summation takes to account contributions of all N_u users. The parameter $p(t)$ models the received pulse waveform. In accordance with Turin's multipath channel model, per-path pulse distortion is neglected [43]. Thus $p(t) \equiv w(t)$ of Eq. 2.5.

All transmitters were assumed dispersed enough such that the channel responses from each transmitter to any receiver are independent. The minimal antenna separation for this is $\lambda_{wave}/2$ (half the transmitted signal wavelength). Considering the permitted operating frequency range of UWB (3.1 to 10.6 GHz), the wavelength of a UWB signal within a vacuum may range from approximately 2.8 cm to 9.7 cm. Hence channel independence is a feasible assumption.

Decisions on the encoded data within a received signal are conducted with the use of a template base waveform, taking the form of [44]:

$$v(t) \triangleq w(t) - w(t - \varepsilon), \tag{2.17}$$

where ε is the binary PPM time shift set equal to the base pulse width T_w. The test statistic Z is constructed by summing the N_s correlations between the template signal $v(t)$ at various time shifts, and the received signal [3]. Representing the template spanning an entire symbol as $v_{symbol}(t)$, the symbol-level decision variable may be expressed as:

$$Z = \int_{t \in T_i} r(t) v_{symbol}(t) dt. \tag{2.18}$$

The polarity of this decision variable estimates the transmitted data bit $b_m^{(u)}$. A decision to $b_m^{(u)} = 0$ is made in the case that:

$$Z = \sum_{m=-\infty}^{\infty} \int_{\varepsilon}^{\varepsilon + T_w} r^{(u)}(t) v(t - mT_f - c_m^{(u)} T_c) dt > 0, \tag{2.19}$$

where $r^{(u)}(t)$ represents the uth user's received signal. The decision of $b_m^{(u)} = 1$ is made in the event that $Z \leq 0$.

As the transmitted signal is deterministic, and the system noise is a Gaussian process, the received signal is also Gaussian. As the correlation between the template and the received signal is a linear function of the latter, it also is a Gaussian random process. Finally, provided the number of users N_u is large, the multi-user interference may be considered a Gaussian process too [31, 37, 3, 45].

Decisions on encoded data may be conducted on the N_s waveforms comprising a transmitted signal either individually or collectively. The former involves correlations over each waveform, with a decision being based upon a simple majority criterion. Conversely, the correlation can be applied to the entire signal representing the transmitted symbol, with a decision determined through the single result. While more complex in design, the latter provides an error performance improvement, this being the method applied in this thesis.

Within binary PPM, two orthogonal functions may be used for data representation. These signal vectors, in terms of the transmit energy, may be expressed as:

$$\mathbf{s_1} = (\sqrt{E_{TX}}, 0), \tag{2.20}$$

$$\mathbf{s_2} = (0, \sqrt{E_{TX}}). \tag{2.21}$$

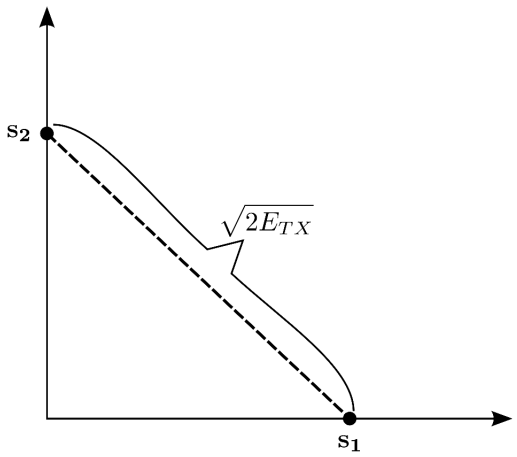

Figure 2.5 Signal points for orthogonal binary PPM signaling

The signal points for these orthogonal signal are shown in Fig. 2.5. An optimal detector applies the maximum likelihood (ML) criterion on the received symbols. Without loss of generality, the single user probability of error may be derived through the assumption that $\mathbf{s_1}$ was transmitted, assuming equiprobable data transmission. The subsequent received vector is:

$$\mathbf{r} = (\sqrt{E_{TX}} + n_1, n_2). \tag{2.22}$$

An error event may now be considered if the received signal is demodulated to be $\mathbf{s_2}$ [46, 47], with error probability:

$$\mathrm{P}(e|\mathbf{s_1}) = \mathrm{P}(n_2 - n_1 > \sqrt{E_{RX}}), \tag{2.23}$$

where noises are assumed statistically independent. The average error probability may be reduced to:

$$\begin{aligned}
\mathrm{P}(n_2 - n_1 > \sqrt{E_{RX}}) &= \frac{1}{\sqrt{2\pi N_0}} \int_{\sqrt{E_{RX}}}^{\infty} \mathrm{e}^{-x^2/2N_0} dx && (2.24)\\
&= \frac{1}{\sqrt{2\pi}} \int_{\sqrt{E_{RX}/N_0}}^{\infty} \mathrm{e}^{-x^2/2} dx && (2.25)\\
&= Q\left(\sqrt{\frac{E_{RX}}{N_0}}\right) && (2.26)\\
&= \frac{1}{2} erfc\left(\sqrt{\frac{E_{RX}}{2N_0}}\right), && (2.27)
\end{aligned}$$

with:

$$erfc(y) = \frac{2}{\sqrt{\pi}} \int_{y}^{+\infty} e^{-\xi^2} d\xi, \tag{2.28}$$

$$Q(x) = \int_{x}^{\infty} \frac{1}{\sqrt{2\pi}} e^{-\frac{x^2}{2}} dx. \tag{2.29}$$

Where multiple pulses are used per data bit representation ($N_s > 1$), the transmitted signal energy is effectively increased by a factor of N_s. However, it should be noted that the increase in the number of pulses per bit requires a corresponding increase to the pulse rate. The bit level average error probability may be expressed as:

$$Pr_b = \frac{1}{2} erfc\left(\sqrt{\frac{N_s E_{RX}}{2N_0}}\right). \tag{2.30}$$

The impact of multi-user interference was commonly estimated through the Standard Gaussian Approximation (SGA) hypothesis [17]. It decomposes the decision variable (Z) into the useful signal, multi-user interference, and noise components, following the form: $Z = Z_u + Z_{mui} + Z_n$. The MUI may be removed through the use of orthogonal coding between users. Terms Z_{mui} and Z_n are both assumed to be zero-mean Gaussian processes. The validity of the SGA increases with the number of interfering users, although does not provide adequate realizations for low transmission rates or pulse repetition rates [48, 49, 50].

However, with the general validity of the SGA being questionable [49, 51], the more accurate Generalized Gaussian Approximation (GGA) may be utilized to approximate multi-user interference [52, 53]. The GGA provides a better estimate to the MUI performance floor in TH-UWB systems, taking into account the fourth order moment of the MUI.

2.3 User Multiplexing Codes

Time hopped UWB users are multiplexed through periodic pseudo-random noise sequences, which determine the chips users will transmit within each time frame.

This code division multiple access is represented by $c_m^{(u)}$ in Eq. 2.1, and is based upon a family of near orthogonal codes. These seek to minimize pulse overlap between simultaneously transmitting users, such that $c_m^{(i)} \neq c_m^{(j)}$ in the mth frame. Unfortunately, orthogonality is difficult to maintain in the presence of multipath, or in the absence of user synchronism. Ultimately, the existence of a Johnson bound between sequence parameters ensures that pure orthogonal time hopping sequences may not be designed [54].

This dissertation assumes chip synchronism exists between all user transmissions, as this generally results in a pessimistic error performance [55]. Subsequently, chip level analysis of user performance through sequence comparison may be conducted.

The three classifications of code division multiplexing which may be applied for multi-user access are:

- time hopping;
- frequency hopping;
- and direct sequence (DS) spreading sequences.

Frequency hopping sequences modulate information onto a carrier signal which systematically alternates through the available frequency bands. Direct sequence spreading is applied by phase-shift-keying a carrier with the summation of the code and the information stream to be modulated. The pulse rate of the data is much lower than that of the spreading sequence, therefore creating a wideband signal [56]. Auto- and cross-correlation properties are not consistent between hopping classifications [57], with correlation analysis in a time hopping perspective conducted herein for comparable results.

Mapping may be employed to convert frequency and DS sequences to time hopping codes, discussed further in Chapter 3.

Many applications adopt pseudo-randomly generated unique codes, as in various cluster based wireless sensor networks [58]. These codes are generated and

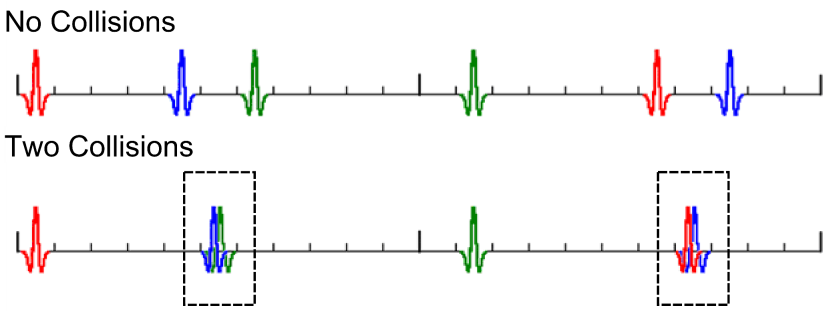

Figure 2.6 Multi-user collisions within a TH-UWB scenario

stored at both the transmitter and receiver. However, use of these random codes can lead to catastrophic collisions between user signals. As shown by Bellorado et al. [59], a significant degradation of data rates in wireless LAN systems may be caused by a UWB device operating with a random time hopping sequence. Proper design of orthogonal codes is also required to decrease the possibility of multi-user interference between UWB devices, lower the effects of multipath interference on communications, and improve synchronization between the transmitter and receiver.

When two user transmissions simultaneously occupy the same chip, a collision or 'hit' occurs. The time multiplexing of three users is shown in Fig. 2.6, using $N_h = 11$ chips. Two signal collisions are evident, where an overlap exists between user monocycles.

There are various aspects which must be considered in the design of orthogonal sequences. Taking a 'slot' to represent either a time interval or a frequency channel, these considerations include:

- efficient and even utilization of the available slots;
- not occupying the same slot for many repetitions;
- avoidance of sub-sequences between user patterns;
- and ensuring the periodicity of the sequence is larger than the number of pulses per symbol ($N_p > N_s$) [60].

Although the simplistic technique of occupying a single slot only throughout communications is feasible, this ultimately leads to a degradation in system performance. The possibility exists that two users may continually enter into the same slot, resulting in complete signal interruption. Rather, sequences are designed to obtain a uniform use of all available slots, as this will aid in minimizing multi-user interference.

For the following code analysis, assume the number of available slots is represented by an arbitrary parameter q, with the hopping pattern being denoted as $x = (x_0, x_1, \ldots, x_{N_p-1})$ of length N_p elements. Denote the composition vector $N(x) = [N_0(x), N_1(x), \ldots, N_{q-1}(x)]$, where $N_i(x)$ indicates the number of times that each of the q slots occur in x. It can be seen $\sum_i N_i(x) = N_p$. Sequences are designed such that [56]:

$$\sum_{i=0}^{q-1} N_i^2(x) = \|N(x)\|^2 \geq N_p \left\lfloor \frac{N_p}{q} \right\rfloor + \left\lceil \frac{N_p}{q} \right\rceil (N_p \bmod q), \tag{2.31}$$

with:

$$N_i(x) = \left\lceil \frac{N_p}{q} \right\rceil \text{ for } (N_p \bmod q) \text{ values of } i, \tag{2.32}$$

$$N_i(x) = \left\lfloor \frac{N_p}{q} \right\rfloor \text{ for } q - (N_p \bmod q) \text{ values of } i. \tag{2.33}$$

This approach evenly utilizes each of the available slots. Additional slot use is selected such that a uniformly spaced selection over the q possibilities is made.

Another requirement in sequence design is controlling the length. Short sequences limit the number of hopping combinations, while long codes may lead to synchronization issues. Also, the cardinality of the time hopping sequence (N_h) must be greater than or equal to the number of users in the system, since this indicates the number of chips (T_c) within a frame (T_f), and subsequently the maximum number of simultaneously transmitting users. Work done by Bellorado et al. [59] shows the gradient-descent based design of hopping codes, optimized for performance within a certain frequency band.

Although time hopping codes are primarily applied to suppress multi-access interference, they also contribute to shaping the power spectral density of the

transmitted signal. This allows better coexistence between UWB and other wireless technologies. Altering the pulse-to-pulse interval in order to remove the inherent periodicity of PPM-UWB signals, the modulated signal produces a lower peak magnitude spectrum [38]. This 'whitening' effect results from the spreading of the signal power over a large number of spectral lines, essentially decreasing the line spacing of the spectral density from $1/T_f$ to $1/(N_p T_f)$. The power spectral density (PSD) of a typical UWB signal with a constant pulse repetition interval is shown in Fig. 2.7(a). The evident periodicity in the spectrum may be offset by a time hopping sequence and PPM data encoding, resulting in the PSD illustrated in Fig. 2.7(b).

As previously stated, it is not possible to obtain a family of time hopping sequences which exhibit completely orthogonal properties. However, provided a quasi-synchronization state exists between users, 'zero-correlation zone' (ZCZ) sequences may be used. Here, an interference-free window exists for a certain level of asynchronicity between user hopping codes, although this is generally achieved through an increase in the cardinality of the sequences [61]. This concept was first introduced for direct sequence code division multiple access (DS-CDMA) as 'zero correlation duration direct sequences' [62]. They were later adopted by DS-UWB [63,64], also FH-UWB as 'no hit zone' sequences [65], and TH-UWB as ZCZ sequences [66]. Unfortunately, this technique is not efficient in terms of chip utilization, with many time slots left unoccupied in order to achieve this property.

An extension to time hopping exists in the form of pseudo chaotic time hopping (PCTH). Rather than only a static and periodic user code, PCTH exploits symbolic dynamics to generate aperiodic (chaotic) spreading sequences [67]. A pseudo-chaotic encoder operates on the input data, with the output used to generate a N-PPM (non-binary) signal which modulates a user-specific time hopping or pulse train 'signature' sequence. This random-like inter-pulse interval removes outstanding spectral features, resulting in a lower probability of intercept with other transmissions [68,69].

A pseudo-chaotic encoder achieves chaotic dynamics through a shift mapping.

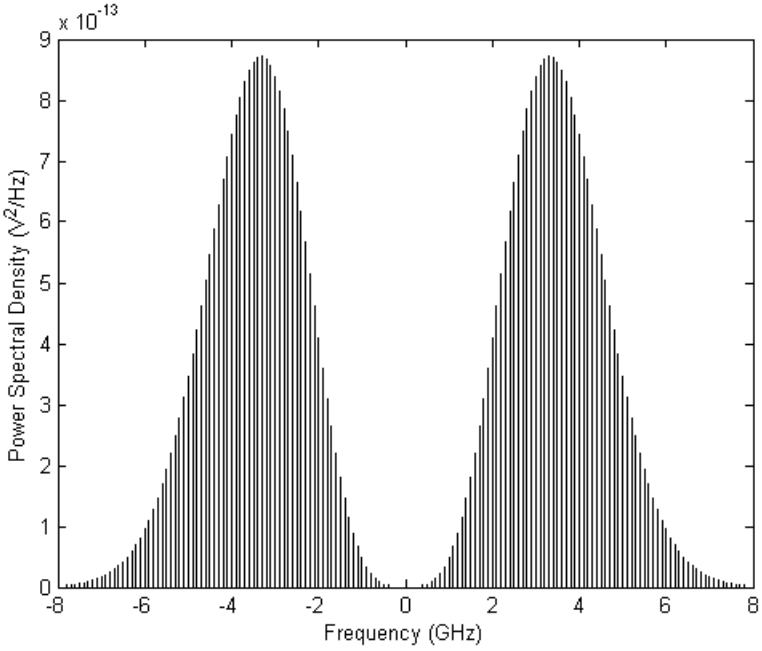

(a)

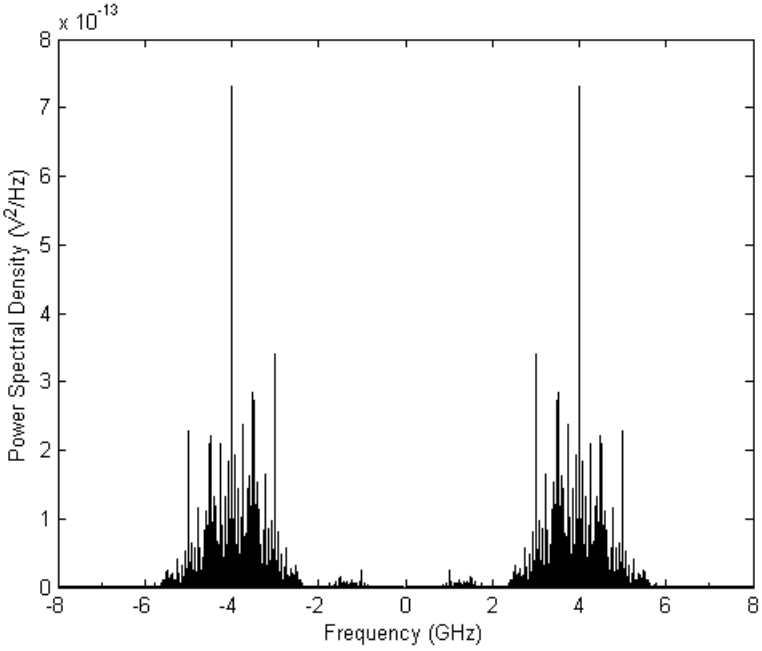

(b)

Figure 2.7 Power spectral characteristics for a UWB system with (a) regular pulse repetition interval and (b) time hopped multiplexing and data encoding through PPM

An example is the Bernoulli shift, which is approximated through the use of a finite-length shift register. This shift is expressed through the function $x_{k+1} = (2x_k)\%1$, where x_k represents the current encoder state. The next encoder state is determined by the current state multiplied by 2, then mapped through the modulo operation onto the states $\{0, 1\}$. This shifting may be followed by successive complex mappings, such as a 'tent map' by using a grey/binary converter (of the form $x_{k+1} = 1 - 2\,|x_k - 0.5|$) [68, 70].

The PCTH receiver applies a simple algorithm based on knowledge of the transmitter's chaotic circuit, hence alleviating the need for additional synchronization circuitry at any level [69, 71]. Unfortunately, the system requires multilevel PPM, and subsequently a convolutional decoder with a large number of states. It also requires higher data rates that conventional orthogonal N-ary PPM [70]. This is coupled with a sensitive dependence on initial conditions of the transmit encoder.

2.4 Channel Equalization

2.4.1 Receiver-side (RAKE)

Conventional UWB schemes have several commercially appealing aspects, including low implementation cost, and low power consumption. Another benefit is that multipath components are capable of being fully resolvable, provided that the duration of each pulse is shorter than the difference between propagation delays of different multipath components [45]. Unfortunately, typical UWB indoor channel responses may have a delay spread of up to 80 to 200 ns, with 60 to 200 paths [41, 72, 73]. It is a result of signal reflection, penetration through materials, and diffraction with interfering objects. Therefore, multipath presents a severe degradation to system performance.

Channel equalization is a common technique applied to circumvent the negative effects of channel multipath. However, while this concept does present benefits in terms of user error performance, it inevitably leads to an increase in the

level of complexity for the system. Increased memory, channel tracking, and additional processing are a few of the requirements. This complexity may be incorporated into either the transmitter or the receiver.

Receiver side equalization, which is more common in wireless communications, entails the collection of channel distorted energy. A common application of receiver equalization is in sensor networks [74, 75]. Here a collection of nodes, each with one or more environment sensors, communicate to higher level node receivers which perform channel equalization. This allows the sensor nodes to be simpler in design, also saving on energy. Existing sensor network methods include 'BTnodes' [76] and Intel's 'Imote' [77], both high bandwidth methods based upon Bluetooth technology.

A RAKE structure is common in UWB, offsetting channel effects through multipath energy collection. It operates by dedicating a 'branch' to each arriving path encompassed in the decision process [78]. The three main types of receiver structures are [79]:

- All-Rake (ARake), which collects all resolved multipath components, and has very high complexity;
- Selective-Rake (SRake), which collects the N_B multipath components which have the largest amplitudes, and has relatively reduced complexity;
- and Partial-Rake (PRake), which collects the first N_B multipath components received, and has the lowest relative complexity.

An example of the selection criteria in these RAKE schemes is shown in Fig. 2.8, with $N_B = 5$.

System complexity poses a significant disadvantage in the design of equalization schemes. RAKE complexity grows linearly in proportion to the number of branches utilized. It has been shown that in order to collect approximately half of the energy in a UWB transmission, RAKE receivers with more than 10 branches are required [80, 81, 82]. Insufficient capturing of multipath energy by

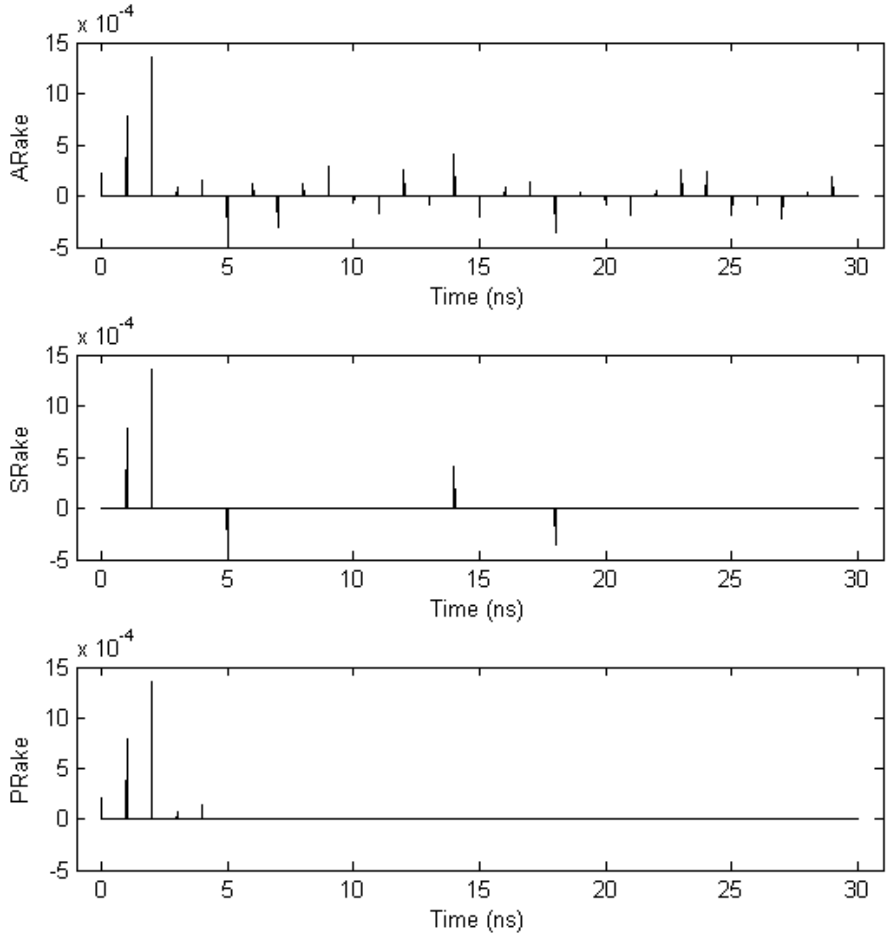

Figure 2.8 Selections for varied RAKE architectures for a LOS propagation channel

the receiver results in a degraded tolerance to intersymbol interference, and also decreases the range of the transmission in a highly dispersive channel. It should be noted that the maximum energy capture of the ARake does not necessarily deliver optimal performance in the presence of ISI. The SRake architecture has been shown to achieve better performance relative to an ARake receiver in certain fading channels [83]. While system improvements exist for increased energy collection, a threshold exists for the number of branches considered, and a deterioration in performance possible for branches past this threshold. However, the SRake receiver must still keep track of all multipath components available in order to perform the selection. Finally, SRake delivers a better

performance than PRake, although this difference is lowered when the highest magnitude paths are located at the beginning of the channel response, as in a LOS scenario.

Integrating the RAKE architecture into the signal defined by Eq. 2.15 over a total of M transmitted frames, the expression for the received UWB waveform for N_u simultaneous users is defined as:

$$r(t) = \sum_{u=1}^{N_u} \sqrt{E_{TX}(u)} \sum_{m=0}^{M-1} w\left(t - mT_f - c_m^{(u)} T_c - \varepsilon b_m^{(u)}\right) \otimes h(u; x_{pos}, t) + n(t) \quad (2.34)$$

$$= \sum_{u=1}^{N_u} \sqrt{E_{TX}(u)} \sum_{m=0}^{M-1} \sum_{k=0}^{L-1} \alpha_k(u; x_{pos}) w\left(t - mT_f - c_m^{(u)} T_c - \varepsilon b_m^{(u)} - \tau_k\right) + n(t). \quad (2.35)$$

Here, the channel is assumed static over the transmission of this M frame block. A RAKE receiver combines the dispersed energy among N_B of the L received paths, thus requiring N_B correlator branches, each aligned in time with their respective multipath component. An ARake receiver considers all replicas of the transmitted pulse ($N_B = L$); an SRake receiver accounts for $N_B < L$ paths, considering the N_B paths with the largest magnitude; and finally a PRake receiver combines energy from the first N_B paths only ($0 \leq l < N_B$). Techniques such as 'Maximal Ratio Combining' may be employed within RAKE systems, where a multiplication is done on each branch with a weighing factor proportional to the path magnitude.

Figures 2.9(a) and 2.9(b) depict the structures of a UWB transmitter and receiver applying a RAKE scheme, respectively. For brevity, frame and time hopping shifts have been omitted in the receiver structures.

2.4.2 Transmitter-side (Time Reversed)

Although not as common in UWB as a RAKE equalizer, transmitter side equalization is also a viable solution to combating multipath. This technique is commonly known as time reversed communications, although has also been referred to as 'pre-rake' [84]. While a conventional system would operate with the trans-

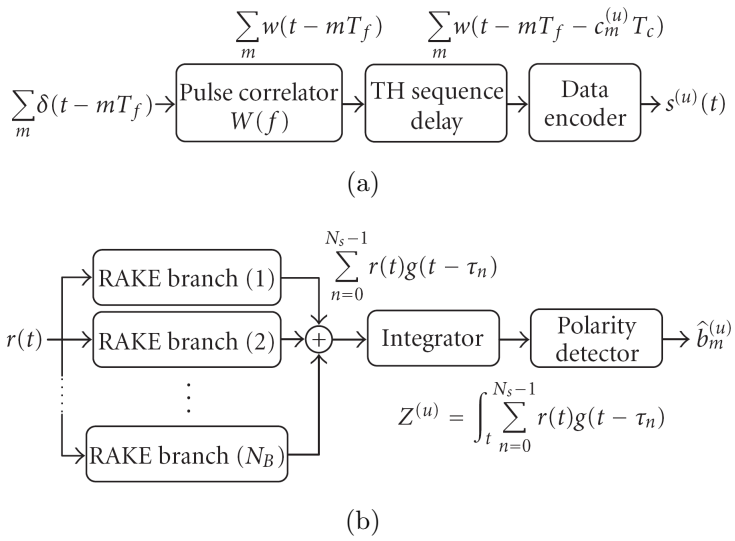

Figure 2.9 UWB structures applying a RAKE scheme (a) transmitter (b) receiver

mission of sub-nanosecond width Gaussian waveforms, a TR-UWB system uses the channel impulse response from the transmitter to the receiver as a transmit pre-filter. The transmitted time reversed signal retraces its path through the channel, resulting in an autocorrelation of the response being received [14, 85].

Time reversed communications was originally developed through underwater acoustics experimentation with sound waves [86], utilizing the ocean as a correlator to save in computation [87, 88]. Testing showed that when energy losses are small, wave equations guarantee that for each sound burst that diverges from a point, there exists a set of waves which would converge through the paths back to the point source.

Relative to a RAKE architecture, TR-UWB shifts the design complexity from the receiver to the transmitter. An ideal application would be in actuator networks, where remote nodes are desired to be simple, inexpensive, and consume minimal power [89]. The received signal is focused in both time (temporal focusing) and space (spatial focusing) at the intended receiver, concentrating the sent energy with a spatial resolution of the order of the wavelength [80, 85, 90]. Through temporal focusing, a TR-UWB system is capable of effectively mitigating intersymbol interference. This is achieved by the very short effec-

tive length of the received signal, a significant advantage over RAKE based UWB [86, 91, 92]. Focusing also allows time reversed communications to be more robust in the presence of narrowband interference relative to receiver-equalization based UWB [93].

Ultimately, there are fundamental drawbacks of a time reversed system. These include:

- determining the channel impulse response from the transmitter to the receiver for use in the former;
- the possibility of channel correlation between users;
- the large time interval required to obtain the response in heterogeneous systems;
- and the degradation in performance if the transmitter does not have perfect knowledge of the channel, or if nonlinearities exist in the transmitter circuitry.

Since the transmitter requires channel state information, TR-UWB is suitable for time-division duplexing schemes, where uplink and downlink radio paths are assumed similar despite the possibility of varied reflective surfacing [94]. Estimation of the channel response can be achieved through the use of the theory of reciprocity for antennas and electromagnetic propagation. It states that the outputs of non-linear antennas for identical excitation signals, as detected at the other antenna, will be identical provided the medium between the antennas is linear and isotropic [95].

In order to draw a correspondence with a RAKE receiver structure, the equivalent N_B multipath components must be incorporated into the transmit pre-filter. An alternate pre-filter design is presented by Guo et al. [91], based upon a digital FIR filter. The discrete representation of the time reversed channel,

considering $N_B = L$ for ARake comparison, is defined as:

$$h\left(u; x_{pos}, -t\right) = \sqrt{G_{H,u;x_{pos}}} \sum_{k=0}^{L-1} \beta_k \left(u; x_{pos}\right) \delta\left(t - \tau_k\right), \tag{2.36}$$

where:

$$\beta_k = \alpha_{(L-1)-k}. \tag{2.37}$$

However, causality requirements mean that $h\left(u; x_{pos}, -t\right)$ is not valid. The time reversed channel response is limited to $h\left(u; x_{pos}, L\tau - t\right)$, where $L\tau$ represents the channel duration. This duration is the effective length of the channel response, encompassing a majority of the channel's multipath components. For ease of notation, $L\tau$ is omitted. The term $G_{H,u;x_{pos}}$ represents the total multipath gain of the channel required for normalization, for user u, and the receiver located at position x_{pos}. This normalization factor is designed such that $G_{H,u;x_{pos}} = \sum_{k=0}^{L-1} \beta_k^2$.

The signal $s^{(u)}(t)$ transmitted for the uth user in a time-hopped time-reversed UWB system, with the time shift ε remaining equal to the pulse width, and equiprobable data $b_m^{(u)} \in \{-1, 1\}$ mapped through binary PPM, is given by:

$$s^{(u)}(t) = \sqrt{\frac{E_{TX}(u)}{G_{H,u;x_{pos}}}} \left(\sum_{m=-\infty}^{\infty} w\left(t - mT_f - c_m^{(u)} T_c - \varepsilon b_m^{(u)}\right) \right) \otimes h^*(u; x_{pos}, -t) \tag{2.38}$$

$$= \sqrt{\frac{E_{TX}(u)}{G_{H,u;x_{pos}}}} \sum_{m=-\infty}^{\infty} \sum_{k=0}^{L-1} \beta_k(u; x_{pos}) w\left(t - mT_f - c_m^{(u)} T_c - \varepsilon b_m^{(u)} - \tau_k\right). \tag{2.39}$$

It can be noted that this transmitted signal is pre-filtered using the time-reversed complex conjugate of the forward link channel response. Considering a single-input-single-output system, time reversal properties still apply provided that the bandwidth occupied by transmissions is significantly larger than the correlation frequency exhibited by the channel [96, 97].

Without loss of generality, user 1 is taken as the desired user, with the signal detected at its receiver in location x_1 given by:

$$r_{TR}^{(1)}(t) \;=\; \left(\sum_{u=1}^{N_u} s_{TR}^{(u)}(t) \otimes h(u; x_1, t) \right) + n(t) \tag{2.40}$$

$$= \left(\sum_{u=1}^{N_u} \sqrt{\frac{E_{TX}(u)}{G_{H,u;x_1}}} \sum_{m=-\infty}^{\infty} R_{h(1)h(u)} \left(t - mT_f - c_m^{(u)} T_c - \varepsilon b_m^{(u)} \right) \otimes w(t) \right) + n(t), \quad (2.41)$$

where:

$$R_{h(1)h(u)}(t) = h(1; x_1, t) \otimes h^*(u; x_1, -t) \quad (2.42)$$

is the correlation of the channel impulse responses from the first and the uth user to user 1's receiver at location x_1.

The decision variable Z within a time reversed scheme is constructed as an inner product of the received signal $r_{TR}^{(u)}(t)$ with the receiver template $v(t)$, giving the estimated received data of $\hat{b}_m^{(u)}$:

$$Z = \int_{(m-1)T_f + c_m^{(u)} T_c + \tau_{(L-1)}}^{(m-1)T_f + c_m^{(u)} T_c + \tau_{(L-1)} + 2T_w} r_{TR}^{(u)}(t) \cdot g \left(t - \left[(m-1) T_f + c_m^{(u)} T_c + \tau_{(L-1)} \right] \right) dt, \quad (2.43)$$

with:

$$\hat{b}_m^{(u)} = \begin{cases} 0, & Z > 0 \\ 1, & Z \leq 0 \end{cases},$$
$$v(t) = w(t) - w(t - \varepsilon).$$

It can be seen in Eq. 2.43 there is an additional shift of τ_{L-1} for the integration, which is required to align the template with the $(L-1)$th path in the received signal of the desired user. This is the largest correlation peak, representing the in-phase autocorrelation peak position for the channel response. This peak has a magnitude related to the number of paths present within the channel.

The template $v(t)$ for free-space propagation was applied within this dissertation in order to characterize a system which is performance-equivalent to a UWB system employing an ARake receiver [98]. When the guard time T_g is chosen such that ISI is avoided, an ARake and a TR-UWB system exhibit identical diversity orders and thus have the same error performance, even in the presence of multi-user interference (MUI). However, temporal focusing allows TR-UWB to be more resilient in the presence of ISI.

With the received signal taking the form of the autocorrelation of the channel impulse response, it can be inferred that inherent sidelobe energy will exist.

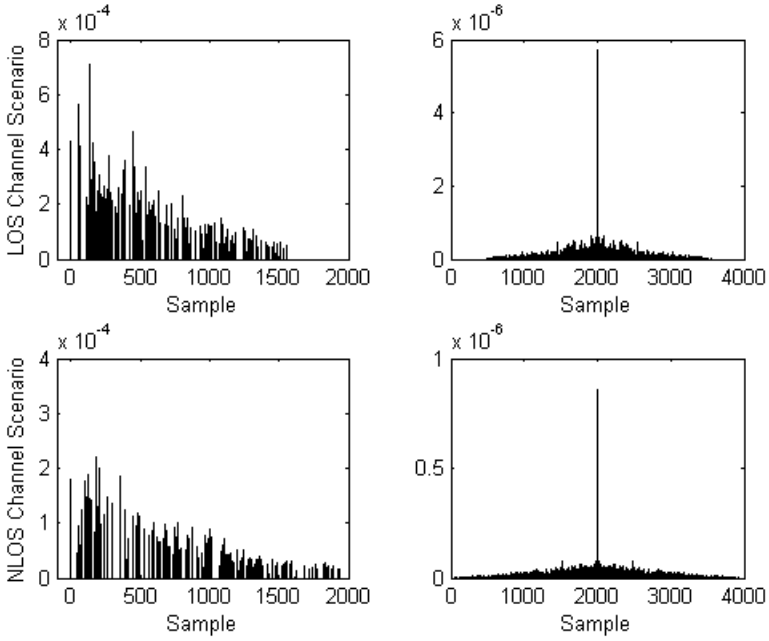

Figure 2.10 Time and autocorrelation profiles for LOS and NLOS scenarios of the IEEE 802.15.3a channel model

Following from this, it can be seen that increasing the randomness of a channel response results in lower sidelobe energy. Thus, a NLOS system which characteristically has lower tail energy is expected to out-perform a LOS system. However, larger lengths of the NLOS channels will ultimately lead to an increase in the duration of the sidelobe energy. This is due to longer channel responses increasing the autocorrelation peak to sidelobe energy ratio, but also increase the sidelobe temporal span. The characteristic differences between a LOS and NLOS are illustrated in Fig. 2.10, showing their time and autocorrelation profiles. For the NLOS scenario, a reference attenuation of $A_{dB} = 51$ dB with a path loss exponent of $\gamma = 3.5$ were applied.

Transmitter and receiver structures for a time reversed approach are shown in Fig. 2.11(a) and Fig. 2.11(b) respectively. It can be noted that the main variations relative to the receiver-side equalization structures are the added pre-filtering stage, and subsequently simplified receiver design.

Several additional techniques may be employed to increase system performance.

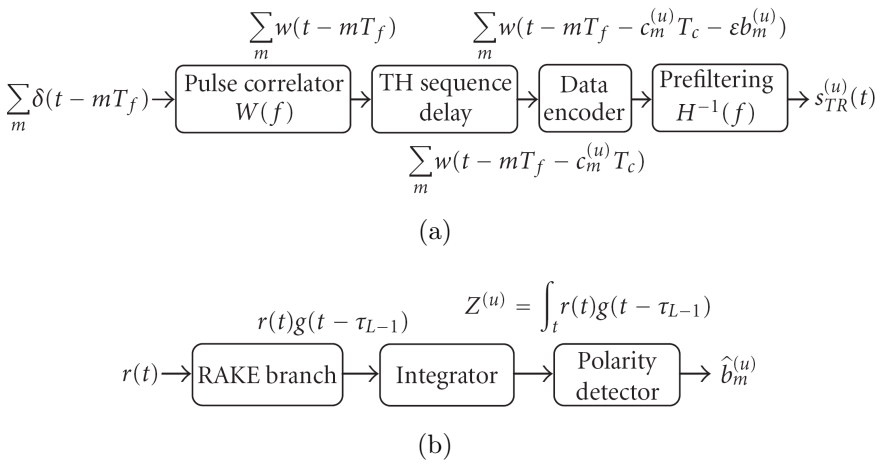

Figure 2.11 UWB structures applying a time reversed scheme (a) transmitter (b) receiver

A MMSE equalizer may be adapted into a time-reversed UWB receiver to increase energy collection [85], also MMSE decision feedback applying stochastic gradient descent algorithms may be used for receiver-side equalization [99]. While not studied in this dissertation, a TR-UWB system may adopt only a portion of the channel response as the signal prefilter. An analysis into time-reversed systems utilizing only selected paths of the channel, also referred to as 'dynamic TR' in given by Usuda et al. [84] and Derode et al. [100]. Applying a similar correlation comparison as TR-UWB, pilot assistance and transmitted reference are also methods for combating the effects of multipath interference utilizing decision feedback autocorrelation [101].

Another possible addition to time reversal is the use of iterative channel response reconstruction [102]. Time reversibility is not perfectly ensured in an absorbing medium, which combined with a limited antenna angular aperture means that channel inversion is not guaranteed. Channel reconstruction is based on successive time-reversal operations conducted to obtain an optimal inverse filter of the propagation channel. It is designed to eliminate sidelobes in the received autocorrelation structure by manipulating the signal spectrum. Keeping a static transmit energy, this iterative method harnesses unwanted sidelobe energy as a correction factor to obtain an optimal objective function.

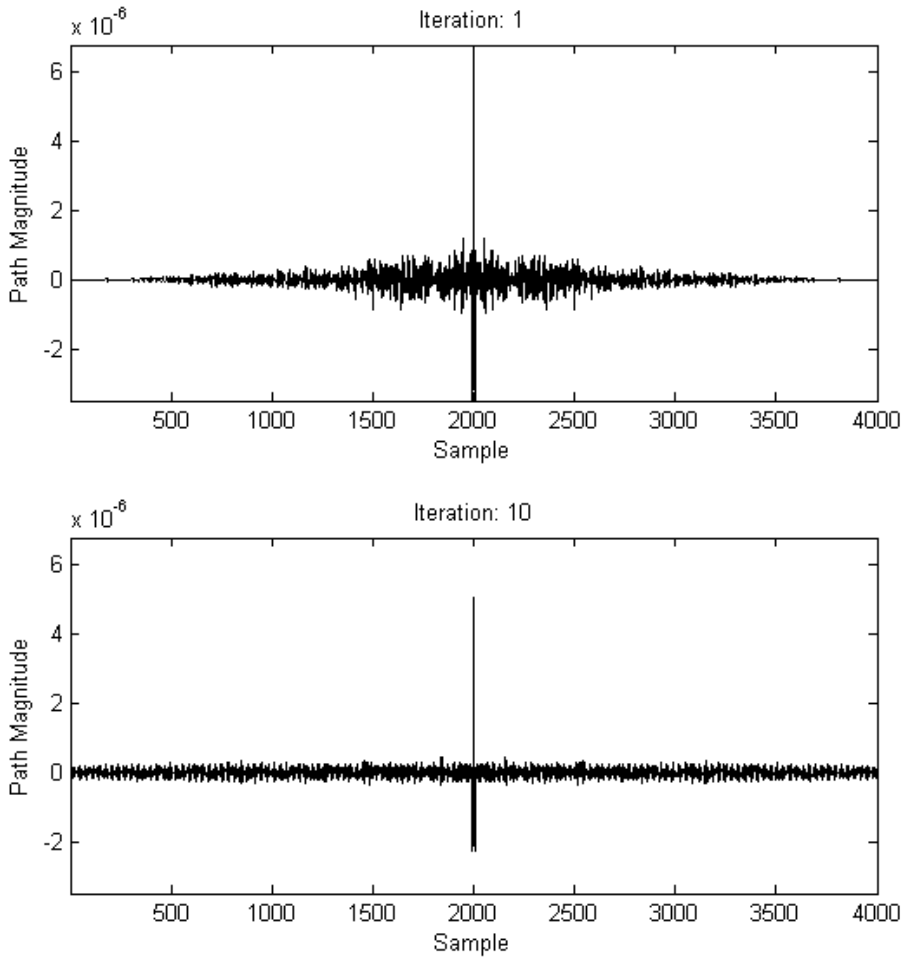

Figure 2.12 Iterative channel reconstruction for a LOS scenario

Unfortunately, the amplitude of the focused pulse is lower than in standard TR focusing. A decrease in SNR is evident in the presence of external noise, and a linear increase in the length of the transmitted signal results from each iteration. The effect of this technique is illustrated in Fig. 2.12 for the CM1 scenario of the 802.15.3a channel model (LOS), operating over 10 iterations.

Using ultrasonic wave transmission in low data rate multiple-input-multiple-output systems, this technique has been shown to produce lower ISI and better performance relative to classical TR communications [102]. However, in electromagnetic single-output-single-input UWB systems this method is not effective,

particularly considering the necessities for high data rate and low processing times.

2.5 Forward Error Correction with Turbo Coding

2.5.1 Binary FEC

Forward error correction (FEC) allows a communication system to add redundancy into a transmitted signal, such that the receiver is capable of correcting a limited number of errors. This is in contrast to backward error correction, which requires a signal re-transmission. A revolutionary method of FEC was developed by Berrou, Glavieux, and Thitimajshima in their 1993 paper: "Near Shannon Limit error-correcting coding and decoding: Turbo-codes". These turbo codes, also known as parallel concatenated convolutional codes, resulted from the strategic combination of three previously developed concepts [103]:

1. systematic convolutional codes;
2. use of reliabilities of the decoded bits (soft-inputs-soft-output or SISO);
3. and the use of two encoders operating on different orders of the data, separated by an interleaver, with two decoders applying iterative feedback.

While achieving near Shannon-limit error performances over limited-bandwidth communication links [104], turbo codes suffer from several drawbacks. These include a high processing latency due to the iterative nature and use of interleaving, and a high complexity due to the use of soft decoding.

The addition of binary turbo coding into a UWB system operates at the binary data level, altering $b_m^{(u)}$ in accordance with a preset convolutional code. This code is based on passing data through a set of linear shift registers, such that n encoder outputs depend on both k encoder inputs and γ previous inputs [103]. The structure of the convolutional encoder is defined by a generator matrix

in the form $G(x) = [g_1, g_2]$, with g_1 and g_2 representing the feedforward and feedback components of the recursive systematic convolutional (RSC) encoder respectively. RSC codes act as pseudo-random scramblers for the transmitted data. Feedforward and feedback components may be represented as octal or binary numbers. For instance, within the transfer function:

$$G(x) = \frac{1 + x^4}{1 + x + x^2 + x^3 + x^4}, \tag{2.44}$$

the numerator/feedforward would be represented as $(21)_8$ or $(10\ 001)_2$, and the denominator/feedback $(37)_8$ or $(11\ 111)_2$.

The turbo transmitter consists of two RSC encoders, generally with the same generator matrix, operating on the same binary input data. However, the second encoder block operates on the permuted data representation using an interleaver [105]. The combined result is a systematic output sequence, together with two parity outputs which have same length as the input. This gives an overall code rate $R_c = k/n = 1/3$. The combination of two RSC component encoders within a binary turbo encoder is illustrated in Fig. 2.13. The parameter $v_t^{(s)}$ represents the encoder's systematic output, with $v_t^{(p_1)}$ and $v_t^{(p_2)}$ representing the parity output of each RSC encoder.

Higher data rates may be achieved by puncturing the filter outputs before multiplexing, alternately selecting between the two possible parity values. This forms a $P = [1\ 0; 0\ 1]$ puncturing scenario, where the column indicates the RSC encoder activated at each time instant. The result is a code rate of $R_c = 1/2$.

Termination bits are appended to the transmitted data sequence in order to force the first RSC component encoder to end in a known state. This improves system performance by initializing the backward recursion applied in the receiver decoding algorithm. The addition of these γ tail bits does not control the final state of the second component encoder however, as it operates on the permuted data sequence. Although not studied within this thesis, methods such as circular termination of the component codes or 'tailbiting' exist such that additional termination bits are not required [104].

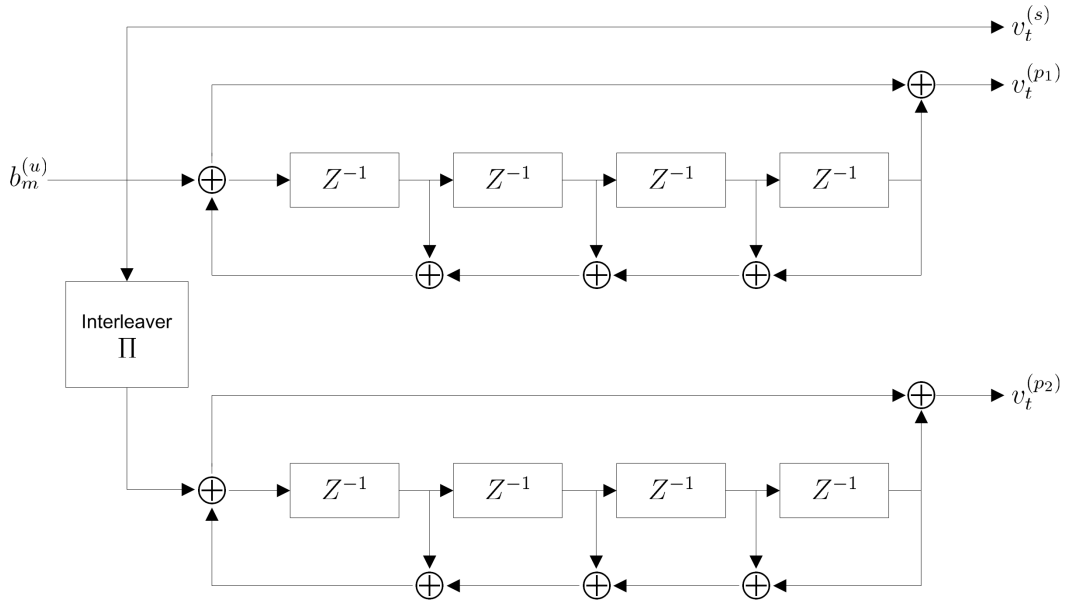

Figure 2.13 Conventional turbo encoder

The size of the interleaver is determined by the parameter n, with larger interleaver sizes generally associated with lower error rates. The interleaver spreads adjacent symbols in the transmission, making them independent of adjacent symbols in reception [103]. This has the effects of reducing degradations due to impulsive noise and burst errors. Unfortunately, an error floor exists in turbo coding caused by the presence of low-weight codewords in the interleaver. The characteristic performance of a turbo system is depicted in Fig. 2.14. Shown is the transition from noise dominated errors, next to the 'waterfall' region of increased user performance, and finally to the error floor arising from inefficiencies in the interleaver's design.

Two types of interleavers are an element-wise interleaver, and a block interleaver. The mapping function of an element-wise interleaver is given by:

$$\Pi(Z \rightarrow Z) \ : \ j = \Pi(i), \ i, j \in \{0, 1\}, \tag{2.45}$$

where i and j represent the indices of elements within the original and interleaved sequences respectively. Conversely, a block interleaver has elements

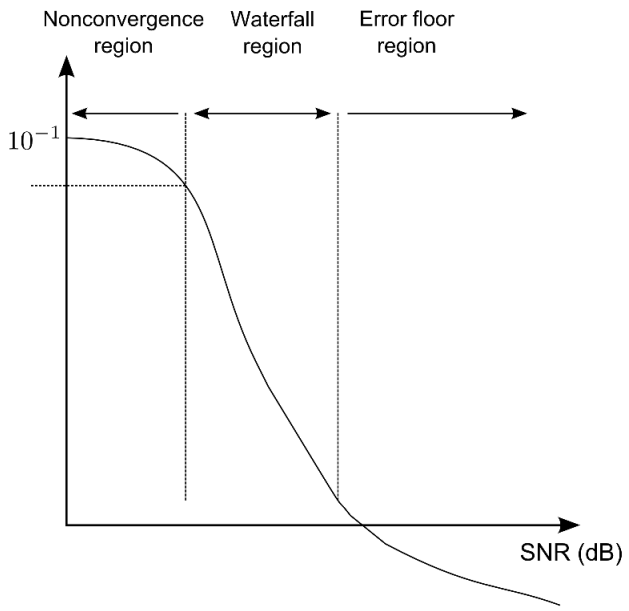

Figure 2.14 Characteristic turbo coding performance

written row by row, and read column by column, having a mapping function of:

$$\Pi(i) = \left\lfloor \frac{i}{I} \right\rfloor + I \bmod \left(\frac{i}{J} \right), \tag{2.46}$$

where I is the number of rows and J the number of columns within the interleaver. However, a block interleaver exhibits a worse coding performance compared to a random element-wise interleaver due to its regularity.

Through correlation of the PPM signal with a static template, the receiver front-end produces a soft magnitude representation for each bit in the encoded data stream. These are used by two component SISO decoders, and indicate the likelihood that the bit is a '0' or a '1'. A negative value indicates a bit '0', a positive value indicates a bit '1', and a value near zero shows equal possibility of either data bit. The output values from each decoder are known as 'extrinsic' probabilities, and are passed to the alternate decoder where they are interleaved and applied as 'prior' probabilities. This iteration is repeated to converge to an estimate of the transmitted codeword.

Two well-known SISO decoding methods are the maximum a posteriori (MAP) algorithm, and the soft-output Viterbi algorithm (SOVA). The latter is generally

selected for practical decoder implementations. It is a maximum likelihood sequence estimator, minimizing the negative log of the likelihood function [105].

A trellis diagram may be applied to illustrate the state transitions in the convolutional encoders. With m shift registers per component encoder, 2^m states are possible in the trellis. Transitions that are not possible through the trellis cannot be transmitted codewords, and thus represent errors. The decoder establishes a path through the trellis which is closest to the actual received sequence when applying the likelihood function. This is referred to as the 'survivor path' through the trellis. Trellis transitions are discussed further in Chapter 6.

2.5.2 Non-Binary FEC (TTCM)

The combination of data modulation with an expanded modulation set is evident in schemes such as interleaved convolutional time hopping (ICTH) [106]. ICTH is based upon a low-rate convolutional code combined with multilevel PPM. It is an alternative to PCTH, replacing the shift registers with a distance optimized convolutional code exhibiting the same rate and number of states.

This dissertation proposes the combination of data encoding with time hopping through the use of non-binary turbo codes. It is proposed to encode information symbols onto an expanded modulation set, rather than binary pulse encoding combined with a preset time hopping code. Turbo trellis coded modulation (TTCM) is utilized, which was first presented by Robertson and Worz [107]. Similarly to binary turbo codes, TTCM uses a parallel concatenation of two binary trellis coded modulation (TCM) encoders. TCM combines rate $R_c = m/(m+1)$ binary convolutional codes with an M-ary signal constellation ($M = 2^{k+1} > 2$), optimizing the Euclidean distance between codewords [108]. A TCM encoder is illustrated in Fig. 2.15, with v_k representing the encoded output stream. By replacing the component codes in a binary encoder with trellis codes, coding gains are achievable without a subsequent bandwidth expansion [109, 110]. However, an expanded signal constellation set is required, restricted to having the same average energy as an uncoded constellation.

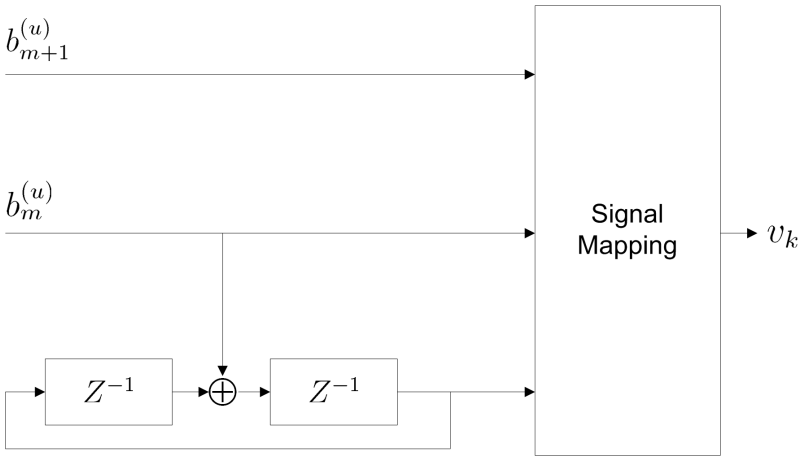

Figure 2.15 Trellis coded modulation encoder

TCM introduces dependency between all successive symbols, with its performance proportional to the square of the free distance of the convolutional code applied. The coding gain of TCM compared to uncoded schemes asymptotically achieved at high SNR may be expressed as [110]:

$$G_{TCM} = 10\log_{10}\left[\left(\frac{\delta_{free}^2}{\delta_{free,u}^2}\right) \times \left(\frac{E_{s,u}}{E_s}\right)\right], \tag{2.47}$$

where δ_{free}^2 and $\delta_{free,u}^2$ represent the squared free distances of the TCM and uncoded schemes respectively, with E_s and $E_{s,u}$ being the average signal energies of the encoding methods.

TTCM offers increased performance relative to classical binary coding. It benefits from a better convergence of the iterative decoding due to reduced correlation effects between the decoder, less sensitivity to puncturing patterns, an additional degree of freedom in the permutation design due to the non-binary symbols, and greater robustness toward the flaws of the decoding algorithm [111]. Non-binary convolutional turbo codes have been adopted in several standards, including DVB-RCS, DVB-RCT and the IEEE 802.16a standard (WiMAX) [104]. Unfortunately, TTCM requires more edges to be introduced in the receiver trellis structure, inevitably increasing the complexity of the decoder.

A memoryless mapper $\bar{\Pi}(j)$ generates a one-to-one relationship between the coded bits and the time hopping chip positions. This is required when the output constellation size of the TTCM encoder is not equivalent to the number of chips within a single time frame (N_h). Also, an additional degree of user differentiation is achieved through a random PPM shifting in the TTCM system. This is necessary considering the chip synchronous architecture studied.

Decoding is conducted symbol-by-symbol, rather than bit by bit as in conventional turbo coding. A modified symbol based SOVA decoding algorithm is applied, based upon maximum likelihood accumulated metrics through the trellis. While it is well known that the MAP decoding algorithm achieves a better performance than SOVA, this gap is decreased when using non-binary turbo coding [104,111,112]. With a large interleaver size, non-binary SOVA has a performance loss of approximately 0.3 dB at a bit error rate of 10^{-4} relative to the MAP algorithm [113].

2.6 Chapter Summary and Conclusions

Ultra wideband is an emerging wireless communication method, which has seen considerable attention by both industry and academia. Operating below the noise floor, it enables unlicensed short range communications at very high data rates. Time hopping codes allow user multiplexing to be achieved simply by additional time shifting, with codes designed to obtain orthogonality between all users.

With an IEEE standardized channel model, time hopped UWB generally requires equalization measures in order to collect a significant portion of the transmit signal energy. Although receiver side equalization is more common, transmitter side pre-filtering is also a viable method of accommodating for channel distortion.

Forward error correction allows receiver-side rectification of transmission errors, and may be applied in both binary or non-binary methods. Binary convolutional

techniques such as turbo coding are increasingly popular, while non-binary methods such as TTCM also have promising applications. TTCM may be applied to combine data modulation with time hopping coding, re-constructing the transmitter and receiver models.

Therefore, several wireless communication methods may be applied to UWB in order to increase user performance. From channel equalization to error correction, every addition is designed to combat degradations inevitably prevalent in telecommunications.

Chapter 3

Multi-user Hopping Codes

3.1 Introduction

Wireless communications are inherently exposed to various signal degradations, including channel noise, multipathing reflections, and refraction of energy by interfering objects. However, in multi-access systems, the most substantial errors occur primarily due to multi-user interference [114]. Multi-user codes are applied to achieve an orthogonality between user transmissions, although interference is inevitable in asynchronous systems. These codes consist of a set of codewords, also referred to as a set of sequences. Commonly known as 'hopping codes', they are strategically designed to obtain specific performance limits. They are dependent upon many factors, including the range of values permitted by the system, the periodicity of each sequence, and target correlation values between sequences.

This chapter overviews several correlation measures which exist for multi-user sequence analysis. Varied approaches may be applied for time, frequency, and direct sequence domains. An alternate method introduced within this thesis is based upon separation probability analysis. It is derived through the averaging of differences between consecutive and non-consecutive values within the hopping codewords. This chapter also covers multi-user sequence design methods for time, frequency, and direct sequence domains. All codes were converted

to the time domain for comparative analysis. Finally, the application of time hopping codes for the design of a UWB chip interleaver is discussed.

3.2 Conventional Performance Measures

Multi-user interference poses a severe degradation risk to any wireless communication link. In terms of time hopping, a user code consists of a series of numbers signifying which chip each pulse will occur in for a certain time frame (see Sec. 2.2.1). Hopping codes are designed to minimize mutual interference between users. A collision of user transmissions, also referred to as a 'hit', occurs when two or more users attempt to occupy the same time slot. Of significant concern are identical subsequences between patterns, which may cause bursts of collisions. The use of the same slot for prolonged periods may also have adverse effects. Inefficient code design increases vulnerability to jamming, susceptibility to intrusion, and the possibility of continuous collisions between user sequences.

Codes are characterized by their self-correlation (autocorrelation) and their correlation with other codes (cross-correlation). An impulsive autocorrelation profile (with near zero out-of-phase correlation results) guarantees robust synchronization (avoiding false locks), optimal channel estimation, and ISI mitigation abilities. Favorable cross-correlation profiles (near zero for all code asynchronization) ensure a minimization of multi-access interference, with orthogonal codes providing a better bit error rate performance [30, 70]. Unfortunately, an inverse optimization relationship exists between the two correlation properties, with an improvement in one method generally resulting in a degradation of the other.

Three conventional performance measures commonly adopted for the calculation of autocorrelation and cross-correlation results are:

- Hamming correlation, for time and frequency hopping codes;
- frequency difference function, for frequency hopping codes;

- and direct sequence correlation, for direct sequence codes.

The Hamming correlation is a periodic measure of the number of collisions between sequences for a certain relative time delay. Since patterns within different families may be of different length, division by the sequence periodicity is used to normalize the correlation results. Taking N_p as the period of the sequences, it is defined as [33]:

$$H_{XY}(\tau) = \frac{1}{N_p} \sum_{i=0}^{N_p-1} h_{xy}\left(x_i, y_{i+\tau}\right), \quad 0 \leq \tau \leq N_p - 1, \tag{3.1}$$

$$h_{xy}(a,b) = \begin{cases} 0, & \text{a} \neq \text{b} \\ 1, & \text{a} = \text{b} \end{cases}. \tag{3.2}$$

Here, τ represents the time asynchronicity between the codes. Values are obtained using cyclically shifted sequences (represented as x_i and $y_{i+\tau}$, with $(i+\tau)$ taken modulo N_p), averaged over all possible sequence pairs within a family of codes.

The frequency difference function is applied to find the number of collisions between frequency multiplexing codes. Similarly to time hopping, N_h frequency carriers are defined, with a hopping sequence designating slot allocation for each user. The system bandwidth (W) is divided into N_h equal channels of width W/N_h. The difference equation takes into account both a time lag and a Doppler/frequency shift between user codes. This is the intentional Doppler shift implementing spreading sequences, not the frequency shift degradation caused by device mobility. Utilizing notation commonly found in literature, the difference function is defined as [115, 116]:

$$\begin{aligned} \left(y_2 \Delta y_1\right)(k;t,\omega) &= y_2\left(k+t\right) + \omega - y_1\left(k\right) \pmod{N_h}, \\ &\text{for} \quad 0 \leq k, t, \omega \leq N_h - 1. \end{aligned} \tag{3.3}$$

Here, $y_1(k)$ and $y_2(k)$ are placement operators, referring to user spreading sequences. They represent two frequency hopping code functions. The parameter k indicates each sequence element, and t and ω represent time and frequency shifts respectively. The difference function operates by shifting the placement

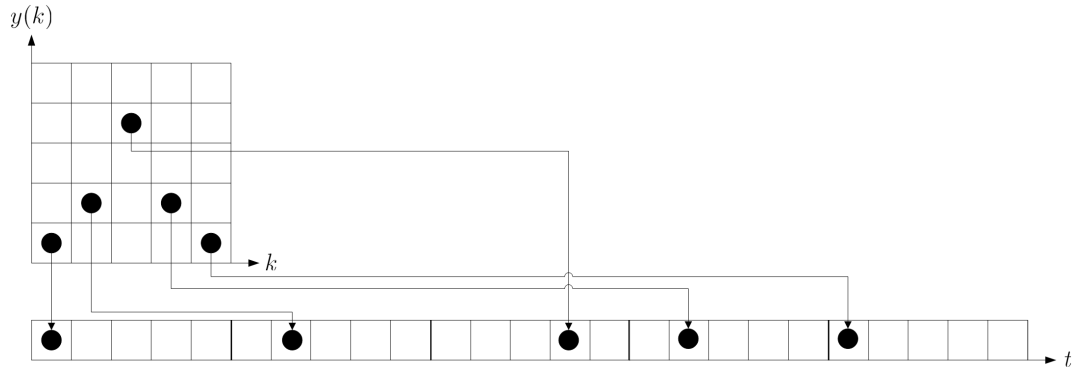

Figure 3.1 2-D and 1-D representations of a frequency hopping code

operators over time and frequency dimensions. When the function is equal to zero for a certain time and frequency shift, a collision is deemed to have occurred. The two dimensional representation of a frequency hopping code is given in Fig. 3.1, together with its mapping to the time domain. Each element in the hopping matrix is given a value of 1 if the frequency is utilized within that time interval, and zero otherwise. A frequency hopping code which uses all available channels once and only once achieves maximum bandwidth usage, and is referred to as a 'full frequency hop code'.

Applying Lagrange's theorem, that the power of a polynomial indicates its maximum number of solutions in the finite field, the maximum number of hits in the two dimensional autocorrelation (AC) and cross-correlation (CC) functions can be established [117]. This is achieved by expanding the frequency difference function for a family of sequences, and determining the highest order of the argument k.

Through simplification, it can be proven that the difference equation reduces to the Hamming cross-correlation for a constant Doppler shift. Frequency hopping codes may be used directly in a time hopped system, although their autocorrelation and cross-correlation characteristics will be altered. In the general case, the use of FH patterns for TH applications gives a slightly degraded performance, with the maximum number of code collisions in the correlation functions for TH sequences being twice that for FH sequences [30].

The final correlation statistic, direct sequence correlation, is utilized as a similarity measure for direct sequence codes. These noise-like spreading codes consist of complex valued elements, which for the purpose of this chapter were mapped into decimal values for application in a TH-UWB architecture. With x_i and $y_{i+\tau}$ representing two spreading codes, N_p the length of the codes, and τ their asynchronicity, the direct sequence orthogonality measure is given as [118]:

$$R_{x,y}(\tau) = \sum_{i=0}^{N_p-1} x_i y_{i+\tau}^*. \tag{3.4}$$

In order to exemplify the trade-off between autocorrelation and cross-correlation functions, consider the correlation properties of 'perfect sequences' [118]:

$$\begin{aligned} R_x(\tau) &= \begin{cases} N_p, & \tau = 0 \\ 0, & \tau \neq 0 \end{cases}, \\ R_{x,y}(\tau) &= \sqrt{N_p}, \text{ for all } \tau. \end{aligned} \tag{3.5}$$

The optimal correlation performance achieved by these nonbinary complex codes are dependent entirely upon the sequence periodicity. Where a more impulsive autocorrelation could be obtained through a increase in the sequence length, this would also increase the cross-correlation statistic and subsequently deteriorate the code's performance.

3.3 Separation Probability Analysis

Assuming a perfectly power controlled TH-UWB system, where users are transmitting at identical data rates, the distinguishing factor for user performance is the time hopping code that is used. A unique method for characterizing hopping codes is introduced herein as the chip separation probability profile S_e. It defines a set of state probabilities which indicate the probability of two transmissions having a certain separation, based upon a family of time hopping sequences. Expanded to $S_e(A, B)$, this measure is determined for a separation of B chip intervals between elements of a hopping sequence, and A intermediate pulses transmitted by the user between those B chips. These parameters are

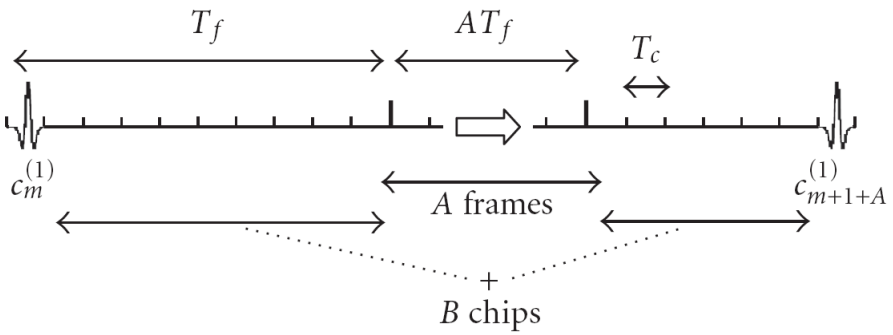

Figure 3.2 Chip separations for pulsed transmissions

illustrated within Fig. 3.2. ISI is controlled by the separation between consecutive elements within a time hopping sequence, while MUI is affected by the relative separation between symbols sent from the interfering users and those from the desired user.

The issue of intermediate pulses over the separation distance is required considering the RMS delay spread of a UWB signal. With the ability to span several time frames, interference from a single transmission may last well over an adjacent frame. However, similarity between the separation probabilities for varying A allows $S_e(A, B)$ to be approximated by $S_e(0, B)$ for all A.

For ISI, S_e must be determined for each individual hopping code within a family of sequences, then averaged over the set. The separations between all sequence elements c_j^i for a family of N_c sequences of length N_p may be expressed as:

$$S_e \in \begin{bmatrix} \Xi_{1,1} & \Xi_{1,2} & \cdots & \Xi_{1,N_p} \\ \Xi_{2,1} & \Xi_{2,2} & \cdots & \Xi_{2,N_p} \\ \vdots & \vdots & \ddots & \vdots \\ \Xi_{N_c,1} & \Xi_{N_c,2} & \cdots & \Xi_{N_c,N_p} \end{bmatrix}, \tag{3.6}$$

where:

$$\Xi_{i,j} = N_h - \left(c_j^i + 1\right) + c_{(j+1+A)\%N_p}^i + AN_h. \tag{3.7}$$

Separations are averaged over the set of N_c sequences. For MUI, the analysis is conducted over all possible sequence pairs within the family. The separation

between two sequence elements within the same time frame is expressed as:

$$\Xi_{u_i,u_j,m_i,m_j} = c^{u_i}_{m_j} - c^{u_j}_{(m_j+m_i)\%N_h+1}, \tag{3.8}$$

where u_i and u_j represent the sequence number, with m_i and m_j the sequence element indexes. Considering sequence elements within different time frames, and assuming the number of intermediate pulses A is negligible, the separations between sequence elements may be calculated as:

$$\Xi_{u_i,u_j,m_i,m_j} = \left(N_h - \left(c^{u_i}_{m_j} + 1\right)\right) + c^{u_j}_{(m_j+m_i)\%N_h+1}. \tag{3.9}$$

The separation probability depends significantly on the range of the hopping code (N_h). A larger value will result in more chips to select from, leading to a more sparse profile. The separation B ranges from AN_h to $(A+2)N_h-2$, where A is zero for adjoining frames. These probabilities were determined through a brute force analysis of all codes within a given family of sequences, and then averaged for each B.

An optimal code design based upon separation probabilities would seek to distance user transmissions as much as possible. Since S_e gives a symmetrical profile, an initial proposal for optimal code design would be a unit probability peak for median separation, and zero elsewhere. However, as discussed in Sec. 2.3, a regular pulse repetition interval results in concentrated spectral lines in the PSD. Hence, an optimal code would have the highest probability for median separation, and linearly decreasing sidelobe probabilities reaching a zero probability for no separation. This triangular profile type is achieved by random sequences with a uniform probability distribution, and a large family of code sequences. This uniform distribution exhibits equi-probable use of all hopping positions, which is a favorable multiplexing property. The separation profile for random codes created using a linear congruential number generator is shown in Fig. 3.3.

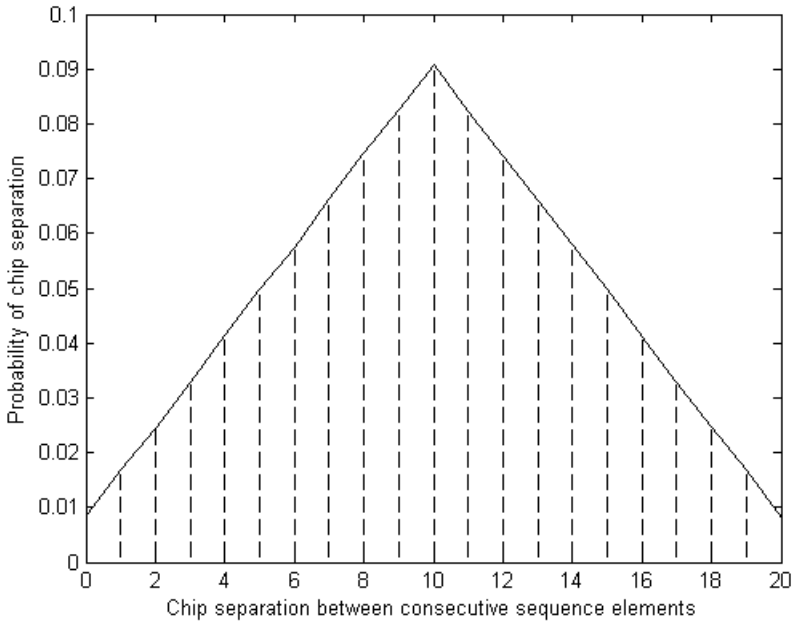

Figure 3.3 Optimal chip separation generated by random codes with uniform distribution

3.4 Sequence Design

3.4.1 Time/Frequency Hopping Approach

Time and frequency hopping sequences may be designed through varied procedures. These include dependence on a predefined distribution, or an equation $y(k)$ relating various parameters of the sequences (the placement operator). The 'user number' is a crucial part of the design procedure, assumed unique over all simultaneously transmitting users. It is required to obtain a sequence from a family of patterns generated from each design. Common parameters in sequence design are: u the user number, k the iteration number for a code ($0 \leq k < N_p$), and variable p selected as a prime value. Most sequences are constructed over a Galois field with p^m elements (m an integer).

3.4.1.1 Random Sequences

A common method for hopping code generation is the use of independent, identically distributed pseudo-random sequences. Considering the number of chip within a UWB frame N_h, the randomly generated integer hopping sequences must be contained within the range of 0 to $N_h - 1$. These may be used as a control set for comparative analysis with sequences which are designed with an underlying structure to achieve orthogonality. However, 'short' hopping sequences are considered within this chapter. While uniformly distributed random codes approach the optimal triangular separation profile discussed in Sec. 3.3 as the code family size increases to infinity, short random codes do not achieve this property.

The probability of at least one user in a K user system hopping either entirely or partially to the same slot as a given user when applying random hopping codes is expressed as [114]:

$$P_{h,K} = 1 - (1 - p_h)^{K-1}, \tag{3.10}$$

where,

$$p_h = \begin{cases} \frac{2}{N_h} - \frac{1}{N_h^2}, \; asynchronous \\ \frac{1}{N_h}, \; synchronous \end{cases}. \tag{3.11}$$

The parameter p_h represents the probability of another user hopping to the same time slot.

3.4.1.2 Linear Congruence Codes

Linear sequences are designed based entirely on two parameters: user number and iteration number. They are defined through the placement operator [115]:

$$y(k) = uk \pmod{p}. \tag{3.12}$$

The parameters $k \in \{0, ..., p-1\}$ and $u \in \{1, ..., p-1\}$, giving a maximum of $p - 1$ users. Also, the cardinality and the periodicity of the codes must be equivalent, equal to the value of p. This method produces a family of p

different sequences. These codes possess ideal cross-correlation properties (at most 1 collision) although poor autocorrelation properties (as many as $p-2$ collisions).

3.4.1.3 Cubic Congruence Codes

Cubic congruence codes are based upon a relationship between the user number and the cubic of the iteration number. This is realized through the placement operator [116]:

$$y(k) = uk^3 \pmod{p}. \tag{3.13}$$

This family of hopping codes provides a set of $p-1$ sequences, with a periodicity of p and a cardinality of $p-1$. However, a restriction that exists on these cubic codes is that the value of p, which is restricted to being a prime value, must also satisfy:

$$p = 3m_c + 2, \tag{3.14}$$

with m_c being a positive integer. This property is required in order to generate a full set of codes, where all of the available time slots are used equally. Cubic codes within this thesis are designed with $m_c = 3$, resulting in $p = 11$.

3.4.1.4 Quadratic Congruence Codes - Construction 1

Quadratic congruence codes are based upon a quadratic polynomial of the iteration parameter k. This construction method deviates from the simplistic approach of a two parameter placement operator, rather including two additional variables α and β. These may be varied in order to obtain a larger set of sequences. The placement operator for these codes is constructed as [119]:

$$y(k) = [u(k+\alpha)^2 + \beta] \pmod{p}. \tag{3.15}$$

The parameters $k \in \{0, ..., p-1\}$, $u \in \{1, ..., p-1\}$ and $\alpha, \beta \in \{0, ..., p-1\}$. This results in a code periodicity equal to p, and a cardinality of $p-1$. The placement operator may be used to obtain a set of $(p-1)p$ sequences through the varying of the available parameters. This family of hopping codes has no

more than two collisions between codes for all sequence asynchronicity. For this dissertation, the value of β was set to equal the iteration number k. Also, the value of α was initially set to 1, and incremented when the user number exceeded $p-1$.

3.4.1.5 Quadratic Congruence Codes - Construction 2

This construction of quadratic codes follows the conventional two parameter approach. Where p is chosen as an odd prime value restricted to being greater than or equal to three [120], this alternate quadratic construction is expressed as:

$$y(k) = uk(k+1)/2 \pmod{p}. \tag{3.16}$$

Sequences based upon quadratic congruences achieve near ideal AC results with a maximum of 1 hit with the shifted replica of itself, and at most 2 collisions in their set of mutual CC functions. Unfortunately, symmetry exists in the 2D frequency hopping matrix representation for quadratic codes [120], forming palindromic codes. This signifies that the placement operator induces a many-to-one correspondence over a Galois field, and a certain time slot/channel may be utilized twice while another is unoccupied. Consequently, the system's performance degrades as some chips are under-utilized.

3.4.1.6 Hyperbolic Congruence Codes

These sequences are based upon a hyperbolic congruence between the user number and the iteration number through the placement operator [117]:

$$y(k) = u/k \pmod{p}. \tag{3.17}$$

This family of codes allows a maximum of $p-1$ users, with a cardinality of $p-1$ and a periodicity of p. The parameter $u \in \{1, ..., p-1\}$ and $k \in \{1, ..., p-1\}$, starting at 1 due to no inverse existing for $k = 0$. Unfortunately, the computation to determine the value of each member of a sequence may not be conducted by direct division by k. Rather, the inverse of k must first be determined, found by considering the Galois field that k belongs to. Here, any

inverse operation that is conducted on a member of the field results in a unique value within the field itself. A simple operation to obtain the inverse of k is: $1/k = k^{p-2} \pmod{p}$.

These codes achieve ideal AC characteristics, with no out-of-phase AC collisions, and also a single CC collision for any code asynchronicity.

3.4.1.7 Additional Sequences

Additional codes are constructed through a simple additional relationship between the user number and the iteration number, contained by the prime p [57]. They are defined as:

$$y(k) = [k + u - 1] \pmod{p}. \tag{3.18}$$

The cardinality of the codes is $p - 1$, with the periodicity and the family size both equal to p. It should be noted that all sequences produced are cyclically shifted versions of a consecutive integer sequence, meaning that although these codes may achieve perfect orthogonality, they have a $1/p$ possibility of complete sequence overlap (p collisions).

3.4.1.8 One-Coincidence Sequences

These sequences are designed through a simple relationship between the user number, the iteration number, and a primitive element r, given by the equation [118]:

$$y(k) = r^k + u \pmod{p}. \tag{3.19}$$

This method requires a Galois field of size p, and the calculation of a primitive element r of the field (which when raised to the powers from 0 to $p-2$ generates all non-zero elements within the field). For testing within this thesis, r was set as 2, this being a primitive element of a Galois field of size 11. The parameter $k \in \{0, ..., p-2\}$ and $u \in \{0, ..., p-1\}$. Hence the maximum number of users is p, and the periodicity of the codes is $p - 1$.

This family of sequences achieves zero out-of-phase AC collisions. It is also char-

acterized by having zero CC collisions for synchronous codes, and 1 collision for all asynchronicity between sequences. The average Hamming cross-correlation function for these codes is defined as $(N_p - 1)/N_p$, with N_p the periodicity of the codes.

3.4.1.9 Reed-Solomon Sequences

These sequences are designed through a subset of Reed-Solomon codewords, which are commonly applied in error correction coding [121, 122]. They are developed by allowing a controlled amount of correlation between sequences [123]. The design of these codes requires the determination of two parameters: N_h the number of time slots available; and s the maximum number of permitted in-phase hits between sequences. However, the out-of-phase correlation between sequences may result in as many as $N_h - 1$ hits. There are $(N_h)^{s-1}$ codewords possible, each of length $N_h - 1$.

The codewords represented by the vector f_x are obtained through the multiplication of the $(s + 1) \times 1$ element matrix $\mathbf{n}$ with the code generator matrix G, as:

$$f_x = [n_0, n_1, ..., n_s]\, G. \tag{3.20}$$

The code generator matrix G is constructed using the primitive element α of N_h. This parameter is raised to the power of $(i-1)j$, with i and j representing the row and column of G respectively. The generator matrix has $s+1$ rows and $N_h - 1$ columns, and is defined as:

$$G = \begin{bmatrix} 1 & 1 & 1 & \cdots & 1 \\ \alpha & \alpha^2 & \alpha^3 & \cdots & \alpha^{N_h-1} = 1 \\ \vdots & \vdots & \vdots & \ddots & \vdots \\ \alpha^s & \alpha^{2s} & \alpha^{3s} & \cdots & 1 \end{bmatrix}. \tag{3.21}$$

Elements of $\mathbf{n}$ may range from 0 to $N_h - 1$. Due to numerous cyclically time shifted versions of a codeword being generated, the complete set of Reed-Solomon codewords is a poor choice of hopping patterns. Thus a subset with better properties is found by limiting the values n_0 and n_1 [123]. Firstly, n_0

is chosen constant for all sequences within a set, as it uniformly increases all element values in accordance with the constant top row of G; and secondly a nonzero value is chosen for n_1, since the second row of G consists of consecutive numbers from 1 to N_h, and will attain a certain level of uniqueness between sequences. All other possible combinations are assigned to the remaining elements of $\mathbf{n}$, forming the sequences within the set. A total $N_h(N_h - 1)$ sets may be obtained by choosing different values for n_0 and n_1.

For this thesis, N_h was set to 11, its primitive element $\alpha = 2$, and finally $s = 2$. This allows 11 unique sequences to be generated for each set. The parameter n_0 was set to 0 and n_1 to 1 in accordance with the aforementioned restrictions.

3.4.1.10 Costas Arrays

Costas arrays are generally utilized in frequency hopping. They are generated as a 2D FH constellation, with an equal number of frequency and time slots. Design is restricted to only a single unique frequency over the set of possible frequencies permitted for each time slot within the constellation. For this $N \times N$ matrix, the $N(N-1)/2$ possible vectors between all time/frequency locations are distinct [124]. Alternatively, a Costas array may be defined as the subset of $N!$ permutations of the numbers $\{1, ..., N\}$, with no repeated entries on any line of its characteristic difference triangle. A difference triangle is an analysis tool utilized to verify correlation properties. An example of a Costas array, together with its corresponding difference triangle, is depicted in Fig. 3.4. The first row of the difference triangle represents the row occupied within each column of the 2D Costas array. Every subsequent line is formed by the differences between adjacent elements in the preceding line. In order for this 2D matrix to represent a Costas array, each row within the difference triangle must consist of only unique elements.

A special characteristic of a Costas array is that the correlation between the matrix and a time and frequency shifted version of itself is less than or equal to 1. Having an ideal 2D AC function, they are the optimum multiplexing choice for single-user frequency hopping systems [117]. Unfortunately, this is

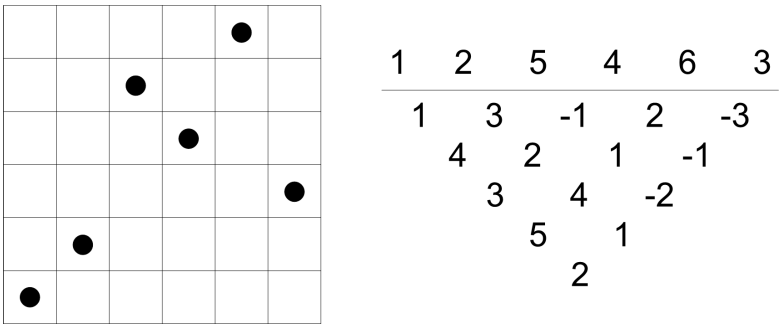

Figure 3.4 A sample Costas array, and associated difference triangle

not the case for CC functions. While in the optimal case individual pairs of Costas arrays have at most 2 coincidences, they may have up to $N/2$ CC hits for certain asynchronicity shifts [116].

The construction of Costas arrays is based upon properties of primitive roots of finite fields [118, 124]. Construction is accomplished through the manipulation of GF(p^m). This Galois field is of order p^m, which designates the number of elements within the set. Taking α and β to represent unique primitive elements of the Galois field, and $a_{i,j}$ representing the array element on the ith row and jth column, two construction methods for a Costas array are:

- Lempel Construction:

$$a_{i-1,j-1} = \begin{cases} 1, & \alpha^i + \alpha^j = 1 \\ 0, & \text{otherwise} \end{cases} ; \tag{3.22}$$

- and Golomb Construction:

$$a_{i-1,j-1} = \begin{cases} 1, & \alpha^i + \beta^j = 1 \\ 0, & \text{otherwise} \end{cases} . \tag{3.23}$$

3.4.1.11 Welch-Costas Arrays

Expanding upon Costas arrays, the Welch-Costas construction delivers full slot utilization. These codes are constructed by taking all primitive roots of the prime p, with the total number of codes possible equivalent to the number of

primitive roots ψ. For an odd prime $\psi = \Phi(p-1) = 2\lambda_p$, where λ_p is an integer and Φ is the Euler Phi function. Taking r as a primitive root of prime p, the placement operator for these codes may be expressed as [125]:

$$y(k) = r^k \pmod{p}. \tag{3.24}$$

This construction results in a Costas array of size $(p-1) \times (p-1)$, with $k \in \{1, ..., p-1\}$. Pairs of Welch-Costas arrays have at most 2 hits in their CC functions, with the upper bound on the number of collisions being $(p-1)/2$ [126]. Similarly to Costas arrays, this construction achieves ideal AC properties.

3.4.1.12 Combinations of Hopping Methods

While several methods exist for the generation of user codes, these methods may be combined to achieve varied sequence properties. This entails the introduction of more than one variable term in the placement operator polynomial, and generally results in a change of correlation characteristics. Various combinations exist [115, 117, 127], including:

- Quadratic and Linear codes:

$$y(k) = uk^2 + bk + c \pmod{p}, \tag{3.25}$$

  where $0 \leq u, b, c \leq p-1$, $u \neq 0$. This combination is also referred to as 'Elliott-Butson' sequencing [128]. The parameters b and c remain static for the generation of all user codes for over u.

- Cubic and Linear codes:

$$y(k) = uk^3 + bk \pmod{p}, \tag{3.26}$$

  where $0 \leq k, b \leq p-1$, and $1 \leq u \leq p-1$. The number of simultaneous users and code correlation properties are dependent upon the number of parameters which remain static.

- Cubic and Quadratic Codes:

$$y(k) = uk^3 + bk^2 \pmod{p}, \tag{3.27}$$

where $0 \leq k, b \leq p-1$, and $1 \leq u \leq p-1$.

- Hyperbolic and Linear Codes:

$$y(k) = u/k + bk \pmod{p}, \tag{3.28}$$

where $0 \leq b \leq p-1$, and $1 \leq u, k \leq p-1$.

- and Hyperbolic and Quadratic Codes:

$$y(k) = u/k + bk^2 \pmod{p}, \tag{3.29}$$

where $0 \leq b \leq p-1$, and $1 \leq u, k \leq p-1$.

3.4.2 Direct Sequence Approach

Direct sequence constructions produce complex valued elements, commonly applied in CDMA systems. Direct mapping from the complex domain to the integer domain was applied to these codes within this thesis, observing the correspondence of correlation properties between domains.

3.4.2.1 Chu Sequences

This spread spectrum coding method considers patterns designed using the complex primitive Nth roots of unity. With N being the length of the sequences, the placement operator for these codes is defined as [118]:

$$y(k) = \begin{cases} e^{\frac{i\pi}{N}u(k+1)k} & N \text{ odd} \\ e^{\frac{i\pi}{N}uk^2} & N \text{ even} \end{cases}. \tag{3.30}$$

The numbers that are relative prime to and less than N signify the user numbers available for this construction. This value is equivalent to the Euler Totient function, representing the maximum number of simultaneous users permitted. The number of possible sequences and their cardinality are equivalent and equal to $N-1$, with $0 \leq k < N$.

Once a direct sequence code is determined, a direct mapping from the complex to the integer domain must be conducted. This is required for a comparative

analysis with time and frequency hopping codes. Unfortunately, this construction leads to palindromic sequences, subsequently increasing the possibility of unwanted sequence prediction.

After a mapping to the integer domain, Chu sequences have a maximum of 1 out-of-phase hit within their Hamming AC function, and a maximum of 2 collisions for their out-of-phase Hamming CC function. Therefore this family of sequences, which is designed to obtain optimal direct sequence correlation properties, retains acceptable properties when mapped to the integer domain.

3.4.2.2 Other Common Spread Spectrum Codes

Other codes which are commonly found in practical direct sequence systems include: Maximal-length sequences (m-sequences), Gold codes and Kasami codes. Maximal-length sequences have several properties which are beneficial for CDMA coding, including near equivalent use of code elements, and limited continuous use of a single element [129]. However, while these sequences may be beneficial for CDMA sequence design, their use in time hopping is not feasible. This is due to multi-user m-sequences within the same family begin cyclically shifted versions of each other [129, 130]. Hence they are used predominantly as a form of chaotic encoding.

Maximal-length sequences may be utilized to generate another family of patterns known as Gold codes. These are created through the use of a 'preferred pair' of m-sequences, which exhibit a three valued CC function. Taking a and b as a preferred pair, and T as a unit code element cyclical shift, a set of Gold sequences is constructed as [118]:

$$G(a,b) = \left\{a, b, a \oplus b, a \oplus Tb, a \oplus T^2b, ..., a \oplus T^{N-1}b\right\}. \tag{3.31}$$

Also based upon m-sequences, the small set of non-binary Kasami sequences over GF(p) form effective CDMA codes [131]. They are created through the use of the trace function as:

$$K(t,i) = \{\kappa_i(t) \mid 0 \leq t \leq N-1,\ 1 \leq i \leq 2^m\}, \tag{3.32}$$

where:

$$\kappa_i(t) = tr_1^m \left\{ tr_m^n \left(\alpha^t \right) + \gamma_i \alpha^{Tt} \right\}. \tag{3.33}$$

Here, $n = 2m$, $N = 2^n - 1$, and $T = (2^n - 1)/(2^m - 1) = 2^m + 1$. The parameter α is a primitive element over GF(2^n), α^T is a primitive element over GF(2^m), and γ_i represents the elements of GF(2^m) for $1 \leq i \leq 2^m$.

3.5 Performance Analysis

The performances of 10 code construction families were analyzed, considering their correlation properties and separation probability profiles. The prime parameter p was chosen to be 11 for all code designs, limiting the number of chips in a frame to 11, and the maximum number of users to 10 (for several constructions). For comparable results, all sequences were tested within two user (one transmitting and one interfering) and 10 user (one transmitting and nine interfering) scenarios.

The chip time T_c was set to 30 ns, and the frame time T_f to 330 ns. All tests performed had each pulse represent a single bit of information ($N_s = 1$). In accordance with IEEE 802.15 UWB standards [132], packet sizes of 1024 octets were used. Channel parameters and user asynchronicity were randomly generated after the transmission of each full packet. Asynchronicity was simulated by adding a random shift from the range $[0, T_c)$ to each user transmission.

The multipath channel parameters were set to simulate a line-of-sight transmission, within a 0 to 4 m range, for all transmitting users. This alters the amplitude of the dispersed paths, and the multipath spread. For the SRake and PRake receivers, 5 multipath components were analyzed ($N_B = 5$).

Hamming correlations conducted on all time hopping sequences within a family returned the maximum, minimum, and average number of in-phase and out-of-phase code collisions. Average values for all sequences constructions was generally equal to 0.1. While some constructions may have exhibited smaller minimum values, this was offset by larger maximum correlation results when

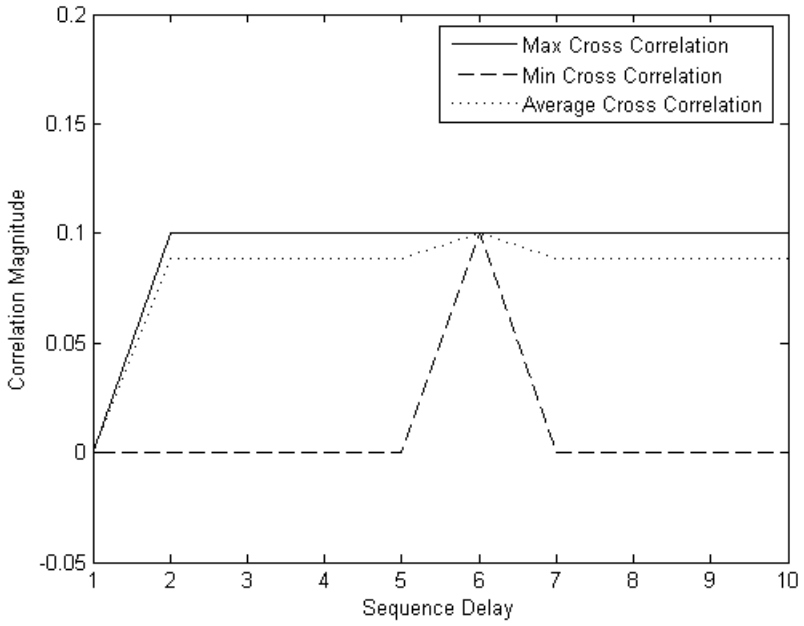

Figure 3.5 Hamming correlation profile for Reed-Solomon multiplexing codes

considering all codes within the family. Reed-Solomon codes were the exception to this property, having an average and maximum out-of-phase correlation of 0.1, and a minimum of predominantly zero. This is depicted in Fig. 3.5.

In order to exemplify a family of multiplexing sequences, shown in Fig. 3.6 and Fig. 3.7 are the hopping values for Reed-Solomon and linear congruence constructions respectively. Arrows indicate code collisions evident within synchronous linear congruence codes. Through a shortened sequence length, Reed-Solomon codes are able to achieve perfect orthogonality for synchronous communications.

Through comparison, it is evident that correlation similarities returned from Hamming correlations coincide with code similarities present in chip separation analysis. Linear, cubic and hyperbolic sequence designs exhibit the same separation profile, depicted in Fig. 3.8(a) for no intermediary pulses ($A = 0$) and separation ranging from 0 to $2N_h - 2$. The profile for the family of Reed-Solomon codes studied is shown in Fig. 3.8(b).

6	9	6	8	0	2	1	1	9	2
10	3	4	0	1	6	6	10	1	3
3	8	2	3	2	10	0	8	4	4
7	2	0	6	3	3	5	6	7	5
0	7	9	9	4	7	10	4	10	6
4	1	7	1	5	0	4	2	2	7
8	6	5	4	6	4	9	0	5	8
1	0	3	7	7	8	3	9	8	9
5	5	1	10	8	1	8	7	0	10
9	10	10	2	9	5	2	5	3	0

Figure 3.6 A family of synchronous Reed-Solomon multiplexing codes

0	1	2	3	4	5	6	7	8	9	10
0	2	4	6	8	10	1	3	5	7	9
0	3	6	9	1	4	7	10	2	5	8
0	4	8	1	5	9	2	6	10	3	7
0	5	10	4	9	3	8	2	7	1	6
0	6	1	7	2	8	3	9	4	10	5
0	7	3	10	6	2	9	5	1	8	4
0	8	5	2	10	7	4	1	9	6	3
0	9	7	5	3	1	10	8	6	4	2
0	10	9	8	7	6	5	4	3	2	1

Figure 3.7 A family of synchronous linear congruence multiplexing codes

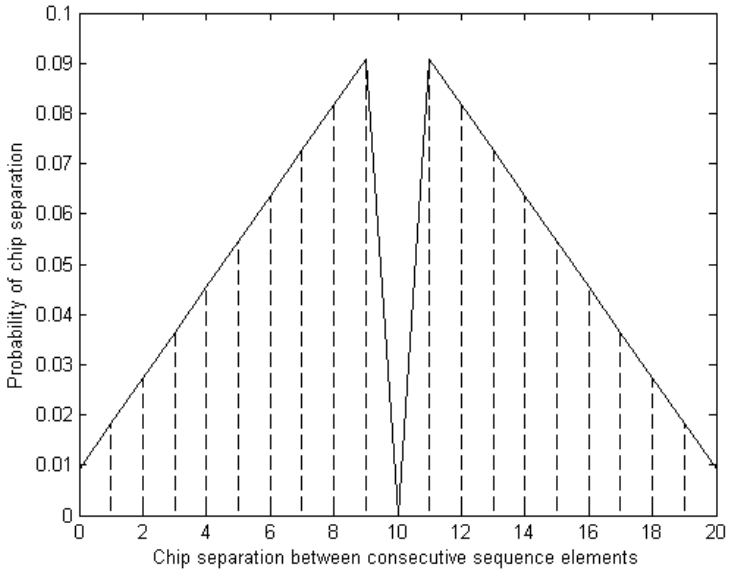

(a)

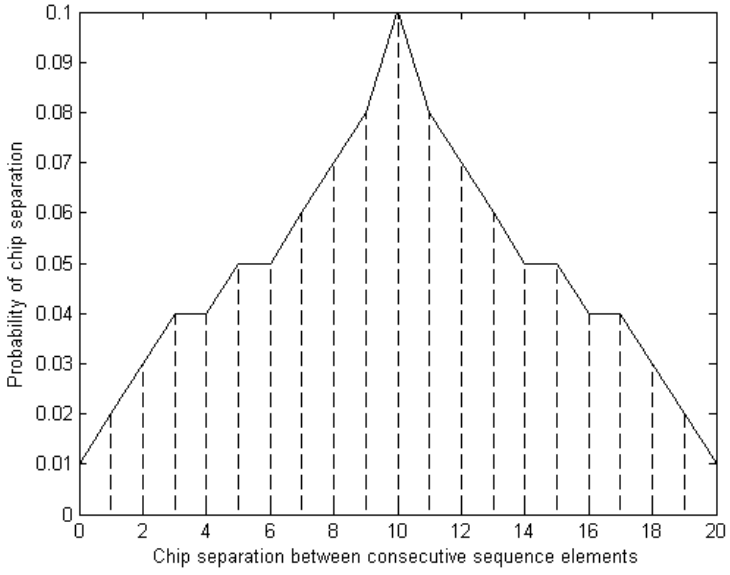

(b)

Figure 3.8 ISI chip separation probabilities for (a) linear, cubic, and hyperbolic congruence codes and (b) Reed-Solomon codes

The bit error rate versus signal to noise ratio plots for the three RAKE receiver types are presented in Fig. 3.9(a) and Fig. 3.9(b) for two user and 10 user scenarios respectively. Initial inspection of the results reveals the transition from noise dominance to interference dominance as the SNR is increased. At low SNR values, decoding errors are mainly caused by noise interfering with the transmission; while at high SNR values errors result from the interference between users.

There exists a minimum BER in each system, which is caused by multi-user interference and shown as a plateau in the high SNR regions. As expected, the BER plateau is lower for the two user case (approximately 10^{-3}) relative to the 10 user case (approximately 10^{-2}), due to the decreased level of user interference. A significant difference can also be seen between RAKE types. The ARake receiver provides optimal performance (lowest BER levels), since it combines all scattered components in the calculation of encoded data. The SRake receiver achieves a relatively worse performance, and the PRake obtains the least favorable results.

An abnormality in the results exists within the two user SRake case for randomly generated hopping codes. Their BER curve falls significantly below other hopping code constructions. Therefore in a system utilizing short code lengths, and operating in a scarce multi-user environment, random codes are capable of surpassing the performance of deterministic codes. However, in a fully utilized system it can be seen that this property is not evident, as shown in Fig. 3.9(b).

It has been determined that in an under utilized system (2 users in a maximum 10 user system, occupying 20% of capacity), both constructions for Quadratic codes, together with Reed-Solomon codes perform well. In the 10 user case (full utilisation), Reed-Solomon codes provide optimal error performance, relative to other constructions. It should be noted that although 'Additional' codes also performed comparatively well, their adoption into wireless devices is not viable due to all codes being cyclical shifts of one another.

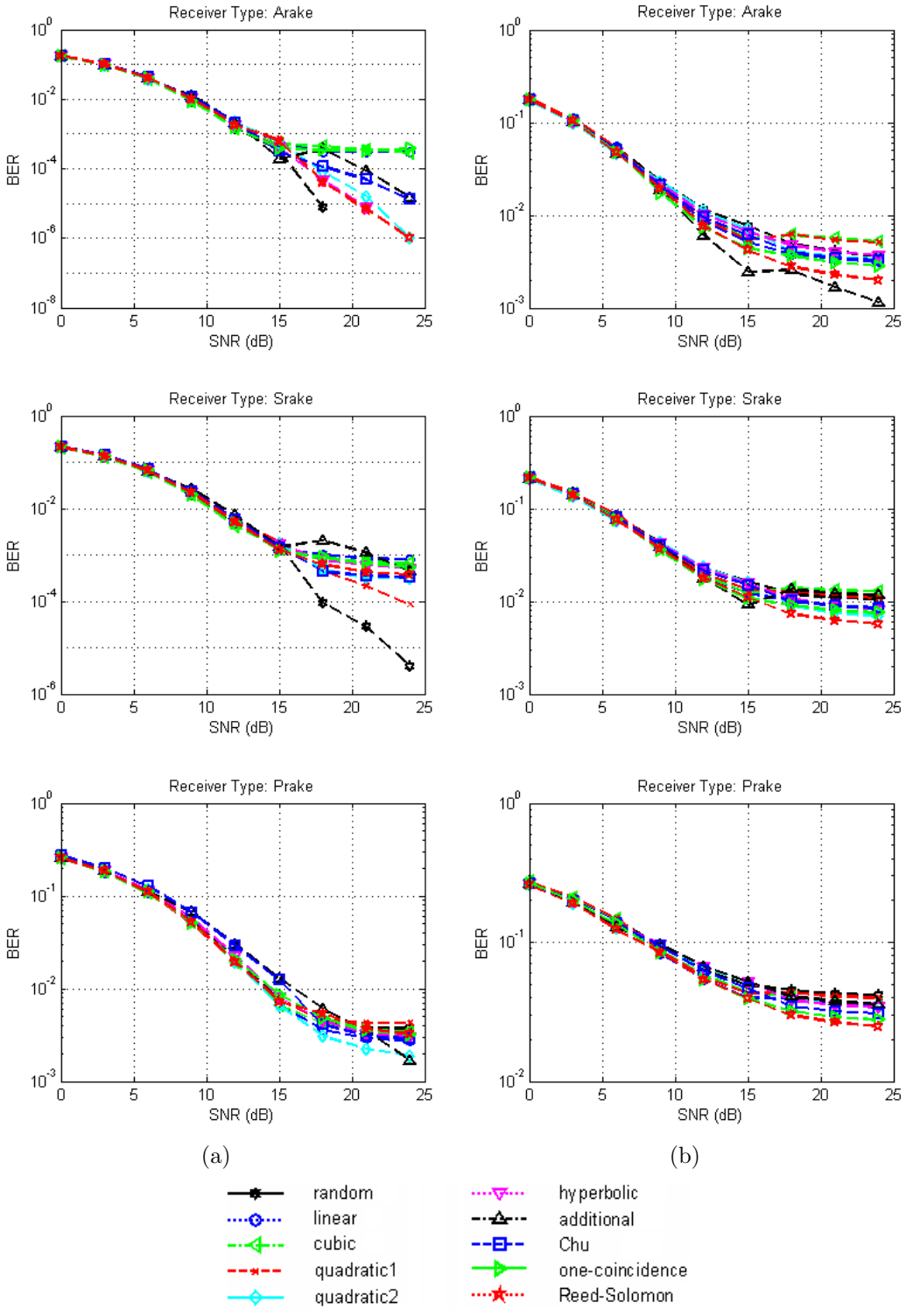

Figure 3.9 BER vs SNR plots for time-hopped UWB with ten time hopping sequence constructions for (a) 2 user case and (b) 10 user case

3.6 Application in UWB Interleaver Design

Multi-user access sequences may be applied to numerous areas of communications. One such application is in the design of interleavers, namely for use in interleaved coding-modulation (ICM). ICM, initially proposed by Pietrzyk and Weber [133], is based on the concept of chip interleaving of UWB signals. The ultimate aim is to reduce ISI common in high data rate systems by interchanging portions of the transmitted signals, in order to spread bursts of errors.

A random interleaver is generally applied, although have a lack of a compact representation. Common hopping codes may be utilized to develop a deterministic chip interleaver, this section considering the application of hyperbolic congruence codes. A considerably larger sequence length was adopted here (up to $N_p = 401$), such that these 'long' random codes could achieve their averaging properties.

The chip interleaver $\Pi_p(x)$ is generated by partitioning the modulation symbols x into subsequences, which may then be rearranged according to random or hyperbolic sequencing. All code construction methods may be utilized, provided that each sequence consists of unique values, and a high level of orthogonality exists between all sequences.

The performance of these interleaver types may be observed through the analysis of scarcely user populated and high data rate (125 Mbit/s) UWB systems operating on IEEE 802.15.3a multipath fading channels. The CM3 NLOS scenario was applied, characterized by a transmitter to receiver separation ranging from 0 to 4 m. Redundancy is added through the use of conventional frame repetition (FR), applying differential autocorrelation signaling with a single delay branch in the receiver. The multi-user performance results with 2000 information bits per packet are shown in Fig. 3.10, with $N_h = 6$ and $N_s = 8$

Apart from a degradation in performance for highly populated systems, and the apparent error floors, it is evident that for a single user scenario the coding gain introduced by the ICM technique is approximately 1 dB at a BER of 10^{-4}.

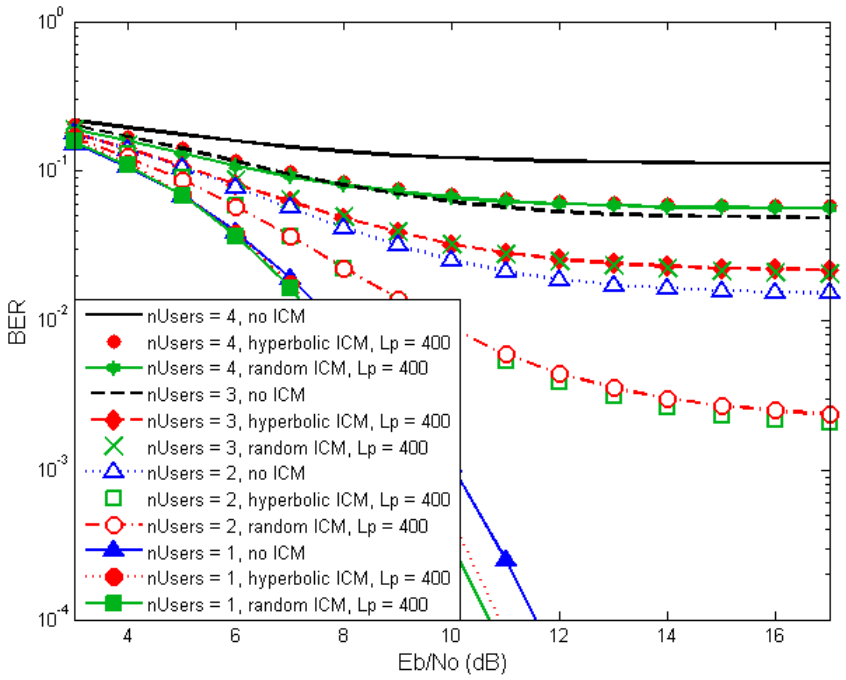

Figure 3.10 Error performance of UWB systems with FR and ICM

This gain increases significantly as more users enter into the system. It can be seen that a deterministic chip interleaver based on hyperbolic sequencing exhibits a similar performance to random interleavers, while having a simpler implementation.

As a further study, work by Li et al. [134] combines the architecture of a time reversed UWB system with the concept of chip-interleaving.

3.7 Chapter Summary and Conclusions

Multi-user hopping codes pose a significant design consideration for modern communications. Many coding methods exist in time, frequency, and direct sequence domains, each with varied correlation measures. Alternate measures, such as a separation probability profile, may be generated in order to further characterize these sequences.

A performance comparison of ten sequence designs reveals that for a system exhibiting low levels of utilization (two user case) short length structured codes attain a similar performance to randomly generated codes. However, this is not true for a fully utilized system, where structured codes slightly out-performed random sequences with a low periodicity. Similarities between random and deterministic codes for a large sequence length were shown in the design of a UWB chip interleaver.

Chapter 4

Intersymbol Interference (ISI) - Derivation and Analysis

4.1 Introduction

Considering the typical RMS delay spread for a UWB multipath channel, intersymbol interference may cause a significant degradation in system performance. This is particularly evident in time reversed UWB, where a longer transmitted waveform approximately doubles the length of the received signal. The level of ISI is influenced by the width of the transmitted pulses, the number of pulses per symbol, the data rate, and the characteristics of the propagation channel. The self-interference within a TR-UWB architecture will diminish significantly provided that the chip time is greater than twice the length of the channel response, allowing enough time for all multipath components to dissipate.

This chapter presents preliminary equations and a closed-form derivation of ISI within a time reversed UWB architecture. Derivations explicitly accommodate multi-user access codes through the 'separation probability' profile introduced in Chapter 3. The chapter concludes with a performance comparison between the derived formulae and simulated analysis.

4.2 Derivation Approach

Temporal diversity in communications systems leads to the adverse effects of self-interference. In order to estimate the performance of a TR-UWB system operating in a scattering environment, the expected ISI variance may be determined. This is accomplished by estimating the level of interference for a single transmission, summed over all overlapping adjacent transmissions by the same user. A similar approach was applied by Deleuze et al. [135] in the context of TH-UWB using a RAKE receiver architecture. In order to obtain a close approximation, the ISI must be Gaussian distributed [136].

The received signal for this system is comprised of Gaussian waveforms ($w(t)$) altered in magnitude and phase by the autocorrelation of the channel response. With these sub-waveforms ideally having a zero average, the ISI has an expected mean of zero. This reduces the variance calculation to:

$$\sigma^2 \equiv \left\langle (Y-\mu)^2 \right\rangle \Rightarrow \left\langle Y^2 \right\rangle, \tag{4.1}$$

where μ represents the signal mean, and $\langle \cdot \rangle$ an ensemble average. The variance is calculated over all overlapping transmissions, also over all possible chip separations by applying the separation probabilities of the user's time multiplexing code.

The derived variance is finally utilized to estimate the BER performance for a TR-UWB system. For a binary PPM architecture, sending N_s transmissions per symbol, the error probability curve is defined as [46]:

$$\mathrm{Pr_e} = Q\left(\sqrt{N_s \cdot SINR}\right) \Rightarrow \frac{1}{2} erfc\left(\sqrt{\frac{N_s \cdot SINR}{2}}\right), \tag{4.2}$$

where $SINR$ represents the signal to combined noise and ISI ratio. In order for this equation to remain valid, all parameters of the $SINR$ must be Gaussian distributed. The additive white noise exhibited by the system is defined as a statistically independent zero mean Gaussian random variable [46]. The ISI term may be brought under the standard Gaussian approximation provided that the number of paths within the channel impulse response (L), the number of

transmissions per symbol (N_s), and the data rate (R) are large [137]. It should be noted that this probability expression is for 'soft' signal reception, where the signal formed by N_s pulses is observed as a single multi-pulse transmission. This is in contrast to 'hard' signal detection, where independent decisions are computed over each of the N_s transmissions, and then a majority criterion applied to determine the encoded data.

Although the received signal power $P_{RX}(u)$ may arrive at the receiver, only the power in the main autocorrelation peak is used for decoding data ($(L-1)$th path). This limitation is accounted for by an additional ratio ϕ, which represents the ratio of power within the strongest path to the remaining sidelobe power. The final *SINR* may therefore be expressed as:

$$SINR = \frac{\phi \cdot P_{RX}(u)}{\sigma^2_{AWGN} + \sigma^2_{ISI}}. \tag{4.3}$$

4.3 Preliminary Equations

The transmitted time reversed signal in terms of path magnitudes and displacements is given by Eq. 2.39, repeated for clarity as:

$$s^{(u)}(t) = \sqrt{\frac{E_{TX}(u)}{G_{H,u;x_{pos}}}} \sum_{m=-\infty}^{\infty} \sum_{k=0}^{L-1} \beta_k(u; x_{pos}) w\left(t - mT_f - c_m^{(u)} T_c - \varepsilon b_m^{(u)} - \tau_k\right). \tag{4.4}$$

The ISI variance derivations presented herein take an average on the $\pm\varepsilon$ shift introduced for the encoding of data through PPM. Assuming $b_m^{(u)}$ is composed of independent identically-distributed ± 1 random variables, the possible time separations between two transmissions are shown in Table 4.1. Here, T_g is the frame guard time, T_w the base pulse width, and the mth transmitted frame is considered relative to an arbitrary nth frame ($n < m$). The result $m - n - 1$ indicates the number of intermediate pulses, also the separation in terms of frame widths, and j represents the chip separation. Analysis shows that taking a mean shift will result in the assumption that there is no additional modulation shift over.

Data Encoded	Time Separation
$\{0,\ 0\}$	$(m-n-1)T_f + jT_c + T_w + T_g + \varepsilon$
$\{1,\ 1\}$	$(m-n-1)T_f + jT_c + T_w + T_g + \varepsilon$
$\{0,\ 1\}$	$(m-n-1)T_f + jT_c + T_w + T_g + 2\varepsilon$
$\{1,\ 0\}$	$(m-n-1)T_f + jT_c + T_w + T_g$

Table 4.1 Binary data modulation separation possibilities

Assuming a total of N symbols transmitted, the variance is calculated for each mth transmission by determining the expected interference from the $m-1$ preceding transmission (pre-symbol interference), and the $N-m$ subsequent transmissions (post-symbol interference). Summations are conducted over all possible separations between the mth and the nth transmissions. The overlaps, as determined at the transmitted side, are convoluted with the user's channel response to obtain the ISI at the receiver side. It should be noted that the transmission channel and the pre-filtering channel are assumed identical for ISI. This response is represented as a combination of L time 'bins' of width τ, such that the length of the channel is $L\tau$.

In terms of pre-symbol interference ($0 \leq n < m$), for each nth symbol only a portion will overlap with the desired mth symbol, accounted for by the parameter N_w. As pre-symbol interference will always dissipate before the end of the mth symbol, N_w specifies the number of time bins to wait until the nth transmission overlaps with the mth. Accountability for post-symbol interference evident when $m < n < N$ takes a similar approach. The parameter N_l represents the number of bins from the beginning of the nth transmission which will overlap with the mth. Taking an average transmission separation from the results of Table 4.1, these overlapping parameters may be represented as:

$$N_w = \left\lceil \frac{(m-n-1)T_f + jT_c + T_w + \varepsilon + T_g}{\tau} \right\rceil, \tag{4.5}$$

$$N_l = \left\lfloor \frac{L\tau - \left((n-m-1)\,T_f + jT_c + T_w + \varepsilon + T_g\right)}{\tau} \right\rfloor. \tag{4.6}$$

The combined overlapping signal is calculated by summing over all possible chip

separation values for all adjacent transmissions $j \in [0, 2(N_h - 1)]$. The entire interfering signal must be considered, with a total length of $2L\tau - \tau$. Without loss of generality, taking user number $u = 1$, the combined interfering signal detected at the receiver may be expressed as:

$$r_{ISI} = \sqrt{\frac{E_{TX}}{U(1)}} \int_0^{2L\tau-\tau} \left[\begin{array}{l} \left(\sum_{n=0}^{m-1} \left(\sum_{j=2(N_h-1)+1}^{0} S_e\left[m-n-1, j\right] \sum_{k=N_w}^{L-1} \beta_k w(t-\tau_k) \right) \right) \otimes h(t;1) \\ + \left(\sum_{n=m+1}^{N-1} \left(\sum_{j=0}^{2(N_h-1)+1} S_e\left[n-m-1, j\right] \sum_{k=0}^{N_l-1} \beta_k w(t-\tau_k) \right) \right) \otimes h(t;1) \end{array} \right] dt. \quad (4.7)$$

For brevity, as the derivation of ISI is concentrated on a single user scenario, user number $u = 1$ and receiver position x_1 are omitted. Simplification of the receiver detected ISI may be conducted by recognizing that not all adjacent transmissions will cause interference. With a channel response length of $L\tau$, the total number of interfering transmissions will be limited to $N_{ov} = \lceil L\tau / T_f \rceil$. Taking the mean $E\left[r_{ISI}\right] = 0$, the second central moment of the ISI may be reduced to:

$$\sigma^2_{ISI} = \sum_{\zeta=1}^{(N_{ov}-1)} \sum_{\varsigma=0}^{2(N_h-1)} (\chi_{\zeta,\varsigma,\xi} + \chi_{\zeta,\varsigma,\psi}), \quad (4.8)$$

where:

$$\chi_{\zeta,\varsigma,\nu} = S_e\left(\zeta - 1, \varsigma\right) \cdot \mathrm{var}\left(h(1; x_1, t) \otimes \left[\sqrt{\frac{E_{TX}(1)}{G_{H,1;x_1}}} \cdot \nu \right] \right), \quad (4.9)$$

$$\xi = \sum_{k=N_w}^{L-1} \beta_k w(t - \tau_{k-N_w}), \quad (4.10)$$

$$\psi = \sum_{k=0}^{N_l-1} \beta_k w(t - \tau_{k+N_w}), \quad (4.11)$$

and:

$$N_w = \left\lceil \frac{(\zeta - 1)T_f + (\varsigma + 1)T_c}{\tau} \right\rceil, \quad (4.12)$$

$$N_l = L - N_w. \quad (4.13)$$

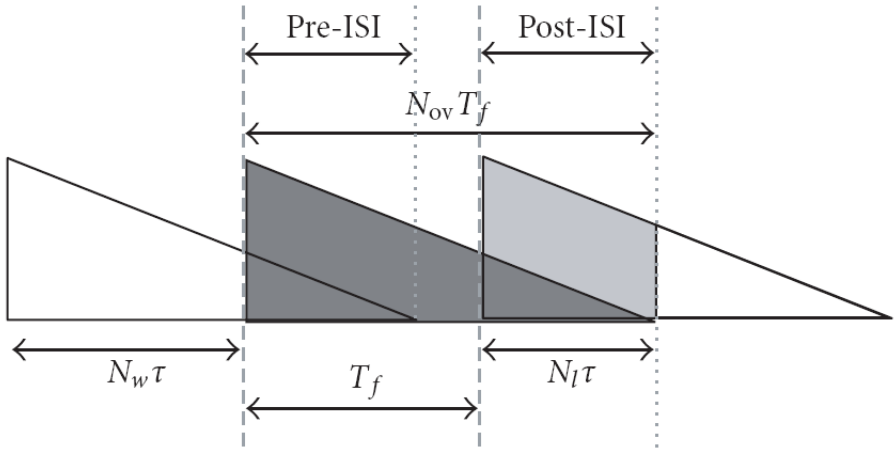

Figure 4.1 Overlapping transmissions in a TR-UWB scenario

The parameter ν represents the portion of the transmitted signal which is regarded as ISI, and is referred to as the third parameter of $\chi_{\zeta,\varsigma,\nu}$. It can be seen that the ISI may be entirely calculated as the summation of partial overlapping signals, with the delay parameters N_w and N_l having an inverse relationship with respect to the number of paths L within a channel. An illustration of the overlapping present in TR-UWB is given in Fig. 4.1, together with all delay parameters. For clarity, a TR transmission is approximated by a simple triangle.

The final non-closed form expression for the ISI present within a TR-UWB system converges to within 5% of the final variance when averaged over approximately 50 independent realizations of Eq. 4.8. An example of this convergence is depicted in Fig. 4.2 for the ISI variance at 30 Mbit/s, $N_s = 1$. The variance magnitude is of the order 10^{-15} due to the incorporation of the signal energy E_{TX}.

4.4 Closed-form Analysis

Presented next is a closed-form representation of the symbol based ISI variance estimation of Eq. 4.8. In order to aid in derivations, a shift of the variance

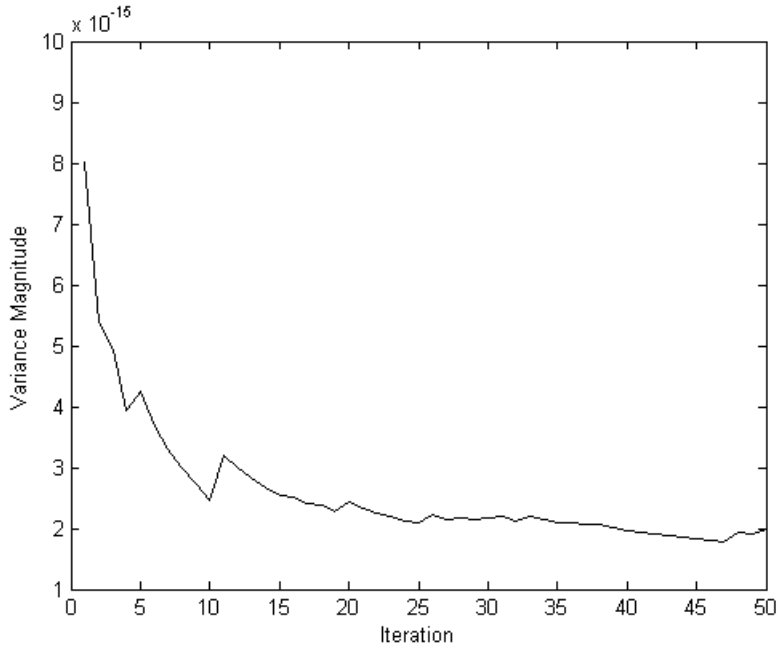

Figure 4.2 ISI variance convergence at 30 Mbit/s, $N_s = 1$

operation was made, forming the 'time combined' version:

$$\sigma^2_{ISI} = \text{var}\left(\sqrt{\frac{E_{TX}(1)}{G_{H,1;x_1}}}\left\{\Omega \otimes h(1;x_1,t)\right\}\right), \tag{4.14}$$

with:

$$\Omega = \sum_{\zeta=1}^{N_{ov}-1}\left\{\sum_{\varsigma=0}^{2(N_h-1)} S_e(\zeta-1,\varsigma)\left(\sum_{k=0}^{N_l-1}\beta_k w(t-\tau_k)+\sum_{k=N_w}^{L-1}\beta_k w(t-\tau_k)\right)\right\} \tag{4.15}$$

representing the summation of all interfering partial signals, together with their respective separation probabilities. This was achieved through a multiplier of $L\tau/T_f$. This multiplier is equivalent to the energy normalization required in Eq. 4.8 to adjust for changing data rate and channel delay spread. Their equivalence is depicted in Fig. 4.3 for varied R and N_s values, at a constant channel delay spread of 40 ns. The order of the variance magnitude is significantly dependent upon the signal energy. An increased N_s value leads to a compaction of transmitted pulses, and subsequently an increase in the signal energy. It should be noted that the multiplier also takes into consideration the movement

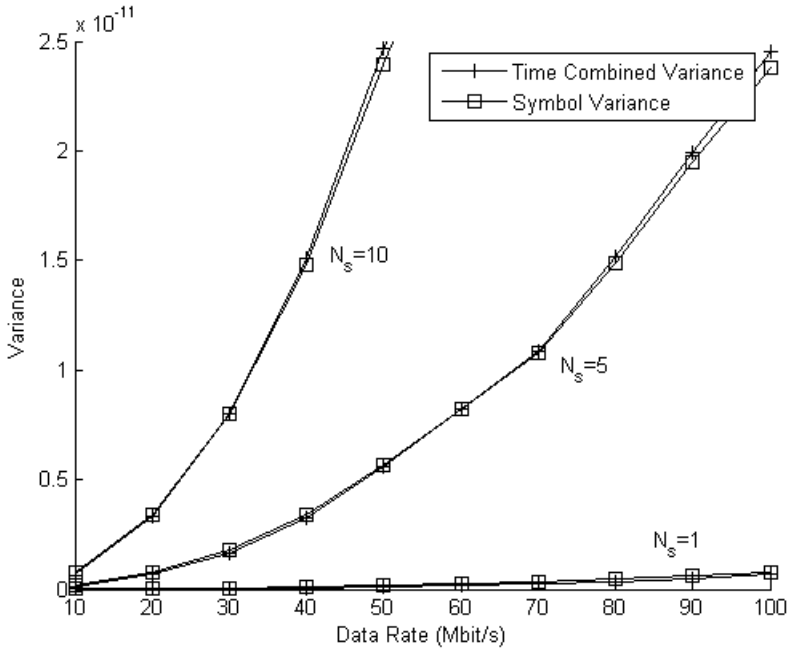

Figure 4.3 Time combined vs symbol based variance comparison

of the separation probability, which will be significant for the MUI derivation of Chapter 5.

Applying the definition $\beta_k = \alpha_{(L-1)-k}$, and assuming that the separation probability is static over ζ, Ω can be altered to:

$$\Omega = \sum_{\zeta=1}^{N_{ov}-1} \left\{ \sum_{\varsigma=0}^{2(N_h-1)} S_e(0,\varsigma) \left(\sum_{k=0}^{N_l-1} \beta_k w(t-\tau_k) + \sum_{k=0}^{(L-1)-N_w} \alpha_k w(t-\tau_{L-1-k}) \right) \right\}. \tag{4.16}$$

Altering the order of summations, Eq. 4.16 reduces to:

$$\Omega = \sum_{\varsigma=0}^{2(N_h-1)} S_e(0,\varsigma) \sum_{\zeta=1}^{N_{ov}-1} \left(\sum_{k=0}^{N_l-1} \beta_k w(t-\tau_k) + \alpha_k w(t-\tau_{L-1-k}) \right). \tag{4.17}$$

To further simplify this expression, the summation over k must be conducted before the summation over ζ. Noting the inverse relationship between ζ and k through N_l, the upper limits on both summations must be changed as:

$$\max\{k\} = N_l - 1, \tag{4.18}$$

$$\zeta = \frac{((L-1) - \max\{k\})\tau - (\varsigma+1)T_c}{T_f} + 1. \tag{4.19}$$

The maximum of k occurs when $\zeta = 1$, and the upper limit of ζ changes to the intersection between k and ζ, forming the limits:

$$k \in \left[0, \frac{L\tau - (\varsigma+1)T_c}{\tau}\right], \tag{4.20}$$

$$\zeta \in \left[1, \frac{((L-1)-k)\tau - (\varsigma+1)T_c}{T_f} + 1\right]. \tag{4.21}$$

Applying this conversion removes the dependence of the β_k and α_k terms on ζ (through N_l), yielding:

$$\Omega = \sum_{\varsigma=0}^{2(N_h-1)} S_e(0,\varsigma) \sum_{k=0}^{L-1} \left\{ \left(\beta_k w(t-\tau_k) + \alpha_k w(t-\tau_{L-1-k})\right) \times \frac{(L-1-k)\tau - (\varsigma+1)T_c}{T_f} \right\}, \tag{4.22}$$

with $\lfloor (L\tau - (\varsigma+1)T_c)/\tau \rfloor \approx L-1$. This assumption is valid provided that $N_h \ll L$, as $\max\{\varsigma\}$ is controlled by N_h.

The parameter Ω can be further simplified by considering the summation of both α_k and β_k for all $k \in [0, L-1]$. Summing time aligned path magnitudes within the expression results in a constant path coefficient for all k over α_k, equal to $((L-1)\tau - 2(\varsigma+1)T_c)/T_f$. Hence the ISI formula of Eq. 4.14 can be reduced to:

$$\sigma^2_{ISI} = \frac{E_{TX}}{G_H} \cdot S_\Xi \cdot V_{ACF}, \tag{4.23}$$

where,

$$S_\Xi = \left(\left[\sum_{\varsigma=0}^{2(N_h-1)} S_e(0,\varsigma) \cdot \frac{(L-1)\tau - 2(\varsigma+1)T_c}{T_f} \right] \right)^2, \tag{4.24}$$

$$V_{ACF} = \mathrm{var}\left\{ [h(-t) \otimes w(t) \otimes h(t)] \right\}, \tag{4.25}$$

with V_{ACF} defining the variance of the autocorrelation of the channel impulse response convoluted with the base waveform $w(t)$.

Considering convolutional and autocorrelation properties over time and frequency domains, the term V_{ACF} may be expressed through the use of Fourier transforms as:

$$V_{ACF} = \mathrm{var}\left\{ \widetilde{W}(f) \cdot |H(f)|^2 \right\}, \tag{4.26}$$

where Parseval's Theorem equates the energy over time and frequency domains, indicating that the Fourier transform is unitary. Here, $\widetilde{W}(f)$ and $H(f)$ refer to the Fourier transforms of the energy normalized base waveform, as in Eq. 2.7, and the channel response respectively.

For the purpose of this derivation, $h(t)$ was estimated through the use of a single exponential function $e(t)$. Since the discrete version of the channel response is used, this exponential was sampled through the use of the Shah function [138], defined in the frequency domain as:

$$\text{Shah}(bf) = \frac{1}{|b|} \sum_{i=-\infty}^{\infty} \delta\left(f - \frac{i}{b}\right). \tag{4.27}$$

A similar channel analysis was conducted by Witrisal [139]. Here, the delay PSD of the 802.15.3a channel model was estimated by a single Dirac pulse at time $t = 0$ to represent the LOS path, followed by an exponentially decaying power distribution. Applying this discrete version of the channel response, Eq. 4.26 yields:

$$V_{ACF} = \text{var}\left\{ \widetilde{W}(f) \cdot \left| E(f) \otimes \frac{1}{\tau} \sum_{i=-\infty}^{\infty} \delta\left(f - \frac{i}{\tau}\right) \right|^2 \right\}, \tag{4.28}$$

with $E(f)$ representing the Fourier transform of $e(t)$, and the Shah function acting as a replicator of $E(f)$ over the frequency domain. Substituting Eq. 2.7 into Eq. 4.28, the variance expression expands to:

$$V_{ACF} = \sqrt{\frac{32}{\pi}} \cdot \frac{4}{3 f_o \tau^4} \cdot \text{var}\left\{ \left(\frac{f}{f_0}\right)^2 e^{\left(-\frac{f^2}{f_0^2}\right)} \cdot \left| \sum_{i=-\infty}^{\infty} E\left(f - \frac{i}{\tau}\right) \right|^2 \right\}. \tag{4.29}$$

Under the assumption that $E(f)$ has a bandwidth spread less than $1/\tau$, which is valid for an exponential $e(t)$, the argument of the variance can be determined by assuming a constant value for the base waveform's frequency response over each $1/\tau$ width, as shown in Fig. 4.4. Here, a zero-order hold filtering has been applied as:

$$\overline{W}(f) = \sum_{i=-\infty}^{\infty} \widetilde{W}\left(\frac{i}{\tau}\right) \cdot \Pi_{\square}\left(\frac{f - iF_{bin}}{F_{bin}}\right), \tag{4.30}$$

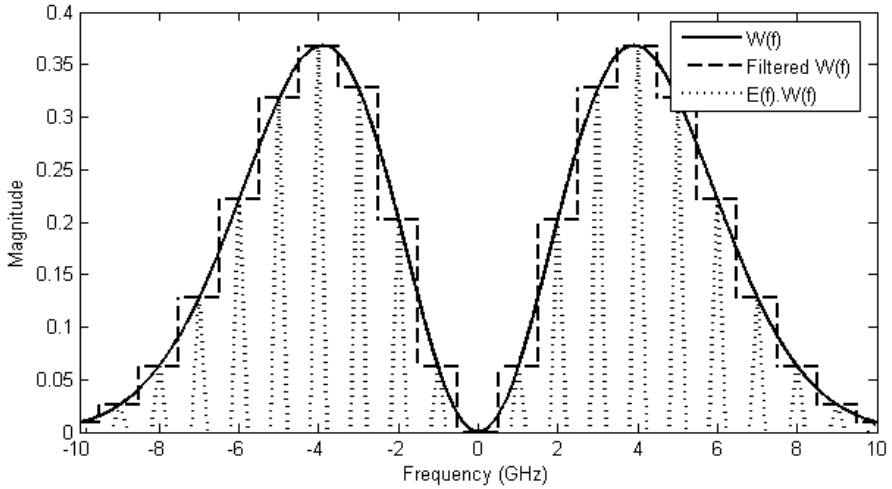

Figure 4.4 Zero-order hold filtering of a Gaussian base waveform

with F_{bin} representing the reciprocal of τ, and $\Pi_{\square}(f)$ the standard rectangular function. This reduces V_{ACF} to:

$$V_{ACF} = \sqrt{\frac{32}{\pi}} \cdot \frac{4}{3f_o\tau^4} \cdot \sum_{i=-\lceil f_{\max}\tau \rceil}^{\lceil f_{\max}\tau \rceil} \widetilde{W}\left(\frac{i}{\tau}\right)^2 \cdot \sum_f |E(f)|^4 \cdot \frac{1}{L\tau} \cdot \frac{1}{T_w f_c}, \qquad (4.31)$$

where f_{max} is the single side frequency over which the majority of the energy within $\widetilde{W}(f)$ exists. The final two terms of this expression are required to determine the PSD variance. The parameter $1/(L\tau)$ represents the inverse of the time width of the channel impulse response, and the final multiplication normalizes the signal based upon the pulse width and sampling frequency.

The final estimate for the ISI variance of a time-reversed system is defined as:

$$\sigma_{ISI}^2 = \frac{E_{TX}}{G_H} \cdot S_\Xi \cdot \mathrm{K} \cdot \Psi, \qquad (4.32)$$

where,

$$\begin{aligned} S_\Xi &= \left(\left[\sum_{\varsigma=0}^{2(N_h-1)} S_e(0,\varsigma) \cdot \frac{(L-1)\tau - 2(\varsigma+1)T_c}{T_f} \right] \right)^2, \\ \mathrm{K} &= \sqrt{\frac{32}{\pi}} \cdot \frac{4}{3f_o\tau^4} \cdot \frac{1}{L\tau} \cdot \frac{1}{T_w f_c}, \\ \Psi &= \sum_{i=-\lceil f_{\max}\tau \rceil}^{\lceil f_{\max}\tau \rceil} \widetilde{W}\left(\frac{i}{\tau}\right)^2 \cdot \sum_f |E(f)|^4. \end{aligned}$$

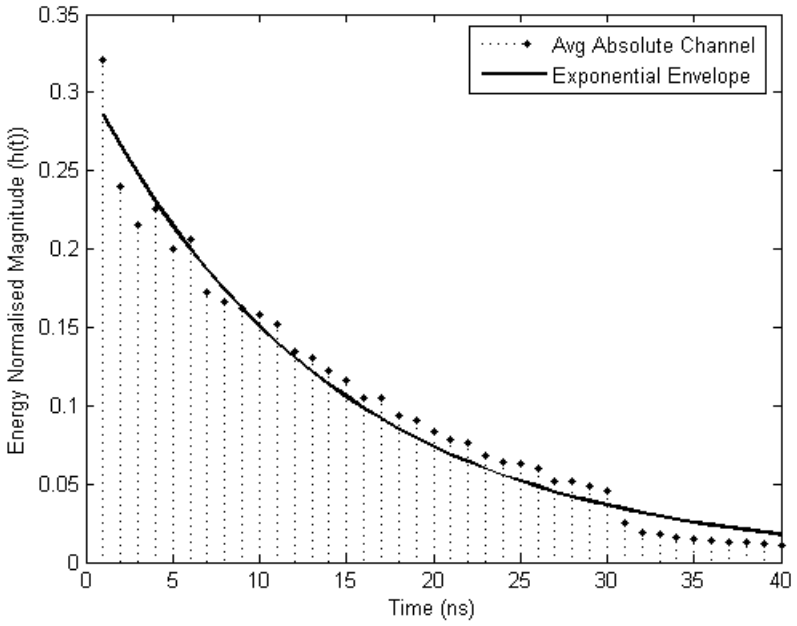

Figure 4.5 Exponential estimation of the IEEE 802.15.3a channel model

The final requirement is the calculation of the $4th$ moment of the channel envelope estimation $E(f)$. With $e(t)$ taken as a single exponential function, its time and frequency domain expressions are [46]:

$$Ae^{-a|t|} \Leftrightarrow \frac{2Aa}{a^2 + 4\pi^2 f^2}. \tag{4.33}$$

The MMSE between this exponential estimation and the energy normalized UWB channel model was analyzed, with the equation parameters for Eq. 4.33 estimated as $A = 0.2858$, $a = 7.1 \times 10^7$ for $h(t)$. Alignments averaged over 1000 realizations are shown in Fig. 4.5.

4.5 Simulation Results

A TR-UWB simulation was adapted from a time hopped PPM UWB simulation by Di Benedetto and Giancola [17]. A LOS system with a transmitter-receiver displacement of 0-4 m was tested (CM1 in the IEEE 802.15.3a model). This requires a ratio of $\phi \approx 0.566$ for the SINR of Eq. 4.3, averaged over 50 realiza-

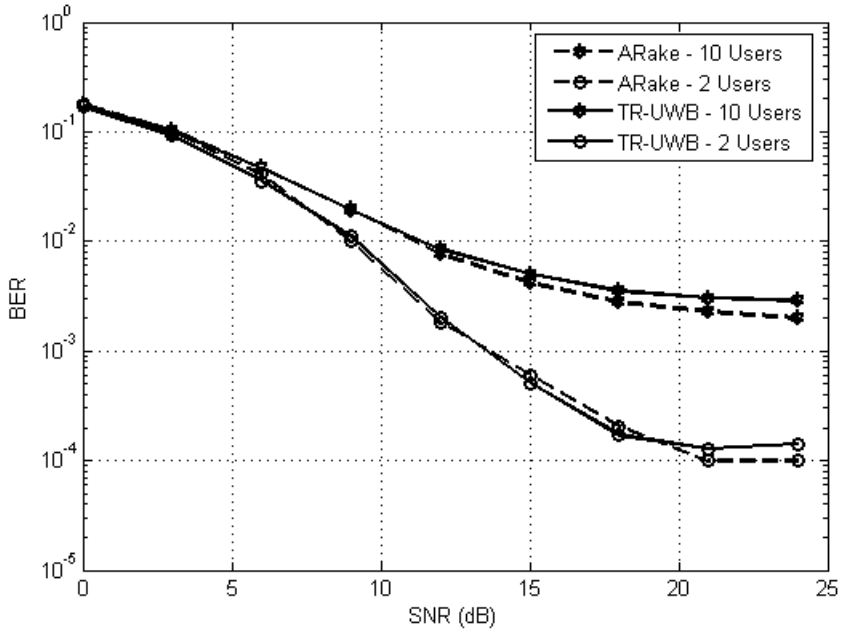

Figure 4.6 Similarity analysis of UWB and TR-UWB in the absence of ISI at 3 Mbit/s, $N_s = 1$

tions of the multipath channel. An independent channel model was generated for each packet transfer, set to a size of 1024 octets. For this LOS scenario, a reference attenuation of 47 dB and attenuation exponent of $\gamma = 1.7$ were applied. The cardinality and periodicity of each time hopping code were set to 11, with a pulse width of 0.5 ns, a data encoding shift of 0.5 ns, and a sampling frequency of 50 GHz. The number of bins per channel (L) was set to 40, and the bin width τ set to 1 ns. The bin width was chosen to be greater than the base waveform duration, and large enough to allow an encoded signal to be orthogonal to its non-encoded counterpart. A transmit power of 1 mW was selected, although scalability allows this work to be extended to alternate power levels easily.

In order to ensure the equivalence of UWB and TR-UWB models in the absence of ISI, simulations were conducted at a data rate of 3 Mbit/s, $N_s = 1$, for 2 and 10 users, with results shown in Fig. 4.6. This data rate and N_s combination allows the majority of the 40 ns channel response tested to pass before the

transmission of the next symbol. Equality between the two methods is shown in the presence of varied MUI.

The closed-form ISI variance equation was tested through comparison with the performance of a simulated single user scenario.

Reed-Solomon time hopping was applied for user multiplexing in the receiver-side ARake tests and the transmitter-side time reversed tests. Labelling the TR-UWB variance derivation results as 'TR-Equ', results for $N_s = 5$ and $N_s = 10$ are shown in Fig. 4.7(a) and Fig. 4.7(b) respectively. Tests were conducted for data rates of 15, 50 and 100 Mbit/s. It can be observed that for all data rates the derived error curve closely traces the simulated performance. A slight over approximation developed for the closed-form analysis relative to the semi-analytical analysis of the preliminary equations, this being due to simplification errors. However, differences were negligible, being at most one third of a decade at an SNR of 20 dB, with a data rate of 100 Mbit/s, $N_s = 5$.

Furthermore, equivalent ARake systems exhibit severely impaired performance in the presence of increased ISI. This difference intensifies for higher data rates, which leads to a proportional elevation in the level of self-interference. These results are supported by RAKE and TR-UWB tests conducted in literature [91].

Finally, as expected an increase in the data rate, which has a proportional decrease in the frame width T_f, significantly degrades system performance. Similarly, as the frame length is dependent upon the parameter N_s, it also has a significant influence on performance. At a data rate of 100 Mbit/s, the comparative ISI plateau is clearly visible. For $N_s = 5$, the formulated plateau occurs at a BER of approximately 10^{-6}, while for $N_s = 10$ it appears at near 10^{-4}.

4.6 Chapter Summary and Conclusions

In this chapter, a closed-form expression for the ISI within a time-reversed UWB system was developed. The approach of these derivations was to analyze all overlapping transmissions, considering the expected overlap and subsequent

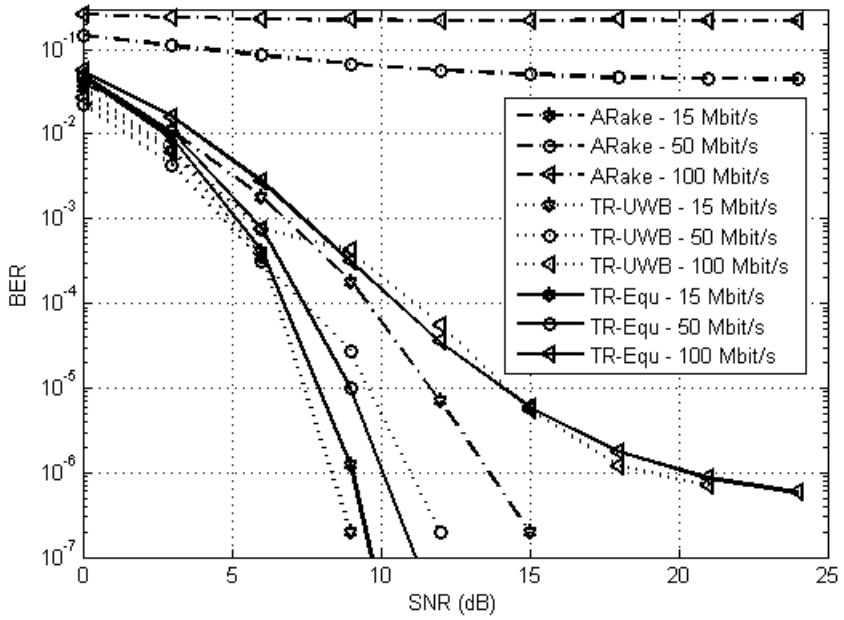

(a)

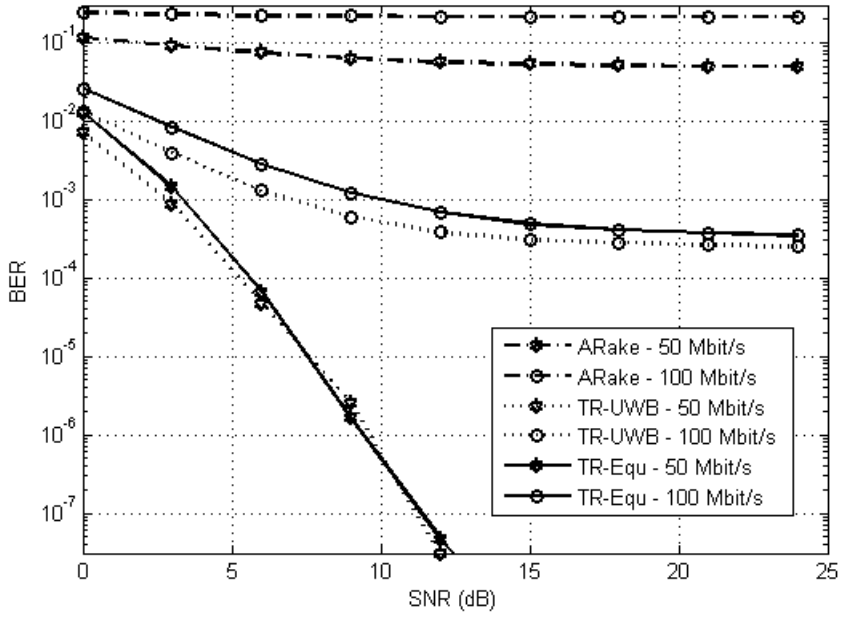

(b)

Figure 4.7 BER curves for ISI with Reed-Solomon coding for (a) $N_s = 5$ and (b) $N_s = 10$

probability of occurrence. This latter probability was determined through the 'separation probability' profile, which characterizes a family of hopping codes. Requiring only the $4th$ moment of the channel response envelope to be calculated, comparative results using an exponential estimation were presented. These indicated a close alignment between simulated and derived error rates.

An over-approximation develops for the formulated performance as the level of interference increases. This results due to approximations made in the derivation process, although the estimated curve always remains within close proximity to simulated results, generally within a decade of the simulated error rate.

Finally, performance similarities between TR-UWB and ARake based UWB were exemplified in the absence of ISI. Within high pulse rate systems, time reversed communications were shown to be an effective method of mitigating ISI. It also benefits from the computational advantage achieved by having the channel perform the necessary convolutional operation. This cumbersome task would otherwise be conducted by the receiver architecture, considerably increasing calculation latency.

Chapter 5

Multi-user Interference (MUI) - Derivation and Analysis

5.1 Introduction

Multi-user interference is an inevitable consequence of multiple users operating in close proximity. For the case of ISI, if the chip time is greater than the transmission duration, no interference from adjacent user transmissions exists. For MUI however, this condition would only remove the partial interference caused by transmissions within adjacent chips, while the issue of same chip collisions between users remains. Similarly to ISI, the level of MUI is affected by the width of the transmitted pulses (T_w), the number of pulses per symbol (N_s), the data rate (R), and the propagation channel ($h(t)$). It is also controlled by the multi-user multiplexing sequences utilized.

This chapter discusses preliminary equations and a closed-form derivation of MUI within a time reversed UWB system. User multiplexing is accommodated through the 'separation probability' profile introduced in Chapter 3. The chapter concludes with a performance comparison between the derived formulae and a simulated multi-user analysis.

5.2 Derivation Approach

The MUI derivations presented within this chapter follow a similar procedure to that of the closed-form ISI derivation of Chapter 4. However, while ISI accounts for only self-interference, MUI comprises of interference from all users in close proximity. For a multi-user scenario, there are three types of interference which must be accounted for: in-phase, where two users transmit in the same chip; pre-out-of-phase, where an interfering user transmission occurs before the current transmission; and post-out-of-phase MUI, where an interfering transmission occurs after the current transmission. The first is dependent upon the separation probabilities of user asynchronism within a single frame; while the latter two are dependent upon user separations for all adjacent frames over which a transmission may exist.

Similarly to the ISI variance calculation, transmission overlaps are analyzed over all possible chip separations. Since the in-phase MUI considers collisions between same frame transmissions, the traditional Hamming cross correlation function is applied, averaged over correlations between all user combinations. The out-of-phase variance adopts the MUI separation probability profile, averaging over asynchronism for all users.

The *SINR* expression of Eq. 4.3, representing the signal to combined noise and interference ratio, must be altered to accommodate for the additional MUI term. It is subsequently changed to include the collective σ^2_{MUI} term as:

$$SINR = \frac{\phi \cdot P_{RX}(u)}{\sigma^2_{AWGN} + \sigma^2_{ISI} + \sigma^2_{MUI}}. \tag{5.1}$$

In order for this expression to remain valid, the MUI term must be Gaussian distributed. This requires analysis to be conducted over a large number of simultaneous users [57].

5.3 Preliminary Equations

MUI variance derivations take an average on the $\pm\varepsilon$ shift introduced for the encoding of data through PPM. This is equivalent to a cancellation of the data modulation displacement, as discussed in Sec. 4.3.

Discrete time signal overlaps are characterized through channel bin delay parameters. Overlap parameters for in-phase and out-of-phase MUI, considering the 1st and the uth ($u \neq 1$) user's transmissions, are shown in Fig. 5.1. ISI parameters are represented also for comparison, with a time reversed transmission approximated by a triangular waveform. The subscripts *(In)* and *(Out)* label the in-phase and out-of-phase components respectively. The parameters $N_{w(In)}$ and $N_{w(Out)}$ represent the number of paths before an overlap of the pre-interference occurs, with $N_{l(In)}$ and $N_{l(Out)}$ indicating the number of paths which are overlapping for post-interference. The dark shading represents the desired signal, while the light shading indicates the interference sources from both ISI and MUI.

The in-phase and out-of-phase variance derivations were accomplished through the same methodology as in the ISI derivation of Chapter 4. The former variance, which encompasses only same frame overlaps between the desired and the interfering signals, estimates the variance through the combination of all partial signals ν which could interfere within the frame of the desired user's symbol. This combination is multiplied by the corresponding separation probability of occurrence, considering all possible chip separations over a single time frame. Taking $u = 1$ as the desired user, and for brevity ignoring receiver positioning and user referencing for path magnitudes, the in-phase variance is formulated as:

$$\sigma^2_{InPhaseMUI} = \sum_{\Theta=-(N_h-1)}^{0} \chi_{\Theta,\xi} + \sum_{\Theta=1}^{N_h-1} \chi_{\Theta,\psi}, \tag{5.2}$$

where:

$$\chi_{\Theta,\nu} = S_e\left(0, \Theta + (N_h - 1) + 1\right) \cdot \mathrm{var}\left(h(u; x_1, t) \otimes \left[\sqrt{\frac{E_{TX}(u)}{G_{H,u;x_1}}} \cdot \nu \right] \right), \tag{5.3}$$

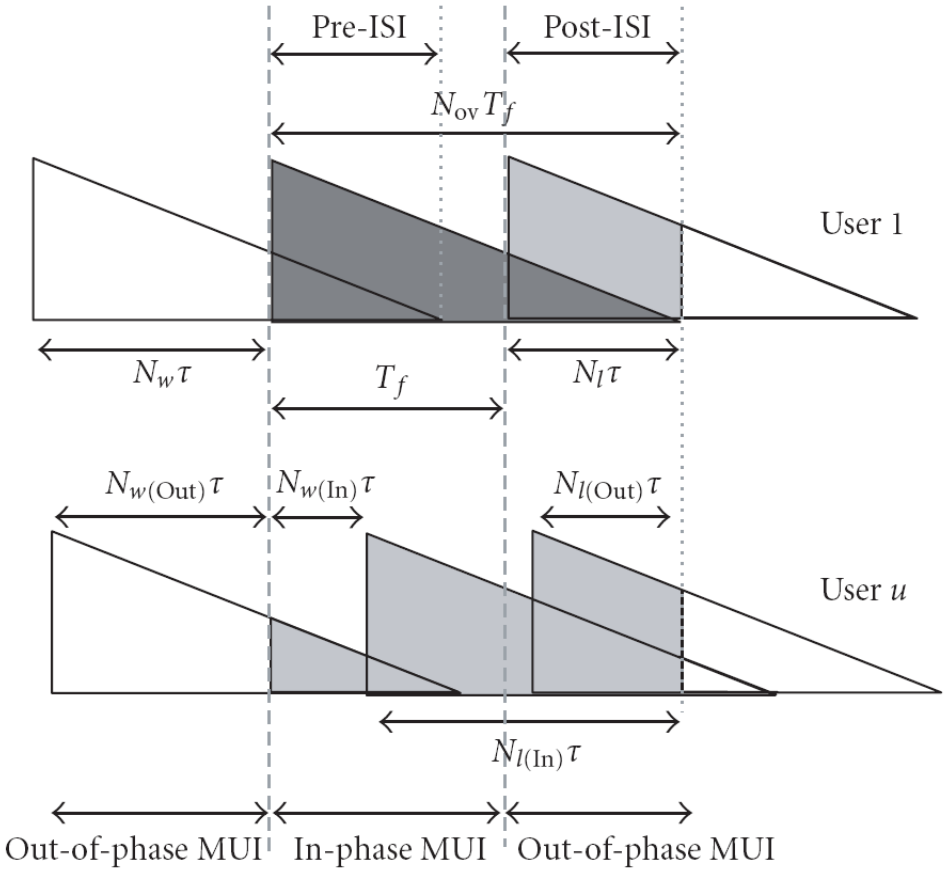

Figure 5.1 Path alignment parameters for MUI variance formulation

$$\xi = \sum_{k=N_{w(In)}}^{L-1} \beta_k w(t - \tau_{k-N_{w(In)}}), \tag{5.4}$$

$$\psi = \sum_{k=0}^{N_{l(In)}-1} \beta_k w(t - \tau_{k+N_{w(In)}}), \tag{5.5}$$

with:

$$N_{w(In)} = \lceil |\Theta| \cdot T_c/\tau \rceil, \tag{5.6}$$

$$N_{l(In)} = L - N_{w(In)}, \tag{5.7}$$

$$N_{ov} = \left\lceil \frac{L\tau}{T_f} \right\rceil. \tag{5.8}$$

The out-of-phase MUI counterpart accounts for overlapping from frames adjacent to the desired user's transmission. It considers all frames over which a transmission may exist, and also all possible chip level separations within the

frames occupied. Applying the separation probability profile, the out-of-phase MUI may be expressed as:

$$\sigma^2_{OutPhaseMUI} = \sum_{\zeta=1}^{(N_{ov}-1)} \sum_{\varsigma=0}^{2(N_h-1)} (\chi_{\zeta,\varsigma,\xi} + \chi_{\zeta,\varsigma,\psi}), \tag{5.9}$$

where:

$$\chi_{\zeta,\varsigma,\nu} = S_e(0,\varsigma) \cdot \mathrm{var}\left(h(u;x_1,t) \otimes \left[\sqrt{\frac{E_{TX}(u)}{G_{H,u;x_1}}} \cdot \nu \right] \right), \tag{5.10}$$

$$\xi = \sum_{k=N_{w(Out)}}^{L-1} \beta_k w(t - \tau_{k-N_{w(Out)}}), \tag{5.11}$$

$$\psi = \sum_{k=0}^{N_{l(Out)}-1} \beta_k w(t - \tau_{k+N_{w(Out)}}), \tag{5.12}$$

$$N_{w(Out)} = \left\lceil \frac{(\zeta-1)T_f + (\varsigma+1)T_c}{\tau} \right\rceil, \tag{5.13}$$

$$N_{l(Out)} = L - N_{w(Out)}. \tag{5.14}$$

For each MUI type, the expected interference signal is convoluted with the channel response from the interferer's transmitter to the desired user's receiver at position x_1. The final variance formula equates to the expected interference from a single interferer, multiplied by the number of interferers present. The total MUI is evaluated as:

$$\sigma^2_{MUI} = \left(\sigma^2_{InPhaseMUI} + \sigma^2_{OutPhaseMUI}\right) \cdot (N_u - 1). \tag{5.15}$$

Through testing, it was determined that a MUI variance within 5% of the final convergent value could be obtained after approximately 100 independent realizations of this MUI formulation. An example of this MUI convergence for a 10 user system is illustrated in Fig. 5.2, operating at 30 Mbit/s, $N_s = 1$. The variance magnitude is of the order 10^{-10} due to the incorporation of the signal energy $E_{TX}(u)$.

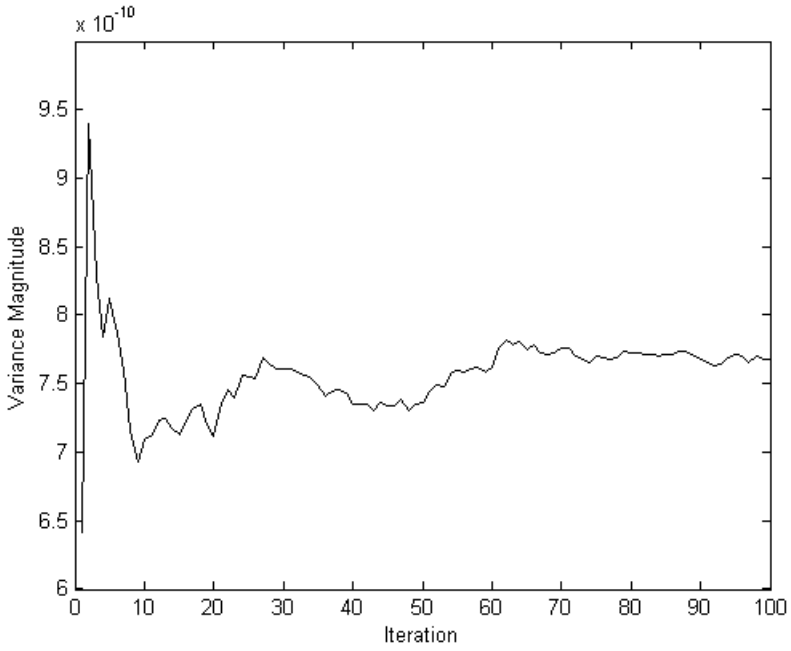

Figure 5.2 MUI variance convergence at 30 Mbit/s, $N_s = 1$

5.4 Closed-form Analysis

5.4.1 In-Phase MUI

The main technique to combat in-phase MUI degradation is the strategic use of time hopping codes. These may be employed to arrange user transmissions to minimize sequence collisions. The in-phase component covers MUI over the $2N_h - 1$ possible chip separations between the desired and interfering user transmissions. It should be noted that the in-phase component poses a minimal degradation relative to out-of-phase MUI, which arises from user transmissions originating in adjacent frames. For comparison, the in-phase component is approximately 10% of the out-of-phase interference at 30 Mbit/s, $N_s = 5$, with this ratio decreasing as the data rate or transmissions/symbol increase.

The base expression for the In-Phase MUI from a single user is presented in Eq. 5.2. In order to obtain a simple solution to this expression, it is assumed that the channel delay spread is significantly larger than the maximum separation

$(2N_h - 1)$. This is valid provided $L\tau \gg (2N_h - 1)T_c$, and allows each partial signal ν to be assumed by an entire channel response. This approximation becomes more valid as the data rate and N_s values are increased, and is achieved through a reduction of the ν equations to give:

$$\upsilon = \xi = \psi = \sum_{k=0}^{L-1} \beta_k w(t - \tau_k). \tag{5.16}$$

The variance can thus be written as:

$$\sigma^2_{InPhaseMUI} \approx \sum_{\Theta=-(N_h-1)}^{N_h-1} Se\left(0, \Theta + (N_h - 1) + 1\right) \cdot \mathrm{var}\Bigg(h(u; x_1, t) \otimes \left[\sqrt{\frac{E_{TX}(u)}{G_{H,u;x_1}}} \cdot \upsilon \right] \Bigg). \tag{5.17}$$

With known channel delay spread $(L\tau)$ and gain $(G_{H,u;x_1})$, the convolution with the propagation channel can be omitted. This results in an estimation of the multi-user interference from a combined signal energy perspective, such that the structure of the interference signal as considered at the transmitter side is determined, then normalized according to the propagation channel. The disadvantage however is that the structure of the channel is not taken into account. Assuming that a correlation of a time reversed signal with a propagation channel (of equal length) doubles the signal vector length, Eq. 5.17 can therefore be simplified to:

$$\sigma^2_{InPhaseMUI} = \frac{E_{TX}(u) \cdot G_{H,u;x_1}}{G_{H,u;x_1}} \cdot \sum_{\Theta=-(N_h-1)}^{N_h-1} Se\left(0, \Theta + (N_h - 1) + 1\right) \cdot \mathrm{var}\left(\sum_{k=0}^{L-1} \beta_k w(t - \tau_k) \right) /2. \tag{5.18}$$

Noting that ν has normalized energy, and taking into account the sampling frequency, this expression can be further reduced to:

$$\sigma^2_{InPhaseMUI} = E_{TX}(u) \cdot G_{H,u;x_1} \cdot \sum_{\Theta=-(N_h-1)}^{N_h-1} Se\left(0, \Theta + (N_h - 1) + 1\right) \cdot f_c/(L\tau f_c - 1)/2 \tag{5.19}$$

$$\approx \frac{E_{TX}(u) \cdot G_{H,u;x_1}}{2L\tau}, \tag{5.20}$$

where the sum of all separation probabilities is equal to unit probability as:

$$\sum_{\Theta=-(N_h-1)}^{N_h-1} Se\left(0, \Theta + (N_h - 1) + 1\right) = 1. \tag{5.21}$$

5.4.2 Out-of-Phase MUI

Out-of-phase MUI considers transmissions by nearby users which originate from frames adjacent to the current frame of the desired user. With the high data rates required by emerging UWB applications, this form of interference poses a significantly higher severity than in-phase MUI.

The variance of this degradation is calculated by summing all partial transmissions which overlap into the desired user's symbol. This summation is conducted over all overlapping time frames (ζ), also all possible chip separations (ς) between the interfering signal and desired signal. Out-of-phase separations are weighted by the separation probability profile of the time hopping code applied. The expression for the out-of-phase MUI by a single user is given by Eq. 5.9. The similarity between this MUI formulation and the ISI equations of Chapter 4 is evident, with the exception that the user number $u \neq 1$. An alternate approach to the ISI derivation was applied for the out-of-phase MUI however, calculating the variance of the overlapping signals on a frame-by-frame basis.

For the initial simplification, the assumption is made that interference originating from frames before the current transmission and that which will interfere in subsequent frames are independent. Also, as for in-phase MUI, the convolution with the propagation channel has been removed, considering the interference from the transmitter's perspective. This requires a division by 2 due to the halving of the output length when converted to the receiver's perspective. For brevity, constant energy/gain multiplications have been omitted. Assuming normalized channels, the out-of-phase expression may be reduced to:

$$\sigma^2_{OutPhaseMUI} = \frac{1}{2} \sum_{\zeta=1}^{(N_{ov}-1)} \sum_{\varsigma=0}^{2(N_h-1)} \left(S_e\left(0, \varsigma\right) \cdot \mathrm{var}\left(\xi + \psi\right)\right). \tag{5.22}$$

As variance is independent of time position when considering the entire signal,

the time shifting τ may be omitted without consequence. Using the relationship that $\beta_k = \alpha_{(L-1)-k}$ to combine ξ and ψ equations, the above formula simplifies to:

$$\sigma^2_{OutPhaseMUI} = \frac{1}{2} \sum_{\varsigma=0}^{2(N_h-1)} S_e(0,\varsigma)\, \Upsilon, \tag{5.23}$$

where:

$$\Upsilon = \sum_{\zeta=1}^{N_{ov}-1} \left(\text{var} \left(\sum_{k=0}^{N_{l(Out)}-1} [\beta_k w(t-\tau_k) + \alpha_k w(t-\tau_{L-1-k})] \right) \right). \tag{5.24}$$

Unfortunately, correlation exists between the signals of different frames within Υ. Consequently the encompassing of the summation over ζ into the variance operation is not feasible. In order to remove this correlation, an additional time shift of twice the channel delay spread must be introduced. This additional displacement will lead to a larger signal length, subsequently requiring a normalization by N_{ov} for the *var* operation. Equation 5.24 is therefore equivalent to:

$$\begin{aligned} \Upsilon \;=\; N_{ov} \cdot \text{var} \Bigg(\sum_{\zeta=1}^{N_{ov}-1} \sum_{k=0}^{N_{l(Out)}-1} & [\beta_k w(t - 2\zeta L\tau - \tau_k) \\ & + \alpha_k w(t - 2\zeta L\tau - \tau_{L-1-k})] \Bigg). \end{aligned} \tag{5.25}$$

In order to remove the $2\zeta L\tau$ shift, the correlation between the variables within the *var* function must be considered. Ignoring this displacement, and taking the summation over k to produce a single independent signal, correlation exists for the $N_{ov}-1$ signals when summed over ζ, herein collectively referred to as v_ζ. This is accounted for by subtracting twice the covariance between all $N_{ov}-1$ signals, denoted as Θ_ζ. Expressing Eq. 5.23 as:

$$\sigma^2_{OutPhaseMUI} = \frac{1}{2} \sum_{\varsigma=0}^{2(N_h-1)} S_e(0,\varsigma) \cdot N_{ov} \cdot \text{var} \left(\sum_{\zeta=1}^{N_{ov}-1} v_\zeta \right), \tag{5.26}$$

the covariance between the dependent signals is:

$$\Theta_\zeta = \sum_{\zeta_1=1}^{N_{ov}-1} \sum_{\substack{\zeta_2=1 \\ \zeta_2 \neq \zeta_1}}^{N_{ov}-1} \text{cov}[\nu_{\zeta_1}, \nu_{\zeta_2}]. \tag{5.27}$$

Conceptually, it can be seen that the $N_{ov}-1$ signals being correlated are replicas of the time reversed channel impulse response, with portions attenuated or nulled. The collection of partial signals for a system operating at 50 Mbit/s, $N_s = 10$, with all channel paths set to unity for ease of visual analysis, is shown in Fig. 5.3. At $N_{l(Out)} = L/2$, the summation over k magnifies all β_k from τ_0 to $\tau_{L/2-1}$, and all α_k values from τ_{L-1} to $\tau_{L/2-1}$. Together these form the complete time reversed response. Through expansion of the covariance of the partial signals within Θ_ζ, individual paths of the channel response may be combined. Simplification of similar path terms reveals the summation of α_k^2 and β_k^2 values, limited by N_{ov}. The summation of the signal energy of all partial responses with $N_{l(Out)} < L/2$ may be extracted, leaving a term θ_{hf} dependent only upon N_{ov} and the variance of the propagation channel. Assuming the channel is zero mean, this variance reduces to the calculation of the gain of the normalized channel, which by definition is unity. Hence, Θ_ζ may be expressed as:

$$\Theta_\zeta = \frac{1}{2L\tau}\left\{\left[\sum_{\xi=\lfloor N_{ov}/2\rfloor+1}^{N_{ov}-1}\sum_{l=0}^{N_l-1}\left(\alpha_{l+1}^2+\beta_{l+1}^2\right)\right]+\theta_{hf}\right\}, \tag{5.28}$$

$$\theta_{hf} = \begin{cases} (N_{ov}-2)+4\sum_{j=1}^{N_{ov}/2-2}(N_{ov}/2-j-1), & N_{ov}\text{ even} \\ 4\sum_{j=1}^{\lceil N_{ov}/2\rceil-2}\left(\lceil N_{ov}/2\rceil-j-1\right), & N_{ov}\text{ odd} \end{cases}. \tag{5.29}$$

While the calculation of the out-of-phase variance operates over $\varsigma \in [0, 2(N_h - 1)]$, the value of Θ_ζ is estimated by the median level of interference over all possible chip separations, this occurring at $\varsigma = N_h - 1$. Also, the normalized base waveform is omitted, rather focusing on the summation of path gains and accounting for the change in signal lengths through the $2L\tau$ division. This entails a path magnitude based estimation of the covariance between all dependent signals of this MUI.

With the $2\zeta L\tau$ shift of Eq. 5.25 removed, the order of summation over ζ and k can be exchanged as in the ISI derivation. The upper limits on these summation parameters are:

$$\max\{k\} = N_{l(Out)} - 1, \tag{5.30}$$

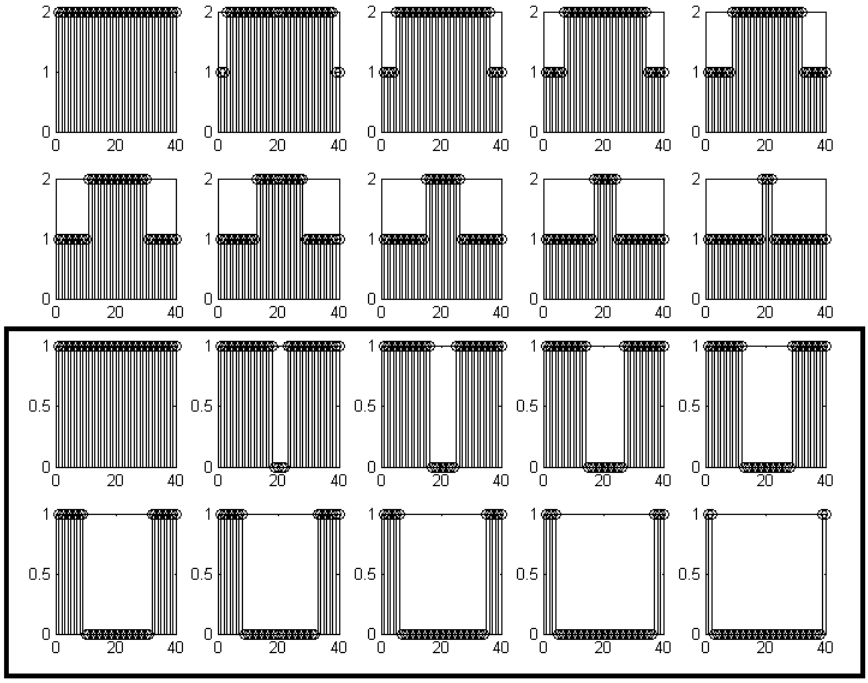

Figure 5.3 Collection of partial signals for covariance summation within out-of-phase MUI, operating at 50 Mbit/s, $N_s = 10$

$$\zeta = \frac{((L-1) - \max\{k\})\tau - (\varsigma+1)T_c}{T_f} + 1. \tag{5.31}$$

With the maximum of k occurring at $\zeta = 1$, the upper limit of ζ becomes the intersection between it and k, resulting in the ranges of:

$$k \in \left[0, \frac{L\tau - (\varsigma+1)T_c}{\tau}\right], \tag{5.32}$$

$$\zeta \in \left[1, \frac{((L-1)-k)\tau - (\varsigma+1)T_c}{T_f} + 1\right]. \tag{5.33}$$

Assuming $\max\{k\} = [L\tau - (\varsigma+1)T_c]/\tau \approx L-1$, the out-of-phase MUI expression simplifies to:

$$\begin{aligned}\sigma^2_{OutPhaseMUI} &= \frac{1}{2}\sum_{\varsigma=0}^{2(N_h-1)} S_e(0,\varsigma) \\ &\cdot \operatorname{var}\left(\sum_{k=0}^{L-1} \sum_{\zeta=1}^{\frac{((L-1)-k)\tau-(\varsigma+1)T_c}{T_f}+1} [\beta_k w(t-\tau_k) + \alpha_k w(t-\tau_{L-1-k})]\right) - 2\Theta_\varsigma. \end{aligned} \tag{5.34}$$

As the α_k and β_k terms are independent of ζ, the expression can be simplified to obtain a constant multiplier of $\lceil([(L-1)-k]\,\tau-[\varsigma+1]\,T_c)\,/T_f\rceil$ over all k.

The combined out-of-phase MUI equation can be reduced by observing that the summation over k adds two instance of each α_k value, each with a multiplier of either $([L-1-k]\,\tau-[\varsigma+1]\,T_c)\,/T_f+1/2$ or $(k\tau-[\varsigma+1]\,T_c)\,/T_f+1/2$, where it is assumed that the *ceil* operation will on average add $1/2$ to the fraction. The summation of these weights results in a constant multiplier over k. Rearranging, the final expression for the multi-user interference from a single user, including the constant energy/gain multiplications, may be presented as:

$$\sigma^2_{OutPhaseMUI} = G\cdot E_{TX}\left(\frac{1}{2}\left\{\sum_{\varsigma=0}^{2(N_h-1)} S_e\,(0,\varsigma)\right.\right.$$
$$\left.\left.\cdot\left[\frac{(L-1)\tau-2(\varsigma+1)T_c}{T_f}+1\right]^2\right\}\cdot \mathrm{var}\,(h(t))-2\Theta_\zeta\right), \quad (5.35)$$

where convolution with the energy normalized independent base waveform $w(t)$ has been ignored. This is valid provided $\tau \geq T_w$.

In order to remove all dependence on individual path magnitudes (α_k, β_k), it is observed that the covariance summation Θ_ζ of Eq. 5.28 consists of a summation of the square of all path amplitudes. Considering the summation limits, paths which exist closer to the response beginning and end ($l = \{0, L\}$) are summed more than those near the center of the response (where $l = L/2$). The partial signals considered here are shown boxed within Fig. 5.3. Expanding the double summation of Θ_ζ, a waveform is generated which consists of the square of all path amplitudes multiplied by an envelope following the form illustrated within Fig. 5.4.

The number of discontinuities within this envelope is equal to $2(\lceil N_{ov}/2\rceil - 1)$, with N_{ov} increments of step width T_f/τ paths. Applying the standard rectangular function $\Pi_\square(t)$, it can be described mathematically as:

$$\widetilde{\Theta}(t) = \sum_{i=1}^{N_{ov}} \Pi_\square\left(\frac{t-T_f/\tau}{T_f/\tau}\right)\cdot\left|\left\lceil\frac{N_{ov}}{2}\right\rceil - i\right|. \quad (5.36)$$

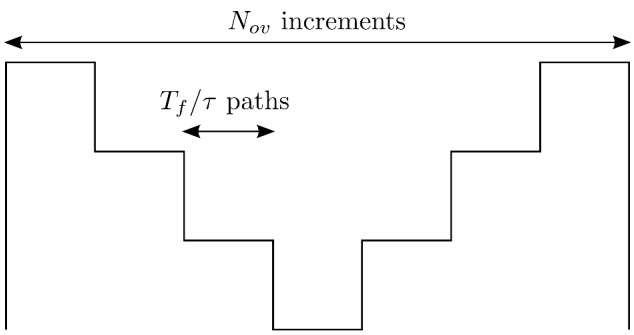

Figure 5.4 Covariance summation envelope for MUI

This reduces the covariance expression to:

$$\Theta_{\zeta} = \frac{1}{2L\tau}\left\{\left[h^2(t)\widetilde{\Theta}(t)\right] + \theta_{hf}\right\}. \tag{5.37}$$

An MMSE exponential estimation was adopted to replicate the structure of the channel response. Estimations on both $h(t)$ and $h^2(t)$ are required for this MUI formulation, both developed using an exponential form. The MMSE parameters for the form of Eq. 4.33 are set as $A = 0.2858$, $a = 7.1 \times 10^7$ for $h(t)$, and $A = 0.122$, $a = 1.3 \times 10^8$ for $h^2(t)$. Alignments averaged over 1000 realizations are shown in Fig. 5.5.

As in the ISI derivation, a normalization by $L\tau/T_f$ is required. However, this multiplier includes the movement of the separation probability between the preliminary and closed-form ISI expressions, which must be compensated here through a multiplication by $1/\sqrt{mean(S_e(0,\varsigma))}$, $\forall\varsigma$.

5.5 Simulation Results

A time reversed UWB simulation was utilized to determine the validity of the closed-form MUI derivations within this chapter. Simulation parameters were set as in the ISI comparison of the preceding chapter. Multi-user error performance analysis presented next also took into account ISI within the system through the closed-form expression of the previous chapter.

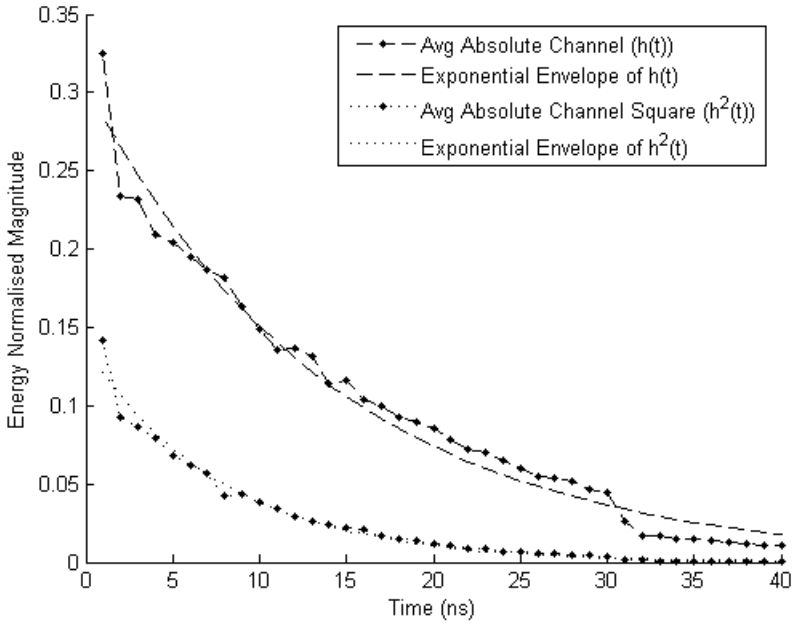

Figure 5.5 Exponential estimation of the UWB channel model $h(t)$ and channel model square $h^2(t)$

The effects of MUI on the expected performance of a time reversed system at 30 Mbit/s, $N_s = 5$, with an SNR of 12 dB, are illustrated in Fig. 5.6. The addition of each user results in an increase in the level of MUI present, following a near exponential rise in the error rate. Although a time-reversed system does have the benefit of mitigating ISI, further measures are required to reduce the degrading effects of interfering users.

MUI variance tests for a 10 user scenario were conducted at a data rate of 30 Mbit/s, with $N_s = 10$. Results are illustrated in Fig. 5.7. They indicate the maximum, minimum, and average BER rates over all users for a TR-UWB system, and also the average performance as based on the variance formulas. It is evident that the formulated curve closely follows the average simulated path.

Figure 5.7 also illustrates an interesting property regarding the variance between user performance in transmitter and receiver side equalization types. While achieving relatively better performance, TR-UWB exhibits severe variations in the error probabilities between users. On the contrary, ARake based UWB

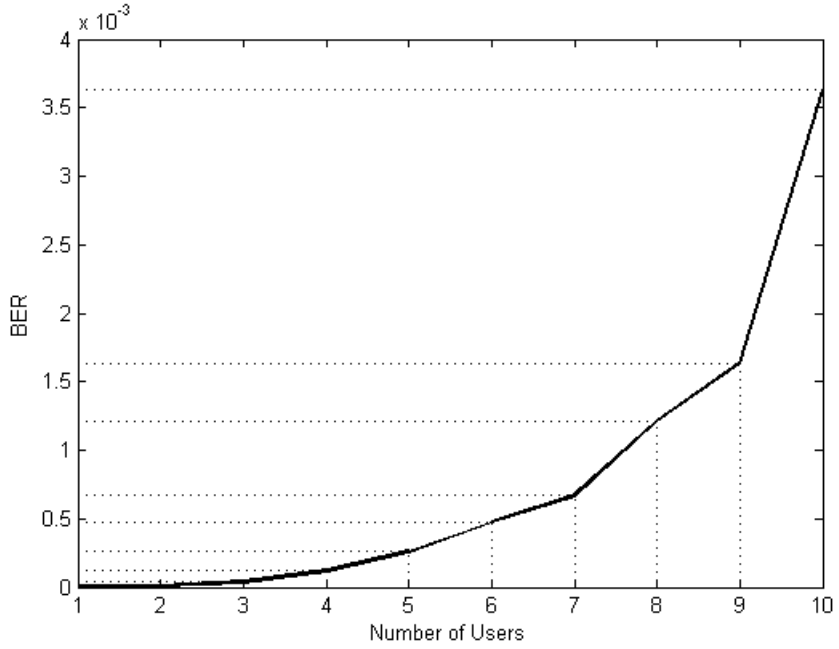

Figure 5.6 BER vs number of users at 12 dB, 30 Mbit/s, $N_s = 5$

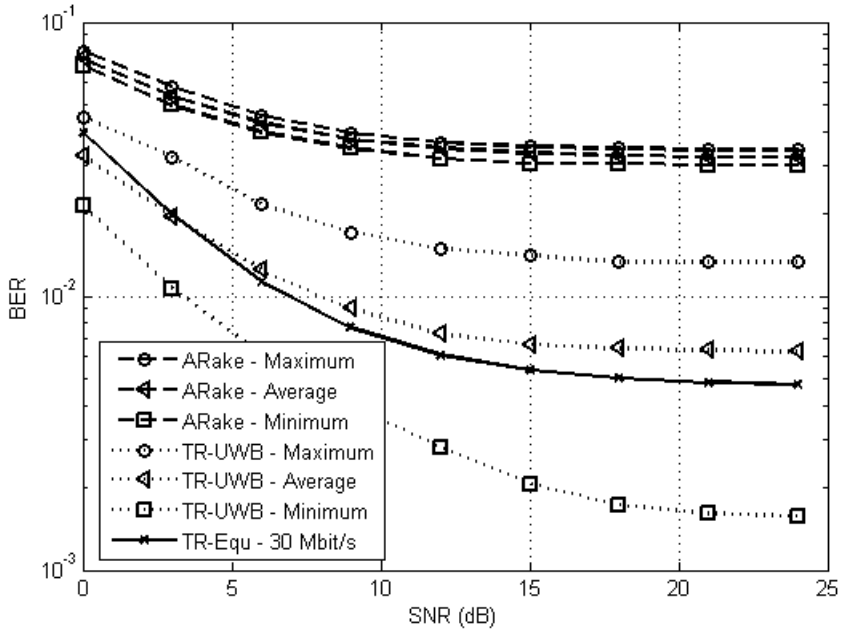

Figure 5.7 MUI BER curves with 10 user Reed-Solomon coding for TR-UWB and ARake at 30 Mbit/s, $N_s = 10$

has a much fairer error distribution, although all users having relatively worse performance than in a time reversed system.

Performance analysis for a system supporting 5 users was also tested, shown in Fig. 5.8 at a data rate of 30 Mbit/s and $N_s = 5$. This was conducted in order to verify the scalability of the derived MUI expressions over a varied number of users. Results indicate a close alignment between simulated and forumated performances when averaged over all user error rates.

To examine the performance of this system with varied hopping schemes, 'Linear Congruence' hopping codes were also adopted. Results for 1 and 10 user tests, at a data rate of 30 Mbit/s and $N_s = 5$, are shown in Fig. 5.9. The equivalence between the formulated and simulated results can be seen. While the maximum and minimum error rates for the 10 user case are not shown, an alignment with the average BER is apparent. The prevailing difference in performance between receiver-side equalization through an ARake architecture and transmitter-side equalization through a time reversed scheme is also present.

5.6 Chapter Summary and Conclusions

In this chapter, a closed-form expression for the MUI within a time-reversed UWB system was developed. As shown through simulation, MUI has a significant effect on the error performance of a UWB system. Expressions were developed for both the interference existing within the same frame as the desired signal, also within adjacent frames. Applying the Hamming cross correlation function and the separation probability profile of the time hopping code used, all overlapping transmissions were analyzed. Comparative results using an exponential estimation for the propagation channel and its square were presented. These indicated a close alignment between simulated and derived error rates for a varied number of interfering users. As in the ISI derivations, an over-approximation develops for the formulated performance as the level of interference increases.

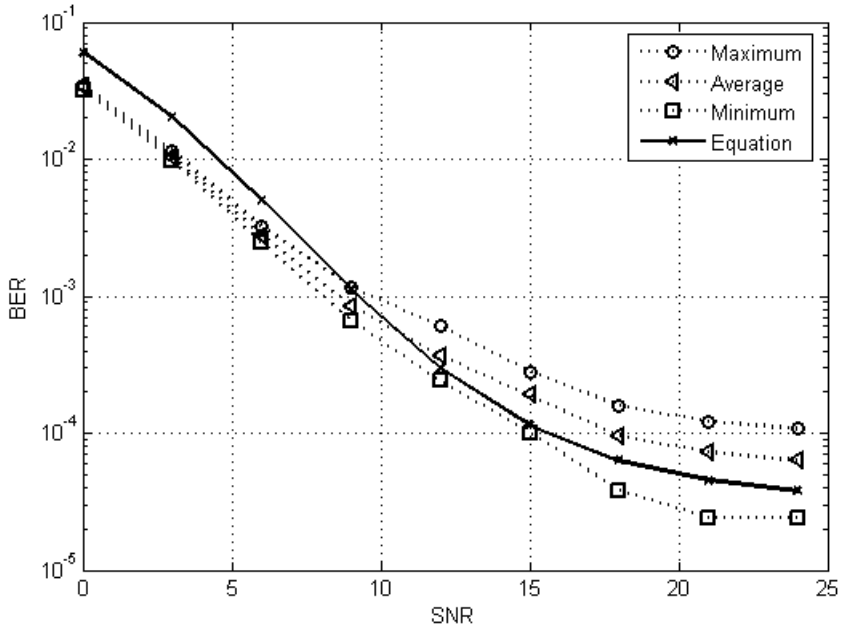

Figure 5.8 MUI BER curves with 5 user Reed-Solomon coding for TR-UWB at 30 Mbit/s, $N_s = 5$

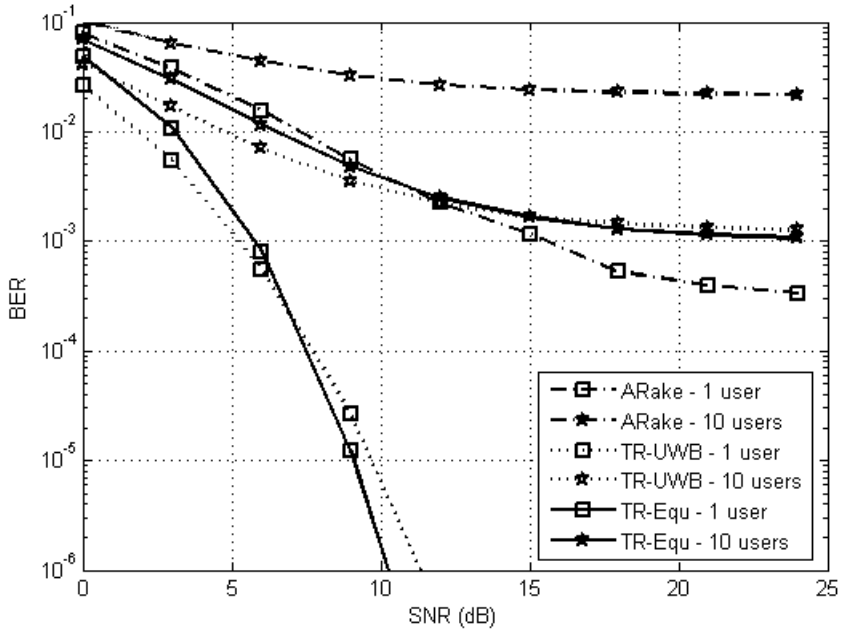

Figure 5.9 BER curves for 1 user and 10 user cases with linear congruence coding at 30 Mbit/s, $N_s = 5$

Finally, larger variances were exhibited between user error performances in a TR-UWB multi-user case when compared to a system using an ARake receiver. This exemplifies the advantages and disadvantages of a TR-UWB system. It may achieve comparatively better performance levels, although at the expense of user equality.

Chapter 6

Forward Error Correction through Turbo Coding

6.1 Introduction

Forward error correction is a common telecommunication technique, whereby a transmitter encodes redundant data into a transmission. A receiver harnesses this extra information to detect and correct propagation errors, without the need for re-transmission. Common error correction methods include serially concatenated convolutional codes [140], low-density parity check codes [141] and space-time block codes [142].

This chapter covers the application of Turbo error correction codes to a time reversed UWB system. This addition may be applied in both the binary and the non-binary form. While the conventional approach targets binary data for encoding, an alternate introduced within this chapter utilizes non-binary Turbo codes at the user multiplexing level. This thesis combines data encoding and user multiplexing stages through the use of turbo trellis coded modulation (TTCM) and a unique mapper to generate a time hopping code. Soft-input-soft-output decoding is applied, using the binary SOVA and the symbol-based SOVA algorithms. Both binary and non-binary systems are presented, together with a comparative analysis of each method's performance. Tests are conducted in single- and multi-user scenarios, and also observe the multi-user interference

effects of signals employing FEC. A final analysis is conducted on the performance gain achievable through the use of structured TTCM constellation mapping as compared to a randomly generated mapping.

In order to align the notation within this chapter with commonly accepted notation for error correction literature, the sampled transmitted and received data for an arbitrary user are represented as x_k and y_k respectively.

6.2 Binary Turbo Coding

6.2.1 Error Correction Approach

Classical turbo codes, also known as parallel concatenated convolutional codes, are based upon the principle of a recursive and systematic convolutional (RSC) encoder. Data bits are encoded through the alternate parsing between two RSC structures, separated by an interleaver. This encoding operates at the binary data level, with the output being an extended data stream with a code rate of either 1/2 or 1/3 depending on whether the system is punctured or not.

The soft-output Viterbi algorithm (SOVA) is employed in the decoding procedures presented herein. Through the use of a trellis, which restricts state transitions, the receiver is able to iteratively parse data through two SOVA component decoders. This enables the capability of transmission at near the capacity of the channel.

6.2.2 Transmitter Design

As discussed in Chapter 2, the architecture of a turbo encoder is based upon the processing of input data by two RSC encoders. These component encoders are separated by a random interleaver in order to foster independent parity output values. As depicted in Fig. 2.13, the turbo encoder operates at the binary data level altering $b_m^{(u)}$. For the following derivations, $v_k^{(s)}$ is taken as the encoder's systematic output at step k, with $v_k^{(p_1)}$ and $v_k^{(p_2)}$ representing the parity output of each RSC encoder. The parity output length of each

component encoder has the same length as the systematic component (original input sequence). In preparation for further processing, these N length output sequences are multiplexed together as:

$$\mathbf{v} = \left\{ \left(v_0^{(s)}, v_0^{(p_1)}, v_0^{(p_2)} \right), \left(v_1^{(s)}, v_1^{(p_1)}, v_1^{(p_2)} \right), ..., \left(v_{N-1}^{(s)}, v_{N-1}^{(p_1)}, v_{N-1}^{(p_2)} \right) \right\}. \quad (6.1)$$

This system has an overall code rate of $R_c = 1/3$, being a linear, systematic code. Higher data rates are achieved through puncturing of the parity elements in the output sequence, while retaining all systematic components. Taking the puncturing pattern as $P = [1\ 0; 0\ 1]$, the output sequence reduces to:

$$\mathbf{v} = \left\{ \left(v_0^{(s)}, v_0^{(p_1)} \right), \left(v_1^{(s)}, v_1^{(p_2)} \right), \left(v_2^{(s)}, v_2^{(p_1)} \right), \left(v_3^{(s)}, v_3^{(p_2)} \right), \cdots \right\}. \quad (6.2)$$

Appending the termination bits into the RSC encoder output forces the first component encoder to end in the all zero state. This provides the advantage of easily known initialization states within the receiver's trellis when conducting backward recursion. A total of γ tail bits are required to achieve this state, with γ representing the number of memory elements in the generator matrix $G(x) = [g_1, g_2]$. Each termination bit is equivalent to the binary addition of the state on all feedback lines, which is then applied as input to the RSC encoder. Feedback lines are represented by g_2 in the generator matrix.

6.2.3 Receiver Design with SOVA Decoder

The turbo receiver structure consists of separate decoding for each of the constituent codes, together with an iterative exchange of reliability information between the two component RSC decoders [103]. Taking the received vector as $\mathbf{y} \in \left(y_k^{(s)}, y_k^{(p_1)}, y_k^{(p_2)} \right)$, demultiplexing at the receiver front-end separates this into its systematic and parity components. The first decoder operates on the combination $\left(y_k^{(s)}, y_k^{(p_1)} \right)$, while the alternate on $\left(\Pi(y_k^{(s)}), y_k^{(p_2)} \right)$. The complete decoder structure is illustrated in Fig. 6.1.

Each SISO component decoder takes as input the a priori information from the alternate decoder, and also the received channel values. A priori values are initialized to a uniform neutral probability when applied as input to the

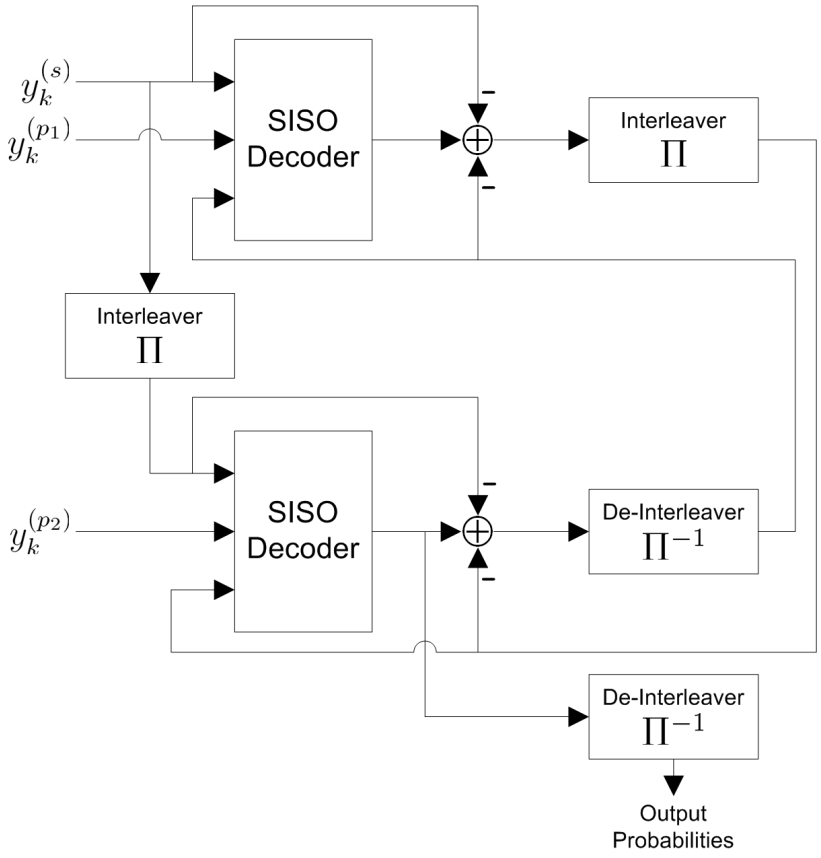

Figure 6.1 Conventional binary turbo decoder structure

first component decoder on the first iteration. The SISO decoder produces as output the extrinsic probabilities on the transmitted data, which are then permuted to give updated a priori information. This is passed to the next component decoder which operates on the next parity sub-block, together with the same systematic data. The systematic probabilities are explicitly available from channel measurements of the $v_k^{(s)}$ factor of Eq. 6.1.

Each iteration seeks to improve the log-likelihood ratio (LLR) $L(d_k)$, where d_k is the kth decoded data bit, converging to an estimate of the transmitted codeword. For a binary symmetric channel, the LLR is defined as [143]:

$$L\left(d_k\right) \triangleq \log \frac{\Pr(d_k = +1)}{\Pr(d_k = -1)}. \tag{6.3}$$

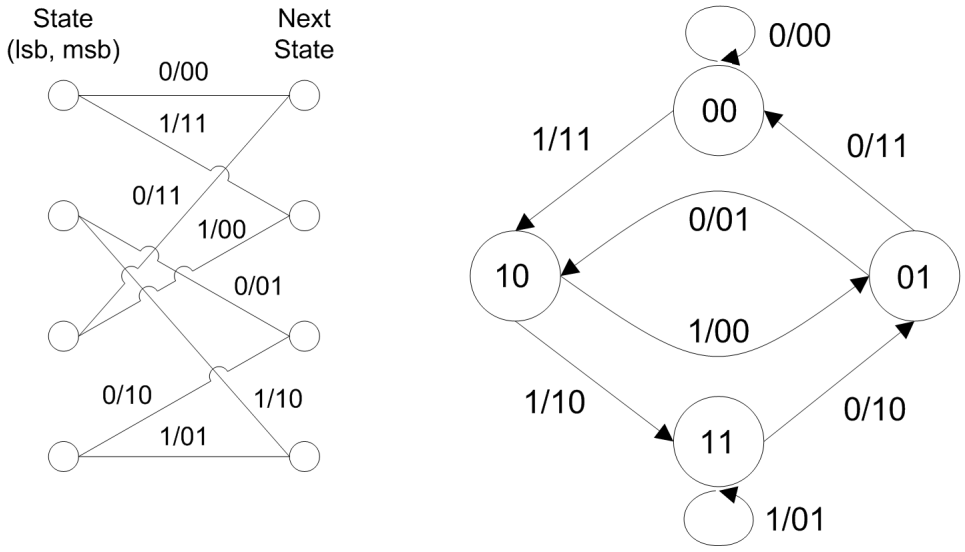

Figure 6.2 Equivalent trellis and state representations of a binary convolutional encoder

Representing the transmit energy as E_{TX}, the LLR can be reduced to:

$$L\left(d_k|\mathbf{y}\right) = \frac{E_{TX}}{2\sigma^2} 4a \cdot y_k, \tag{6.4}$$

where a is the fading amplitude, which has a value of 1 for a Gaussian channel. A 'channel reliability' parameter may be extracted as: $L_c = 4aE_{TX}/2\sigma^2$. This scaling factor is required to compensate distortion evident in the decoding algorithm caused by over-optimistic soft outputs.

Each decoder initiates the SOVA method, which extends on the Viterbi algorithm. It uses a modified path metric to take into account the a priori probabilities of the input symbols, and produces a reliability indicator to the hard decision output for each bit [108]. It analyzes Euclidean distance to determine the highest reliability path through the decoder's trellis structure. With γ memory elements in the convolutional encoder, and m inputs, there are 2^γ possible states in the trellis, with 2^m branches entering, and leaving, each state. A sample trellis diagram, together with its corresponding state diagram, is shown in Fig. 6.2, with $\gamma = 2$, $m = 1$.

The branch metric is defined as [105]:

$$\mu_t\left(y_k, p, q\right) = \log \Pr\left(y_k | B^{(p,q)}\right), \tag{6.5}$$

where $B^{(p,q)}$ represents the transition in the trellis from arbitrary states p to q. The path metric $M_t\left(q\right)$ can therefore be iteratively calculated as:

$$M_t\left(q\right) = M_{t-1}\left(p\right) + \mu_t\left(y_k, p, q\right). \tag{6.6}$$

The terms $M(\vec{S}_k^s)$ and $M(\vec{S}_k^{s'})$ are taken as the metric values of the survivor and the discarded paths terminated at states $S_k = s$ and $S_k = s'$ respectively. Applying these parameters, the incorporation of prior information transforms the path metric to:

$$M\left(\vec{S}_k^s\right) = M\left(\vec{S}_{k-1}^{s'}\right) + \frac{1}{2} d_k L\left(d_k\right) + \frac{L_c}{2} \sum_{l=1}^{n} y_k^l x_k^l, \tag{6.7}$$

where y_k^l and x_k^l represent the lth bit in the n bits of the received and transmitted signals respectively. The decoder initially sets all path metrics for all trellis states to $-\infty$. As the encoder always starts in the all zero state, the metric for the 0^{th} state at the first time instant $\left(M\left(\vec{S}_0^0\right)\right)$ is set to zero.

The metric difference between the survivor metric and each of the discarded metrics may be defined as:

$$\Delta_k^s = M\left(\vec{S}_k^s\right) - M\left(\vec{S}_k^{s'}\right) \geq 0. \tag{6.8}$$

This metric difference is subsequently equivalent to the LLR for the correct decision path, although it requires the consideration of the effects of all discarded paths. The path with minimal length through the trellis is taken as the 'survivor'. If merging paths are determined to produce equal path metrics, a random choice between the options is made.

Reliability vectors store the δ most recent metrics for each surviving path. The minimal distance path at each time instant is determined, and subsequently the bit δ units back on that path is decoded. Typically, a delay time of $\delta = 5\gamma$ is taken. This technique is illustrated in Fig. 6.3 with $\delta = 6$, such that a decision

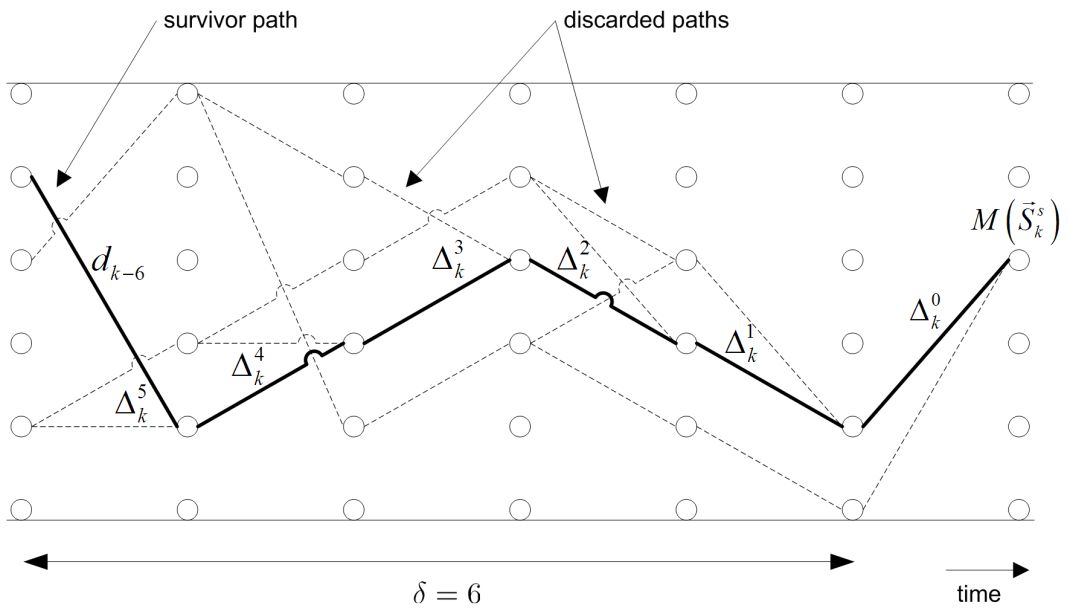

Figure 6.3 Trellis structure with SOVA metric difference decoding over δ time units

is made about bit $d_{k-\delta}$ at time k. Shown in bold is the survivor path, with the dotted paths representing those which were discarded.

The minimal metric difference over all discarded paths which produce an incorrect bit must be calculated. The bit decision reliability is dependent upon the least reliable path decision within the survivor path. This gives the final soft output for the bit d_k as [143]:

$$L(d_k|\mathbf{y}) \approx \mathbf{d_k} \min_{\substack{\mathbf{i=k\ldots k+\delta} \\ \mathbf{d_k \neq d_k^i}}} \mathbf{\Delta_i^{S_i}}. \tag{6.9}$$

Thus, the polarity of the LLR is determined by the decoded data bit, while the magnitude is equivalent to the reliability of the decision. The decoder's systematic input (y_k) is subtracted from this soft output in order to prevent the decoder acting as a positive feedback amplifier [104], giving:

$$L_e(d_k) = L(d_k|\mathbf{y}) - \mathbf{L(d_k)} - \mathbf{L_c y_k}. \tag{6.10}$$

This extrinsic information is then interleaved/deinterleaved to give the a priori information for the alternate decoder. It can be seen that the algorithm behaves

similarly to a Kalman filter. When a reliable channel is apparent, L_c is large relative to the prior reliability, such that the decoder depends more on the channel outputs. Conversely, when the propagation channel has a low signal to noise ratio, L_c is small compared to the prior reliability, and the decoder depends more on the latter.

With a punctured code, double the number of pulses will be transmitted relative to a TR-UWB system without FEC operating at the same data rate (ignoring tailing bits). For comparability, the energy level of each pulse is halved.

6.3 Non-binary Turbo Coding (TTCM)

6.3.1 Error Correction Approach

The transition from a binary turbo system to a non-binary turbo trellis coded modulation scheme requires several alterations to both the transmitter and receiver architectures. The three main alterations are [107]:

- group based interleaving over $m > 1$ bits rather than single bits;
- a changed parity puncturing method in order to achieve the desired spectral efficiency;
- and special constraints on the RSC encoders and interleaver structures.

The TTCM technique may commonly be found in conjunction with phase shift keying modulation [144]. Presented next is the application of TTCM to a UWB system, combining data modulation and user multiplexing stages. The mapping of TTCM output symbols to available chip positions may be conducted through either random or deterministic mapping sequences, and is represented by the function $\bar{\Pi}(j)$.

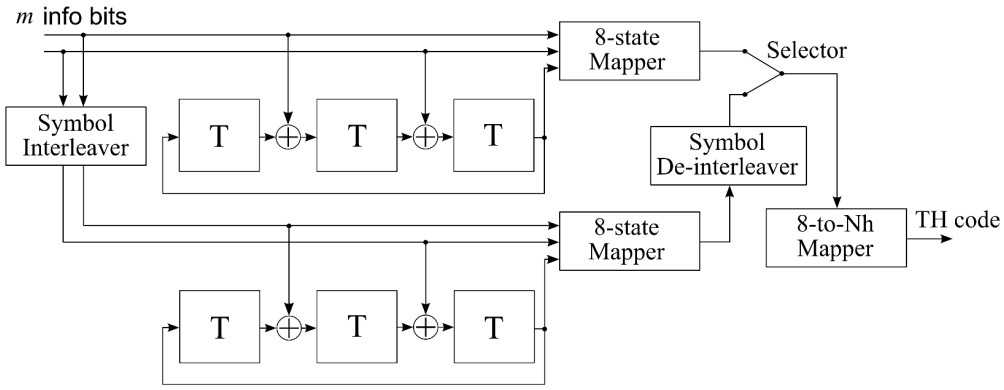

Figure 6.4 TTCM transmitter structure

6.3.2 Transmitter Design

The incorporation of a TTCM transmitter into a UWB system allows the combination of the time hopping stage with data encoding. The structure of a TTCM transmitter is illustrated in Fig. 6.4. It consists of two component RSC encoders, similarly to a conventional turbo transmitter. However, a TTCM encoder operates on m-bit-words, rather than single bit inputs. The 2^m possible inputs are encoded using a code rate of $m/m+1$, with the encoded $m+1$ bits mapped to one of $2^{(m+1)}$ constellation points [109, 113]. This thesis considers TTCM encoding encompassing $m = 2$ data bits. Therefore the $m+1$ bit output consists of two systematic bits, together with a single parity bit, and generates an 8 constellation point output. The encoder selects the symbols alternately from the two component TCM encoders, resulting in an aligned systematic component between the encoders. Consequently only the parity bit is alternately chosen, with the systematic sequence remaining static. A total of $\gamma = m + 1$ shift registers are utilized in each RSC encoder.

Constraints imposed on the component code include that no parallel transitions should exist in the corresponding trellis diagram of the convolutional encoder. This is to ensure each data bit benefits from the interleaving and parallel concatenation. Also, the information bits in an arbitrary step k should not directly influence the parity bit at step k [107]. The final restriction on the TTCM

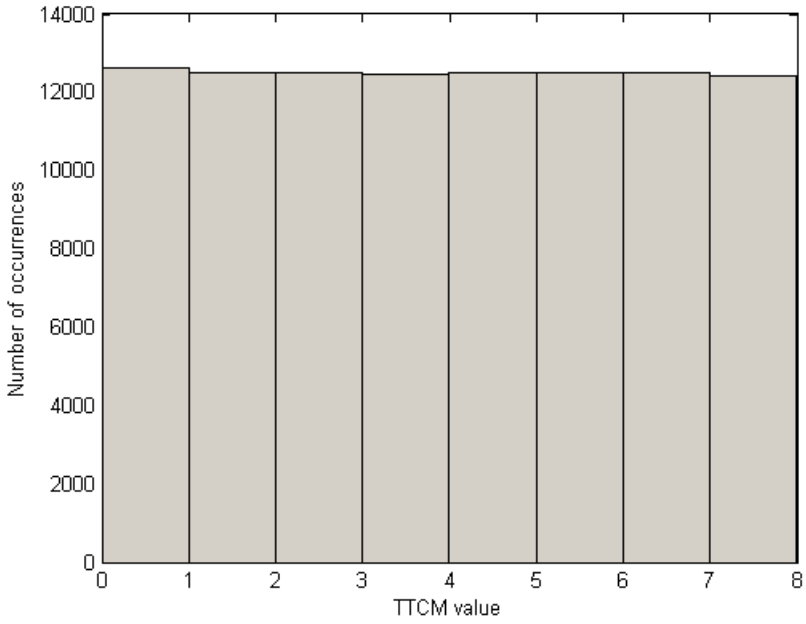

Figure 6.5 Uniform probability of TTCM symbols with a Bernoulli mix binary input stream

transmitter is that the interleaver must operate on a pairwise basis, where even blocks of m bits are mapped to even positions, and odd blocks of m bits mapped to odd positions [109, 113]. This symbol interleaver is applied on the data input before processing with the lower RSC encoder, with a de-interleaving operation conducted on the result to ensure the ordering of the systematic component between both encoders.

It can be noted in this TTCM transmitter that trellis termination is not applied, which will inevitably lead to a slight performance degradation relative to a system with termination capabilities. Also, unlike in the binary turbo coding scheme, this transmitter always applies symbol puncturing. A histogram based analysis of this punctured output, considering a random interleaver design with a Bernoulli mix input binary stream, indicates a uniform probability of the occurrence of each TTCM constellation point. Results are depicted in Fig. 6.5, averaged over 100000 instances.

The final block in the structure of Fig. 6.4 ($8-to-N_h$ Mapper) represents the

function $\bar{\Pi}(j)$, and maps the 8 possible constellation points uniquely onto the N_h possible chip positions utilized for UWB time hopping. This is required as the TTCM symbols have an even $2^{(m+1)}$ constellation range, while in conventional time hopping measures the number of chips within each frame is generally chosen as a prime value.

As simulations conducted in this thesis are chip synchronous, a random PPM shift (ε) must be applied in order to diversify the TTCM signals further. Without this added freedom, all user transmissions would be aligned at the chip level. Scattering is achieved based upon the aforementioned 8 point mapper through mapping onto GF(2).

Since $m = 2$ bits are transmitted per N_s pulses (all N_s pulses having the same chip position), the number of pulses required for data transmission is effectively halved. For comparable results with a binary FEC approach, the energy of each pulse in this TTCM system must be doubled.

6.3.3 Receiver Design with S-B-S Decoder

6.3.3.1 Decoder Structure

A TTCM receiver is similar in structure to a binary turbo coding receiver, both based upon an iterative process. However, sets of log-likelihood ratios are passed between the component decoders in the former, rather than single log-likelihoods [144]. The underlying SOVA procedure is subsequently more complex, as the systematic and extrinsic components cannot be separated due to noise simultaneously affecting the parity and systematic bits [107]. Here, the output is split into two components: the a priori information (L_a) and the combined extrinsic and systematic information ($L_{e\&s}$), with the latter being interleaved/de-interleaved and passed between alternate decoders. A 'hard' decision is conducted on the final LLRs to evaluate the symbol that was received. In order to generate valid results, a large block/interleaver size is required. The TTCM receiver structure applied is shown in Fig. 6.6.

The performance difference between MAP and SOVA decoding is significantly

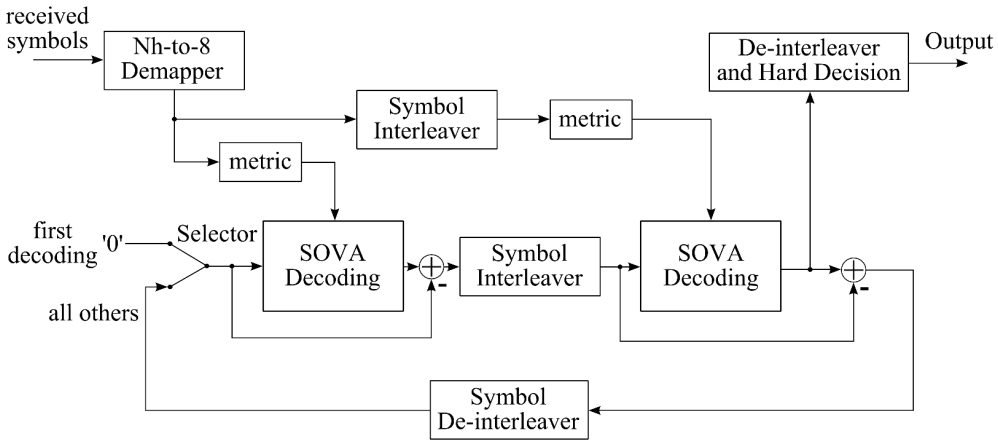

Figure 6.6 TTCM receiver structure

reduced when non-binary coding is applied [111]. The receiver structure and symbol-based SOVA with maximum sequence posteriori probability estimations discussed herein is adapted from Cong et al. [112], also Liu and Tu [113].

Transmitting through TR-UWB, the soft data that is passed to the receiver is the correlation of the received signal in each of the N_h chips with a preset template of the expected received signal. Collection of correlation values is conducted over all N_s transmitted waveforms. The 2^m possible transmission locations are then de-mapped from the N_h chips within each time frame. The required 2^m a priori values are given a zero neutral probability on the first iteration, since the transmitter utilizes puncturing between the component encoders. In contrast, the case of unpunctured encoding would set the a priori probabilities as $\Pr(d_k = i) = 1/2^m$, namely $\log(\Pr(d_k = i)) = -m\log(2)$.

6.3.3.2 Symbol Based SOVA

With γ shift registers utilized in the encoder, the state of each component encoder can be represented as $S_k \in \{0, 1, ..., 2^\gamma - 1\}$. The m bit input is denoted as $d_k \in \{0, 1, ..., 2^m - 1\}$, with received sequence $y_{1\to N} = (y_1, y_2, ..., y_N)$ shown from time 1 to N. The LLR value for each possible symbol i at time k is

calculated as:

$$L\left(d_k = i\right) \triangleq \log \frac{\Pr\left(d_k = i|y_{1\to N}\right)}{\Pr\left(d_k = 0|y_{1\to N}\right)}, \tag{6.11}$$

with the a priori information expressed as:

$$L_a\left(d_k = i\right) = \log \frac{\Pr(d_k = i)}{\Pr(d_k = 0)}. \tag{6.12}$$

Considering the time k and current state s, the cumulated path likelihood metric is represented as $M\left(\vec{S}_k^s\right) = \log\left(\Pr\left(\vec{S}_k^s, \vec{y}_{t\leq k}\right)\right)$. The vector $\vec{y}_{t\leq k}$ represents all received signals leading to and including that at time instant k. The state vector is $\vec{S}_k^s$, which identifies the states along the survivor path terminated at state $S_k = s$.

The TTCM receiver trellis thus assumes that 2^m branches with distinct symbols enter each of the 2^γ trellis nodes. The parameter $q(d_k = i|S_{k-1} = s', S_k = s)$ is defined as the probability that symbol i is associated with the transition from states $S_{k-1} = s'$ to $S_k = s$. Beginning with the metric base equation for binary SOVA shown in Eq. 6.6, and applying the simplification procedure presented in [113], the cumulated path metric may be approximated as:

$$\begin{aligned} M\left(\vec{S}_k^s\right) &= M\left(\vec{S}_{k-1}^{s'}\right) + L_c \cdot \log\left(p\left(y_k|d_k = i, S_k = s, S_{k-1} = s'\right)\right) \\ &\quad + \left[L_a(d_k = i) - \max_{i\in(0,1,\ldots,2^m-1)}(L_a(d_k = i))\right], \end{aligned} \tag{6.13}$$

for $q\left(d_k = i|S_{k-1} = s', S_k = s\right) = 1$, and:

$$M\left(\vec{S}_k^s\right) = -\infty, \tag{6.14}$$

for $q\left(d_k = i|S_{k-1} = s', S_k = s\right) = 0$. As the detected signal must be considered at all iterations, the term $\log(p(y_k|d_k = i, S_k = s, S_{k-1} = s'))$ is calculated from the soft received values. The multiplication by the channel metric L_c ensures that the reliance on received soft values is determined by the channel reliability relative to prior reliabilities.

The log likelihood ratio for each symbol is calculated through the maximum likelihood metric obtained through the Viterbi decoding on the 2^m paths entering each state. The parameter $\Gamma_{k,i}\left(\vec{S}_N^s\right)$ is defined as the reliability difference

between the maximum likelihood symbol at time k and the most likely codeword with $d_k = i$, both terminated at state S_N^s:

$$\Gamma_{k,i}\left(\vec{S}_N^s\right) = \max_{all\ \vec{S}_N^s}\left\{M\left(\vec{S}_N^s\right)\right\} - \max_{\vec{S}_N^s:d_k=i}\left\{M\left(\vec{S}_N^s\right)\right\}. \tag{6.15}$$

The LLR values can be obtained as:

$$L\left(d_k = i\right) = \Gamma_{k,0}\left(\vec{S}_N^s\right) - \Gamma_{k,i}\left(\vec{S}_N^s\right). \tag{6.16}$$

In contrast to a conventional binary turbo decoder, the calculation of the LLR values within a TTCM system accounts for multiple incorrect symbols, not just the inverse of the data bit decoded.

As in the binary SOVA procedure, to simplify calculations and limit the memory requirements at the receiver. The log-likelihood ratio $L\left(d_k = i\right)$ is estimated over $\delta = 5\gamma$ trellis increments. Each state in the trellis stores a $\delta \times 2^m$ reliability measure matrix, under the assumption that the survivor and competition paths have converged over the δ time increments. The selection of δ is dependent upon the trade-off between decoding latency and system performance.

The reliability difference between survivor and competing paths with $d_k = l$, and both terminated at state S_{t+1}^s, is denoted as:

$$\Delta_{t+1,l}^s = \max_{all\ \vec{S}_{t+1}^s}\left(\vec{S}_{t+1}^s\right) - M\left(S_{t,l}, S_{t+1}^s\right), \tag{6.17}$$

where $M\left(S_{t,l}, S_{t+1}^s\right)$ represents the cumulative path metric terminated at state S_{t+1}^s and previous state $S_{t,l}$. It can be noted that $\Delta_{t+1,l}^s = 0$ for the surviving path at state S_{t+1}^s. Initially, $\Gamma_{k,i}\left(\vec{S}_k^s\right) = \Delta_{k,i}^s$, with the remaining reliability values $\Gamma_{k,i}\left(\vec{S}_{t+1}^s\right)$ for $k = t - \delta + 2, ..., k$ updated as [112, 113]:

$$\Gamma_{k,i}\left(\vec{S}_{t+1}^s\right) = \min_{l=0,1,...,2^m-1}\left\{\Delta_{t+1,l}^s + \Gamma_{k,i}\left(\vec{S}_{t,l}\right)\right\}. \tag{6.18}$$

This iterative calculation essentially determines the minimum summation of all branch metrics which lead to a particular state, together with the complete cumulative metric up to each of the previous states. This is in correspondence to each of the possible symbol levels.

Traversal through the trellis to determine the transmitted signals is similar to the conventional binary turbo method. The most probable final state is selected (on the survivor path), and the probability of traversing to each of the survivor states is calculated assuming an alternate symbol was decoded. For the case of $m = 2$ and an 8-point symbol constellation, there are 4 input symbol levels, and thus four paths entering into each trellis state. Considering the possibility of 2^m states within the trellis, half of all decoded path metrics (when considering all possible transitions) will have a cumulated metric value of $-\infty$. As expected, this decoding is significantly more computationally exhaustive than the binary case. A major drawback is the requirement of a four dimensional reliability matrix, with proportions determined by the number of input symbols, the number of states, the recursive parameter δ, and the total number of symbols transmitted plus one. However, as the ML state is chosen after δ time increments only, and this reliability matrix is continually updated, only the next and current time increments in the trellis are required. A TTCM trellis structure with $m = 2$ is depicted in Fig. 6.7.

The reliability updating cannot be conducted over δ time units once the backwards parse through the trellis nears time $k = 0$. A limit in the number of competition paths arises, as the trellis is known to start in the $0th$ state according to the encoder initialization. A limited reliability measure is therefore taken for these $\delta - 1$ trellis increments.

The LLR value for each $d_k = i$ relative to $d_k = 0$ is subsequently estimated over δ time positions in the trellis. $L\left(d_k = 0\right)$ by definition will always give a neutral probability.

6.4 Comparative Performance Analysis

The TR-UWB simulation of Chapter 4 was utilized for simulation verification, together with a binary SOVA decoder adapted from Wu [145]. The cardinality and periodicity of each time hopping code were set to 11, with a pulse width of 0.5 ns, and a data encoding shift of 0.5 ns. Transmit power was set to 1 mW,

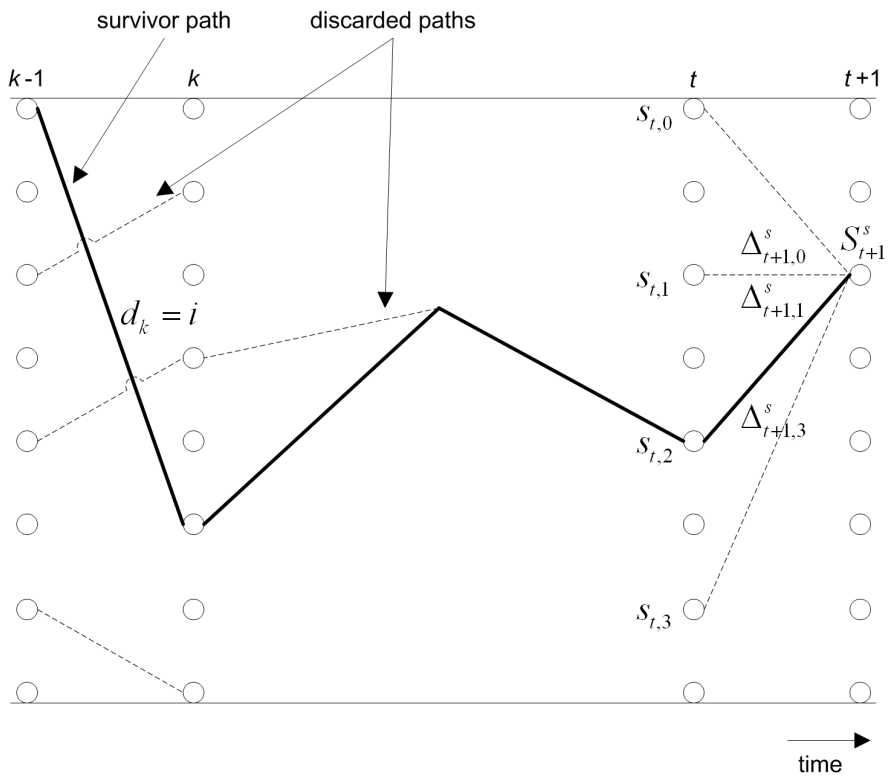

Figure 6.7 TTCM trellis structure with $2^m = 4$ input data symbols

applying the CM1 LOS scenario of the IEEE 802.15.3a UWB channel model. Random interleavers were chosen for both binary and non-binary turbo systems, with the binary system applying a puncturing pattern of $P = [1\ 0; 0\ 1]$. The binary SOVA procedure was defined by a generator matrix with $g_1 = (101)_2$ and $g_2 = (111)_2$. Reed-Solomon time hopping was applied for all cases except in TTCM simulations. The parameter $N_s = 1$ for all tests, and a block length of 400 pulses was utilized. The following results apply a randomly generated mapper $\bar{\Pi}(j)$.

The performances of a single user scenario employing binary SOVA and TTCM systems with a data rate of 50 Mbit/s are depicted in Fig. 6.8 and Fig. 6.9 respectively. The error floor for both scenarios is evident, although more prominent in TTCM. It can be seen that in a single user system, TTCM provides a performance advantage over conventional binary SOVA decoding.

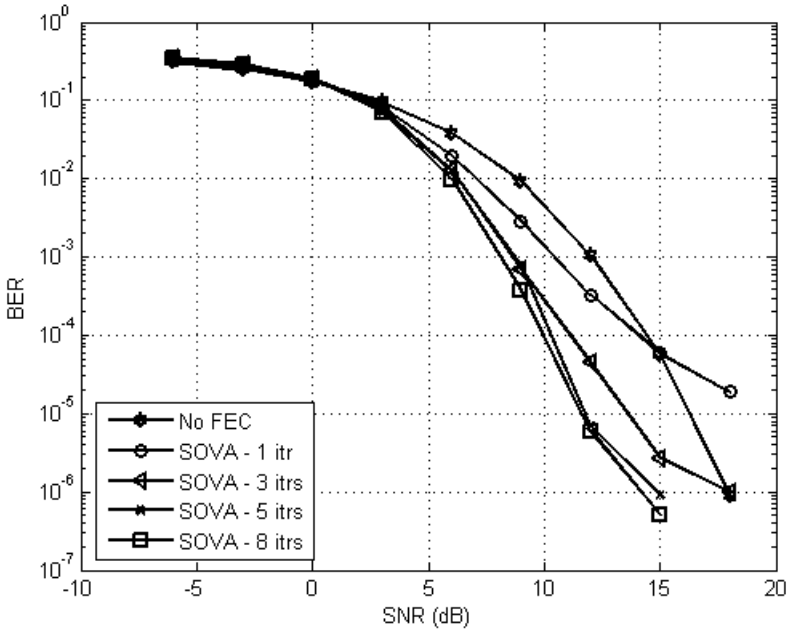

Figure 6.8 Binary SOVA scenario, 1 user performance

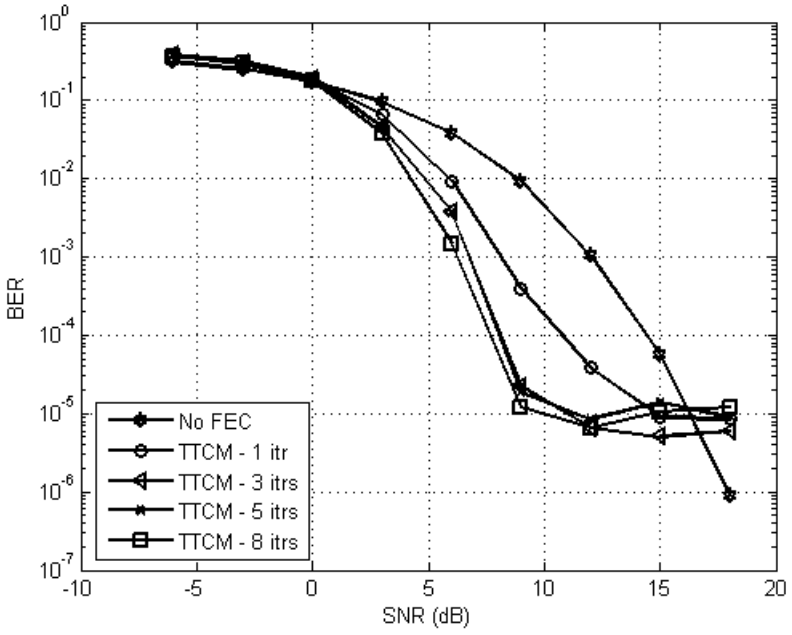

Figure 6.9 TTCM scenario, 1 user performance

Unfortunately, TTCM results exhibit a high SNR error floor as a consequence of the small block size selected. Subsequently, TTCM systems require a large interleaver size in order to overcome this performance limitation.

Shown in Fig. 6.10 and Fig. 6.11 are the bit error rates for binary SOVA and TTCM systems operating at 20 Mbit/s with 10 users applying error correction. It can be seen that multi-user interference has a greater impact on TTCM than binary SOVA, although still achieving a coding gain of over a decade for a high number of turbo iterations.

In order to observe the effects of FEC encoded signals on users not applying error correction, a 10 user system where only one user applied turbo coding was studied. Results for binary SOVA and TTCM scenarios with a data rate of 20 Mbit/s are illustrated in Fig. 6.12 and Fig. 6.13 respectively. Turbo coding was applied over 5 iterations. Although transmitting the same symbol energy, the reduced number of pulses for TTCM resulted in a larger energy per pulse. This is the cause of the larger degradation to non-turbo users relative to the effects of binary SOVA. Also, slightly worse performance was noticed for a user applying TTCM coding rather than conventional binary coding.

6.5 Structured TTCM constellation to symbol mapping

Where non-binary turbo coding modulates data to form an integer sequence, a short length random mapping has so far been applied within this chapter to develop a time hopping sequence. This section explores the possibility of mapping through the application of truncated hyperbolic congruence codes.

The link between the TTCM constellation ($[0, 2^{m+1} - 1]$) and the time hopping integer range ($[0, N_h - 1]$) is achieved through a unique memoryless mapper $\bar{\Pi}(j)$ to generate a one-to-one correspondence between the coded bits and the time hopping chip positions. Random and hyperbolic codes have previously been shown to achieve a similar BER performance in a turbo coded system for

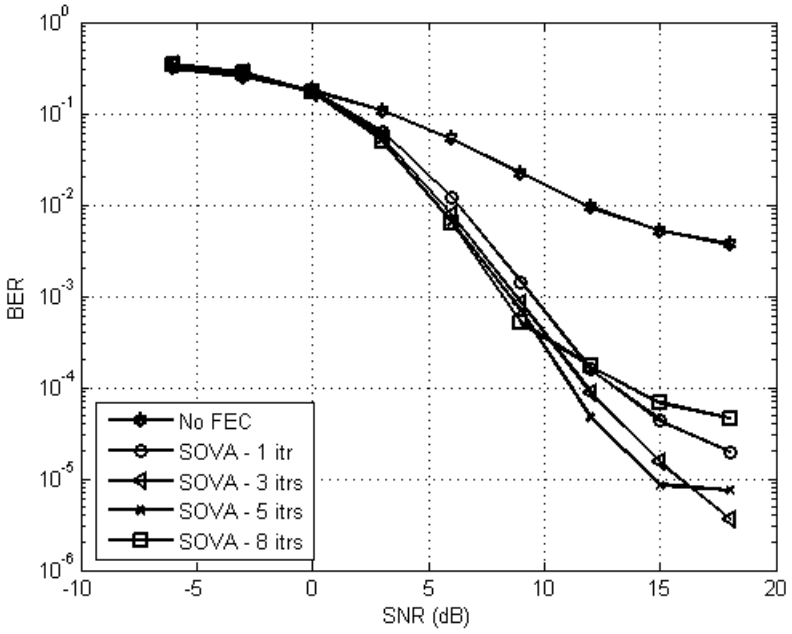

Figure 6.10 Binary SOVA scenario, 10 user performance

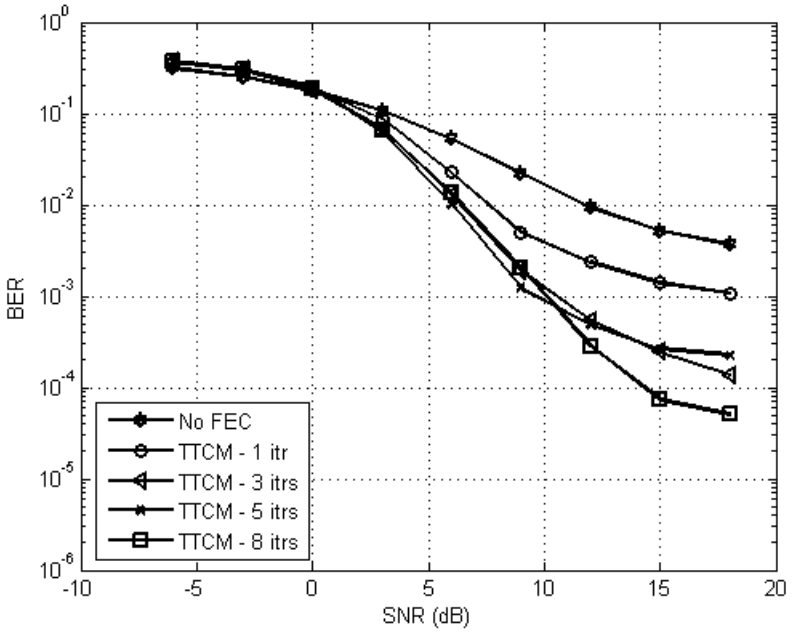

Figure 6.11 TTCM scenario, 10 user performance

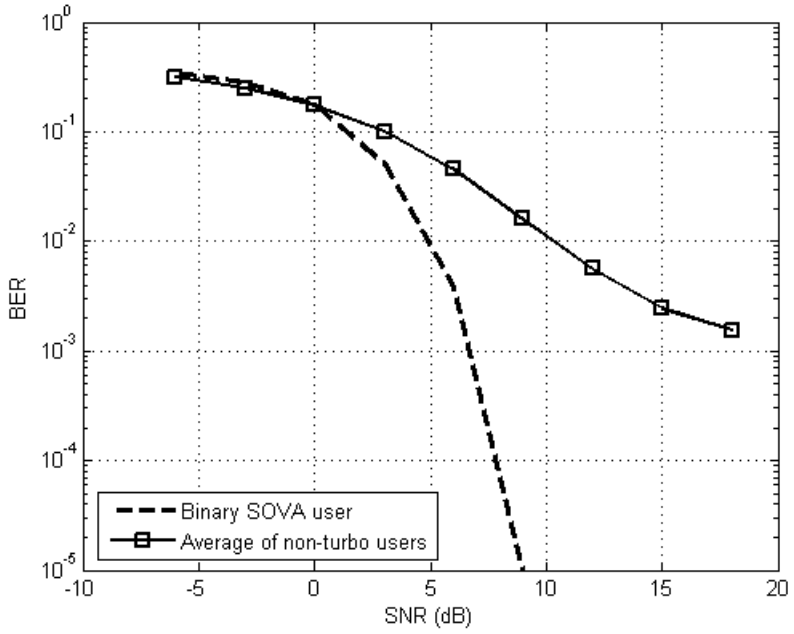

Figure 6.12 Binary SOVA scenario, 10 users with a single user applying FEC

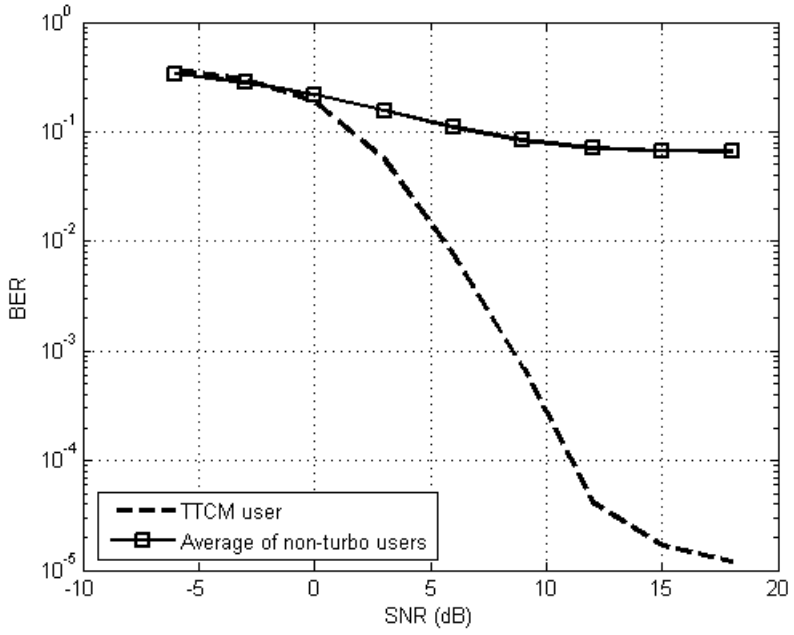

Figure 6.13 TTCM scenario, 10 users with a single user applying FEC

a high interleaver size [6]. Application herein, however, is through truncated codes shorter than the sequence periodicity. This memoryless mapper is represented as the final block in the TTCM structure ($8 - to - N_h$ Mapper). The 2^m possible transmission locations are de-mapped at the receiver through the function $\bar{\Pi}^{-1}(j)$.

A random mapping function is common, although does not provide the design advantages of deterministic codes. Various multi-user sequencing methods may be adopted, provided unique elements are generated. Although the sequence ordering is not sustained, which is vital in obtaining code orthogonality, truncated structured codes will on average obtain a more effective use of the $N_h - 8$ unused time slots over all users. Where a random mapping will uniformly select positions from the N_h possible time chips, a properly designed code family will seek a uniform chip use over all users. This subsequently leads to a uniform selection of the unused slots, thus achieving a better system performance.

This section adopts hyperbolic congruence codes for comparison with randomly selected mapping sequences. The placement operator design of these codes is presented in Chapter 3.

Simulated analysis on hyperbolic codes relative to randomly generated mapping sequences was conducted with the same parameter values as Sec. 6.4. The performances for a single user scenario are depicted in Fig. 6.14. A data rate of 50 Mbit/s was selected, with the error rate for a system not applying error correction shown for comparison. As the benefits of orthogonal sequencing only become apparent in a multi-user scenario, random and the hyperbolic mapping achieve similar error performance levels. Once again, an error floor for both scenarios is evident, which is a consequence of the small block size selected.

Shown in Fig. 6.15 are the averaged bit error rates for TTCM error correction at 20 Mbit/s with 10 equi-power users. It can be seen that for low turbo iteration levels, there is no performance gain in the use of structured codes. As the number of iterations increases, however, an average improvement of half a decade is achieved at SNR=18 dB. This indicates that system improvement does

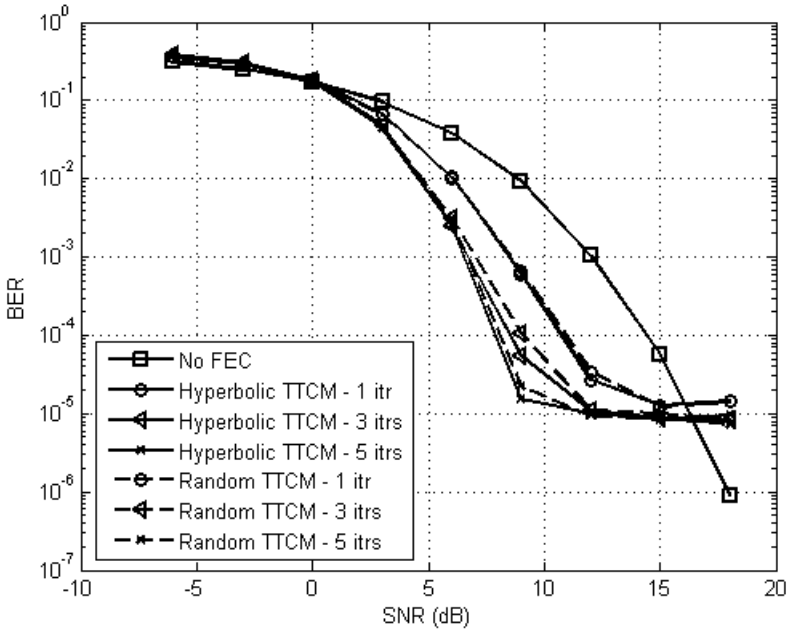

Figure 6.14 Random vs hyperbolic symbol mapping within a single user scenario

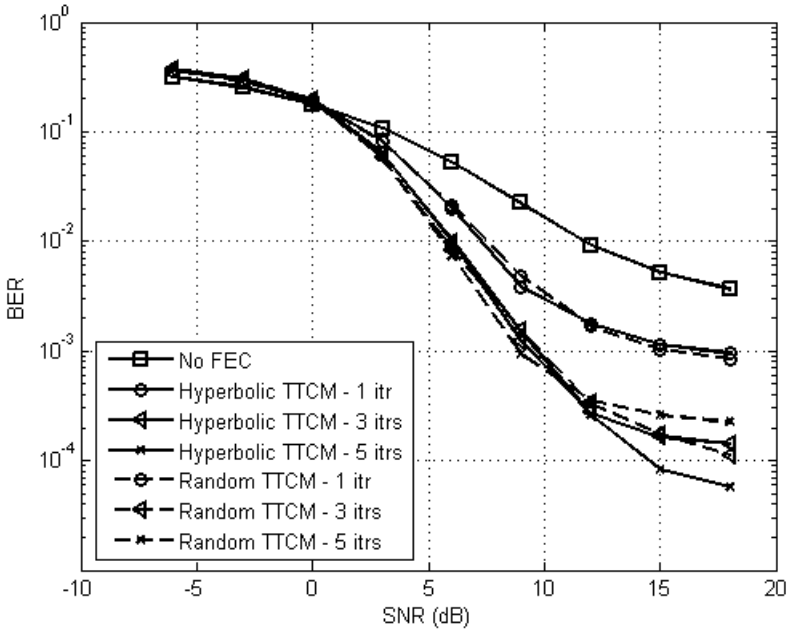

Figure 6.15 Random vs hyperbolic symbol mapping within a multi-user scenario

result from the use of structured mapping codes, which subsequently increase the free distance within the trellis decoder. Thus, with an increased number of iterations the receiver is converging closer to the correct path through the trellis.

6.6 Chapter Summary and Conclusions

The combining of user time hopping with data modulation is proposed, applying non-binary turbo codes with a symbol based decoding algorithm. It was seen that a performance improvement is possible relative to a UWB system not adopting forward error correction. In contrast to conventional binary turbo coding with a SOVA decoder, a bit error rate improvement was noticed for a low number of users, although slight performance degradations for a higher number of interfering users. Unfortunately, the increase in single pulse energy resulted in a detrimental effect to users not applying error correction.

Finally, the use of short truncated hyperbolic congruence codes for the constellation to hopping code mapping has been shown to achieve the same performance level as short length random codes in a single user system, while having the benefit of simpler design. For high traffic systems, it was shown that structured codes achieve lower error rates for higher turbo iteration levels in the receiver.

Chapter 7

Summary, Conclusions and Future Work

7.1 Introduction

This dissertation presented a thorough investigation into modern ultra wideband systems. Together with a literature review on recent developments and standardizations, several communication techniques were discussed which may be applied to achieve a performance advantage. Although requiring increased computation and processing, the expansion in complexity is generally surpassed by the performance gain possible. Ultimately, varied techniques are suited to specific conditions, whether it is the number of users, the propagation channel, or the physical device.

The major conclusions within this thesis are presented next, together with suggestions for future research. Considering the range of communication methods available in the wireless marketplace, all diversity improvements for the UWB architecture earn it a greater capability of addressing common communication issues, and subsequently a more prominent commercial appeal.

7.2 Thesis Summary and Conclusions

Chapter 1 provided a brief introduction to the considerations of this thesis and its aims. The major contributions of each chapter were discussed, together with the publications resulting from the research conducted.

Chapter 2 presented a literature review on the concept of ultra wideband communications, which has seen considerable attention in both industry and academic institutions. Seeking full standardization through the IEEE, several methods exist by which a UWB signal may be generated. Considering its unlicensed and low noise transmission means, it is a strong candidate in the wireless communications arena. Numerous user multiplexing techniques exist, applied to achieve orthogonal transmission sequencing and minimize multi-user interference. Receiver-side equalization techniques employing a RAKE architecture were studied, outlining the differences between each implementation. A transmitter-side equalization approach through a time reversed scheme was also considered. This involves a shift of the equalization complexity required to the transmitter side, which is advantageous for wireless actuator networks. Finally, forward error correction techniques to achieve receiver-side rectification of transmission errors was discussed in terms of both binary and non-binary methods. Binary techniques are increasingly popular and widely accepted, although non-binary methods such as TTCM also have promising properties. TTCM may be applied to combine data modulation with time hopping coding, re-constructing the transmitter and receiver models.

Chapter 3 considered the effects of multi-user interference in modern communication systems. Orthogonal sequencing through time, frequency, and direct sequence domains was researched, each with varied correlation measures. Sequence characterization through a separation probability profile was introduced, exhibiting the same characteristic similarities between sequences as noticed through conventional correlation measures. After presenting numerous sequence constructions over all domains, a comparative analysis of ten designs was given. Results reveal that for a system with low levels of utilization, short

periodicity deterministic codes attain a similar performance to randomly generated sequences. However, within a fully utilized system deterministic codes slightly out-perform random sequences with short length. Lastly, similarities between random and deterministic codes for a large sequence length were exemplified in the design of a UWB chip interleaver.

Chapter 4 presented preliminary and closed-form expressions for the ISI within a time-reversed UWB system. Overlapping transmissions were analyzed considering the expected signal overlap and subsequent probability of its occurrence. This latter probability was determined through the 'separation probability' profile, which characterizes a family of hopping codes. This closed-form solution only requires the calculation of the $4th$ moment of the channel response envelope to be developed. Comparative results of the derived formulae were presented, using an exponential estimation of the channel envelope. A close alignment between simulated and error curves was evident, although a slight over-approximation develops for the formulated performance as the level of interference increases. Performance similarities between a time reversed UWB system and an ARake based architecture were studied within an ISI-free scenario. Within ISI degraded systems, however, TR-UWB was noted to effectively mitigate the subsequent interference caused.

Chapter 5 presented preliminary and closed-form expressions for the MUI within a time-reversed UWB system. Multi-user interference was shown to have a very significant effect on performance, considerably more than that caused by ISI. Expressions were developed for the interference within the same frame as the desired signal, and also within adjacent frames. Both the Hamming cross-correlation function and the separation probability profile were employed in the development of these closed-form MUI expressions. Comparative results of the derived formulae against a simulated multi-user system were given. Although a close correspondence was evident, an over-approximation within the formulated expressions was noticed as the level of interference increased. Finally, larger variances were exhibited between users adopting a TR-UWB architecture relative to an ARake receiver. While TR-UWB may achieve a better performance

compared to the ARake case, it does so at the expense of user performance equality.

Chapter 6 discussed the proposition of combining user multiplexing with the data modulation stage. This was conducted through the use of non-binary turbo codes with a symbol based decoding algorithm. A performance improvement was evident relative to a UWB system not adopting forward error correction. Comparison with a conventional binary turbo coding scheme employing a SOVA decoder showed a performance improvement for a low number of users. Unfortunately, a slight performance degradation was evident for a higher number of interfering transmitters. The increase in pulse energy due to this error control was also noted to degrade the performance of users not applying error correction. Finally, although common to use short random hopping codes for the constellation to hopping code mapping, it was shown that the same performance level could be achieved using short length truncated hyperbolic congruence codes in a single user system. These deterministic codes have the advantage of simpler design relative to randomly generated sequences. It was also shown that for high traffic systems, the use of deterministic codes provides lower error rates for higher turbo iteration levels in the receiver.

7.3 Future Work

Further research that may be conducted to elaborate the work encompassed within this thesis includes:

1. extending the range of multi-user sequencing methods analyzed. Although the majority of near orthogonal constructions have approximately identical auto- and cross-correlation results, a sequence design which achieves the triangular separation profile characteristic to long random codes would provide optimal multiplexing performance. The comparative performance of sequence constructions for a varied number of pulses per bit may also be examined;

2. researching the application of varied propagation channel estimates, where an exponential estimation was adopted within this dissertation. Considering more features of the channel impulse response improves the accuracy of ISI and MUI derivations. While the LOS channel scenario of the 802.15.3a protocol was tested for this thesis, the remaining three scenarios may also be applied to observe the performance of UWB systems in NLOS environments;

3. observing the effects of non-perfectly power controlled systems on multi-user performance. Equi-power user transmissions were considered within this thesis for the ease of derivation, although dominant and overwhelming signal transmissions are a significant concern for all wireless communication systems;

4. the strategic design of pairwise interleavers for a TTCM encoder. Proper interleaver design is capable of providing considerable performance gains relative to randomly generated structures. Trellis termination for non-binary systems may also be researched, as this feature has been shown to achieve better performance levels within binary systems;

5. and finally the examining of a UWB system with TTCM integration which has the number of chip positions per time frame equivalent to the output constellation range of the turbo encoder. For comparability, the range of chip positions within this thesis was set to a prime value, as the majority of orthogonal sequence constructions rely on this property. This required a memoryless mapper to be employed for the TTCM assimilation, always leaving several chips unoccupied. A UWB design which has full use of all available chip positions may provide a greater performance gain for the TTCM decoder, and ultimately lead to an increased viability of UWB communications.

Bibliography

[1] X. Shen, M. Guizani, R. C. Qiu, and T. Le-Ngoc, *Ultra-wideband - Wireless Communications and Networks*. West Sussex, England: John Wiley & Sons, 2006.

[2] T. W. Barrett, "History of ultrawideband (uwb) radar & communications: Pioneers and innovators," in *Progress in Electromagnetics Symposium 2000 (PIERS2000)*, July 2000.

[3] M. Z. Win and R. A. Scholtz, "Impulse radio: How it works," in *IEEE Communications Letters*, vol. 2, no. 2. IEEE, Feb 1998, pp. 36–38.

[4] ITU, "Measurement techniques of emissions from devices using uwb technology," Task Group 1/8: WG4 - Measurement - International Telecommunication Union Radiocommunication Study Groups, June 2004, document 1-8/TEMP/40-E.

[5] K. Popovski, B. J. Wysocki, and T. A. Wysocki, "Performance comparison of uwb hopping codes in a multi-user rich scattering environment," in *63rd Vehicular Technology Conference*, vol. 4, Spring 2006, pp. 1864–1868.

[6] M. M. Pietrzyk, K. Popovski, T. A. Wysocki, B. J. Wysocki, and J. H. Weber, "Scarcely populated uwb-ir systems with interleaved coding-modulation on multipath fading channels," in *The 2006 IEEE 2006 International Conference on Ultra-Wideband*, September 2006, pp. 55–60.

[7] ——, "Multi-user uwb-ir systems with interleaved coding-modulation on multipath fading channels," in *The Institution of Engineering and Tech-*

nology Forum on Waveform Diversity and Design in Communications, Radar and Sonar, November 2006, pp. 91–98.

[8] M. M. Pietrzyk, K. Popovski, T. A. Wysocki, B. Wysocki, and J. H. Weber, "On the performance of scarcely populated coded uwb-ir systems on multipath fading channels," in *27th Symposium on Information Theory in the Benelux*, June 2006, pp. 235–242.

[9] K. Popovski, B. J. Wysocki, and T. A. Wysocki, "Modelling and comparative performance analysis of a time-reversed uwb system," *EURASIP Journal on Wireless Communications and Networking*, vol. 2007, pp. Article ID 71 610, 11 pages, 2007, doi:10.1155/2007/71610.

[10] K. Popovski, T. A. Wysocki, and B. J. Wysocki, "Closed-form derivations of isi and mui for time-reversed ultra wideband," in *International Conference on Signal Processing and Communication Systems (9th International Symposium on DSP and Communication Systems, DSPCS2007, and 6th Workshop on the Internet, Telecommunications and Signal Processing, WITSP'2007*, December 2007.

[11] ——, "A closed-form derivation of self and multi-user interference for time-reversed uwb communications," in *Accepted in Elsevier Special Issue of the Computers & Electrical Engineering Journal*, 2008.

[12] ——, "Combined user multiplexing and data modulation through non-binary turbo codes for uwb," in *to appear in WCNC'08*, 2008.

[13] ——, "Truncated hyperbolic mapping for non-binary turbo coding in uwb," in *Submitted to IEEE International Symposium on Personal, Indoor and Mobile Radio Communications (PIMRC)*, 2008.

[14] R. C. Qiu, H. Liu, and X. Shen, "Ultra-wideband for multiple access communications," *IEEE Communications Magazine*, vol. 43, no. 2, pp. 80 – 87, February 2005.

[15] K. Siwiak and D. McKeown, *Ultra-wideband radio technology.* West Sussex, England: John Wiley & Sons, 2004.

[16] FCC, "Revision of part 15 of the commission's rules regarding ultra-wideband transmission systems," Document 00-163, ET Docket No. 98-153, April 2002. [Online]. Available: www.fcc.gov/Bureaus/Engineering_Technology/Orders/2002/fcc02048.pdf

[17] M.-. G. D. Benedetto and G. Giancola, *Understanding Ultra Wide Band - Radio Fundamentals*. Prentice Hall, 2004.

[18] A. Batra, J. Balakrishnan, G. R. Aiello, J. R. Foerster, and A. Dabak, "Design of a multiband ofdm system for realistic uwb channel environments," in *IEEE Transactions on Microwave Theory and Techniques*, vol. 52, no. 9, September 2004, pp. 2123 – 2138.

[19] J. Bellorado, S. S. Ghassemzadeh, L. J. Greenstein, T. Sveinsson, and V. Tarokh, "Coexistence of ultra-wideband systems with ieee-802.11 a wireless lans," in *IEEE Global Telecommunications Conference*, vol. 1, December 2003, pp. 410 – 414.

[20] WiMedia, November 2007. [Online]. Available: http://www.wimedia.org

[21] G. Hiertz, Y. Zang, J. Habetha, and H. Sirin, "Multiband ofdm alliance - the next generation of wireless personal area networks," in *2005 IEEE/Sarnoff Symposium on Advances in Wired and Wireless Communication*, April 2005, pp. 208 – 214, 10.1109/SARNOF.2005.1426547.

[22] A. H. Tewfik and E. Saberinia, "High bit rate ultra-wideband ofdm," in *Global Telecommunications Conference*, vol. 3, November 2002, pp. 2260 – 2264.

[23] S. Lemon, "Standards deadlock hits uwb - the market will have to decide," IDG News Service, May 2005. [Online]. Available: http://www.techworld.com/

[24] E. Saberinia and A. H. Tewfik, "Multi-user uwb-ofdm communications," in *IEEE Pacific Rim Conference on Communications, Computers and Signal Processing*, vol. 1, August 2003, pp. 127 – 130.

[25] J. Balakrishnan, A. Batra, and A. Dabak, "A multi-band ofdm system for uwb communication," in *IEEE Conference on Ultra Wideband Systems and Technologies*, November 2003, pp. 354 – 358.

[26] S. Deffree, "No standard for ultra wideband comms," Electronic News, ElectronicsWeekly.com, 20th January 2006.

[27] HiddenWires, "Haier corporation and freescale semiconductor unveil world's first uwb-enabled consumer tv," http://hiddenwires.co.uk/, 27th June 2005.

[28] B. W. E. Magazine, "Ds-ofdm ultrawideband modulation technique wins approval from fcc," 15th December 2006.

[29] M. Hamalainen, V. Hovinen, R. Tesi, J. Iinatti, and M. Latva-aho, "On the uwb system coexistence with gsm900, umts/wcdma, and gps," *IEEE Journal on Selected Areas in Communications*, vol. 20, no. 9, pp. 1712 – 1721, December 2002.

[30] T. Erseghe, "Time-hopping patterns derived from permutation sequences for ultra-wide-band impulse-radio applications," in *In Proceedings of 6th WSEAS International Conference on Communications*, University di Padova, July 2002, pp. 109–115. [Online]. Available: http://primo.ismb.it/firb/docs/uwb-wseas02.pdf

[31] R. Z. Scholtz, "Multiple access with time-hopping impulse modulation," in *Military Communications Conference*, vol. 2, October 1993, pp. 447 – 450.

[32] J. D. Choi and W. E. Stark, "Performance of ultra-wideband communications with suboptimal receivers in multipath channels," *IEEE Journal on Selected Areas in Communications*, vol. 20, no. 9, pp. 1754–1766, December 2002.

[33] M. S. Iacobucci and M. G. D. Benedetto, "Multiple access design for impulse radio communication systems," in *IEEE International Conference on Communications*, vol. 2, April 2002, pp. 817 – 820.

[34] F. Heliot, M. Ghavami, R. Nakhai, and A. H. Aghvami, "Performance of space-time block coding and space-time trellis coding for impulse radio," in *IEEE Global Telecommunications Conference*, vol. 5, no. 29, November 2004, pp. 3225–3229.

[35] J. A. Salehi, "Code division multiple-access techniques in optical fiber networks. i. fundamental principles," *IEEE Transactions on Communications*, vol. 37, no. 8, pp. 824 – 833, August 1989.

[36] A. Swami, B. Sadler, and J. Turner, "On the coexistence of ultra-wideband and narrowband radio systems," in *Military Communications Conference, Communications for Network-Centric Operations: Creating the Information Force*, vol. 1, October 2001, pp. 16–19.

[37] H. J. Park, M. J. Kim, Y. J. So, Y. H. You, and H. K. Song, "Uwb communication system for home entertainment network," *IEEE Transactions on Consumer Electronics*, vol. 49, no. 2, pp. 302 – 311, May 2003.

[38] E. H. K. Yeung and K. Mitchell, "Modelling of ultra-wideband (uwb) radio system," University College London, April 2005. [Online]. Available: www.ee.ucl.ac.uk/lcs/papers2002/LCS040.pdf

[39] B. Parr, B. Cho, K. Wallace, and Z. Ding, "A novel ultra-wideband pulse design algorithm," in *IEEE Communications Letters*, vol. 7, no. 5, May 2003, pp. 219 – 221.

[40] L. Bin, E. Gunawan, and L. C. Look, "On the ber performance of th-ppm uwb using parr's monocycle in the awgn channel," in *IEEE Conference on Ultra Wideband Systems and Technologies*, November 2003, pp. 403 – 407.

[41] J. Foerster, "Channel modelling sub-committee report - final," IEEE 802.15.SG3a, Tech. Rep., December 2002.

[42] A. Saleh and R. Valenzuela, "A statistical model for indoor multipath propagation," *IEEE Journal on Selected Areas in Communications*, vol. 5, no. 2, pp. 128–137, February 1987.

[43] R. Rappaport, *Wireless Communications: Theory and Practice*, N. Englewood Cliffs, Ed. Prentice Hall, 1995.

[44] B. Hu and N. Beaulieu, "Comparison of modulation schemes and rake receiver structures for uwb systems on an ieee 802.15.3 indoor channel," in *Global Telecommunications Conference*, vol. 6, November 2005, pp. 3493 – 3497.

[45] G. Yue, L. Ge, and S. Li, "Performance of uwb time-hopping spread-spectrum impulse radio in multipath environments," in *Vehicular Technology Conference*, vol. 3, April 2003, pp. 1644–1648.

[46] J. G. Proakis and M. Salehi, *Communication Systems Engineering*, 2nd ed. Prentice Hall, New Jersey, USA, 2002.

[47] J. G. Proakis, *Digital Communications*, 4th ed., U. New York, Ed. McGraw-Hill Companies, Inc., 2001.

[48] M. Z. Win and R. A. Scholtz, "Ultra-wide bandwidth time-hopping spread-spectrum impulse radio for wireless multiple access communications," *IEEE Transactions on Communications*, vol. 48, no. 4, pp. 679–691, April 2000.

[49] G. Durisi and G. Romano, "On the validity of gaussian approximation to characterize the multiuser capacity of uwb th-ppm," in *IEEE Conference on Ultra Wideband Systems and Technologies*, May 2002, pp. 157–161.

[50] J. R. Foerster, "The performance of a direct-sequence spread ultra-wideband system in the presence of multipath," in *IEEE Conference on Ultra Wideband Systems and Technologies*, May 2002, pp. 87–91.

[51] J. Fiorina and W. Hachem, "On the asymptotic distribution of the correlation receiver output for time-hopped uwb signals," *IEEE Transactions on Signal Processing*, vol. 54, no. 7, pp. 2529–2545, July 2006.

[52] J. Fiorina and D. Domenicali, "Revisiting th-ir-uwb performance limits dependency on essential system parameters using the generalized gaussian

approximation," in *IEEE International Conference on Ultra-Wideband*, September 2007, pp. 751 – 754.

[53] J. Fiorina, "Elaboration of a simple receiver adapted to multi-user interferences in impulse radio ultra wide band," in *IEEE Globecom*, November 2006.

[54] R. A. Scholtz, P. V. Kumar, and C. C. Bravo, "Some problems and results in ultra-wideband signal design," in *in Proc. SETA'01*, May 2001.

[55] S. Gezici, H. Kobayashi, H. V. Poor, and A. F. Molisch, "Performance evaluation of impulse radio uwb systems with pulse-based polarity randomization in asynchronous multiuser environments," in *IEEE Wireless Communications Networking Conference*, March 2004, atlanta.

[56] S. B. Wicker and V. K. Bhargava, *Reed-Solomon Codes and Their Applications*, N. York, Ed. Institute of Electrical and Electronics Engineers, 1994, chapters 1 & 9.

[57] I. Guvenc and H. Arslan, "Design and performance analysis of th sequences for uwb-ir systems," in *Wireless Communications and Networking Conference*, vol. 2, March 2004, pp. 914–919.

[58] I. Guvenc, H. Arslan, S. Gezici, and H. Kobayashi, "Adaptation of multiple access parameters in time hopping uwb cluster based wireless sensor networks," in *Proc. IEEE 1st International Conference on Mobile Ad-hoc and Sensor Systems*, October 2004, pp. 235–244.

[59] J. Bellorado, S. S. Ghassenzadeh, A. Kavcic, B. Tarokh, and V. Tarokh, "Time-hopping sequence design for narrowband interference suppression," in *Vehicular Technology Conference*, vol. 6, September 2004, pp. 3925 – 3929.

[60] F. Ramirez-Mireles and R. Scholtz, "Multiple-access with time hopping and block waveform ppm modulation," in *IEEE International Conference on Communications*, vol. 2, June 1998, pp. 775 – 779.

[61] Z. Zhang, F. Zeng, and L. Ge, "Two-stage time-hopping sequences with zero correlation zone for quasi-synchronous thss-uwb systems," in *IEEE International Conference on Acoustics, Speech, and Signal Processing*, vol. 3, March 2005, pp. 609 – 612.

[62] N. Suehiro, "A signal design without co-channel interference for approximately synchronized cdma system," *IEEE Journal on Selected Areas in Communications*, vol. 12, pp. 837–841, June 1994.

[63] J. Cha, N. Hur, K. Moon, and C. Lee, "Zcd-uwb system using enhanced zcd codes," in *International Workshop on Ultra Wideband Systems, joint with Conference on Ultrawideband Systems and Technologies*, May 2004, pp. 371 – 375.

[64] F. Xeng, Z. Zhang, and L. Ge, "Theoretical limit on two dimensional generalized complementary orthogonal sequence set with zero correlation zone in ultra wideband communications," in *International Workshop on Ultra Wideband Systems, joint with Conference on Ultrawideband Systems and Technologies*, May 2004, pp. 197 – 201.

[65] X. Wang and P. Fan, "A class of frequency hopping sequences with no hit zone," in *Proceedings of the Fourth International Conference on Parallel and Distributed Computing, Applications and Technologies*, August 2003, pp. 896 – 898.

[66] Z. Zhang, F. Zeng, and L. Ge, "Time-hopping sequences with zero correlation zone for approximately synchronized thss-uwb systems," in *The Ninth International Conference on Communications Systems*, September 2004, pp. 20 – 24.

[67] G. M. Maggio, D. Laney, F. Lehmann, and L. Larson, "A multi-access scheme for uwb radio using pseudo-chaotic time hopping," in *IEEE Conference on Ultra Wideband Systems and Technologies*, May 2002, pp. 225–230.

[68] G. M. Maggio, N. Rulkov, and L. Reggiani, "Pseudo-chaotic time hopping for uwb impulse radio," *IEEE Transactions on Circuits and Systems*, vol. 48, no. 12, pp. 1425–1435, December 2001.

[69] T. Yang and L. O. Chua, "Chaotic impulse radio: A novel chaotic secure communication system," *International Journal of Bifurcation and Chaos*, vol. 10, no. 2, pp. 345–357, 2000.

[70] D. C. Laney, G. M. Maggio, F. Lehmann, and L. Larson, "Multiple access for uwb impulse radio with pseudochaotic time hopping," *IEEE Journal on Selected Areas in Communications*, vol. 20, no. 9, pp. 1692–1700, December 2002.

[71] J. M. Sushchik, N. Rulkov, L. Larson, L. Tsimring, H. Abarbanel, K. Yao, and A. Volkovskii, "Chaotic pulse position modulation: A robust method of communicating with chaos," *IEEE Communication Letters*, vol. 4, no. 4, pp. 128–130, April 2000.

[72] Y. Zhang and A. K. Brown, "Complex multipath effects in uwb communication channels," in *IEE Proceedings on Communications*, vol. 153, no. 1, February 2006, pp. 120 – 126.

[73] J. M. Cramer, R. A. Scholtz, and M. Z. Win, "Spatio-temporal diversity in ultra-wideband radio," in *IEEE Wireless Communications and Networking Conference*, vol. 2, September 1999, pp. 888 – 892.

[74] M. Coates and I. Psaromiligkos, "Evaluating average causal effect using wireless sensor networks," in *Proc. IEEE ICASSP Proceedings*, May 2004.

[75] M. E. R. Laboratories, "Wireless sensor networks." [Online]. Available: http://www.merl.com/projects/sensornet/

[76] E. Zurich, "Btnodes - a distributed environment for prototyping ad hoc networks," 2005. [Online]. Available: http://www.btnode.ethz.ch/

[77] R. Kling, R. Adler, J. Huang, V. Hummel, and L. Nachman, "Intel mote: Sensor network technology for industrial applications,"

Intel Corporation, 2005. [Online]. Available: http://dawn.cs.umbc.edu/INFOCOM2005/kling-abs.pdf

[78] M. Z. Win and Z. A. Kostic, "Virtual path analysis of selective rake receiver in dense multipath channels," in *IEEE Communication Letters*, vol. 3, November 1999, pp. 308–310.

[79] H. R. Ahmadi and M. Nasiri-Kenari, "Performance analysis of time-hopping ultra-wideband systems in multipath fading channels (uncoded and coded schemes)," in *The 13th IEEE International Symposium on Personal, Indoor and Mobile Radio Communications*, vol. 4, September 2002, pp. 1694 – 1698.

[80] M. Chen and X. Li, "Transmitter-based channel equalization and mui suppression for uwb systems," in *Proceedings of the International Conference on Modern Problems of Radio Engineering, Telecommunications and Computer Science*, February 2004, pp. 501 – 504.

[81] M. Z. Win and R. A. Scholtz, "On the energy capture of ultrawide bandwidth signals in dense multipath environments," in *IEEE Communication Letters*, vol. 2, no. 9, September 1998, pp. 245–247.

[82] ——, "Characterization of ultra-wide bandwidth wireless indoor channels: A communication-theoretic view," *IEEE Journal on Selected Areas in Communications*, vol. 20, no. 9, pp. 1613–1627, December 2002.

[83] B. Hu and N. Beaulieu, "Comparison of modulation schemes and rake receiver structures for uwb systems on an ieee 802.15.3 indoor channel," in *Global Telecommunications Conference*, vol. 6, November 2005, pp. 3493 – 3497.

[84] K. Usuda, H. Zhang, and M. Nakagawa, "Pre-rake performance for pulse based uwb system in a standardized uwb short-range channel," in *Wireless Communications and Networking Conference*, vol. 2, March 2004, pp. 920–925.

[85] T. Strohmer, M. Emami, J. Hansen, G. Papanicolaou, and A. J. Paulraj, "Application of time-reversal with mmse equalizer to uwb communications," in *Global Telecommunications Conference*, vol. 5, November 2004, pp. 3123–3127.

[86] G. F. Edelmann, T. Akal, W. S. Hodgkiss, S. Kim, W. A. Kuperman, and H. C. Song, "An initial demonstration of underwater acoustic communication using time reversal," *IEEE Journal of Oceanic Engineering*, vol. 27, no. 3, pp. 602–609, July 2002.

[87] M. Fink, "Time-reversed acoustics," in *Scientific American*, November 1999, pp. 91–97.

[88] R. Qiu, "A theory of time-reversed impulse multiple-input multiple-output (mimo) for ultra-wideband (uwb) communications," in *The 2006 IEEE 2006 International Conference on Ultra-Wideband*, September 2006, pp. 587 – 592.

[89] M.-Y. Chow and Y. Tipsuwan, "Network-based control systems: a tutorial," in *The 27th Annual Conference of the IEEE Industrial Electronics Society*, vol. 3, November 2001, pp. 1593 – 1602.

[90] A. E. Akogun, R. C. Qiu, and N. Guo, "Demonstrating time reversal in ultra-wideband communications using time domain measurements," in *51st International Instrumentation Symposium*, May 2005.

[91] N. Guo, R. C. Qiu, and B. M. Sadler, "An ultra-wideband autocorrelation demodulation scheme with low-complexity time reversal enhancement," in *Military Communications Conference*, vol. 5, October 2005, pp. 3066 – 3072.

[92] M. Jun and T. Oh, "Performance of pre-rake combining time hopping uwb system," *IEEE Transactions on Consumer Electronics*, vol. 50, no. 4, pp. 1033 – 1037, November 2004.

[93] S. Zhao and H. Liu, "Prerake diversity combining for pulsed uwb systems considering realistic channels with pulse overlapping and narrow-band

interference," in *Global Telecommunications Conference*, vol. 6, November 2005, pp. 3784 – 3788.

[94] M. Fink, "Time reversal of ultrasonic fields - - i. basic principles," *IEEE Transactions on Ultrasonics, Ferroelectrics and Frequency Control*, vol. 39, no. 5, pp. 555 – 566, September 1992.

[95] C. A. Balanis, *Antenna Theory: Analysis and Design*, 2nd ed., N. York, Ed. John Wiley & Sons, 1997.

[96] A. Derode, A. Tourin, J. de Rosny, M. Tanter, S. Yon, and M. Fink, "Taking advantage of multiple scattering to communicate with time-reversal antennas," *Phys. Rev. Lett*, vol. 90, no. 1, pp. 014 301–1 – 014 301–4, 2003.

[97] G. Lerosey, J. de Rosny, A. Tourin, A. Derode, G. Montaldo, and M. Fink, "Time reversal of electromagnetic waves," in *Phys. Rev. Lett.*, vol. 92, no. 19, 2004, pp. 193 904–1 – 193 904–3.

[98] M. A. Rahman, S. Sasaki, J. Zhou, S. Muramatsu, and H. Kikuchi, "Performance evaluation of rake reception of ultra wideband signals over multipath channels from energy capture perspective," in *Joint UWBST & IWUWBS International Workshop on Ultra Wideband Systems*, May 2004, pp. 231 – 235.

[99] A. G. Klein and J. C. R. Johnson, "Mmse decision feedback equalization of pulse position modulated signals," in *IEEE International Conference on Communications*, vol. 5, June 2004, pp. 2648 – 2652.

[100] A. Derode, A. Tourin, and M. Fink, "Random multiple scattering of ultrasound. ii. is time reversal a self-averaging process?" in *Phys. Rev. E*, vol. 64, no. 3, August 2001.

[101] L. Yang and G. B. Giannakis, "Optimal pilot waveform assisted modulation for ultrawideband communications," *IEEE Transactions on Wireless Communications*, vol. 3, no. 4, p. 1236 1249, July 2004.

[102] G. Montaldo, G. Lerosey, A. Derode, A. Tourin, J. de Rosny, and M. Fink, "Telecommunication in a disordered environment with iterative time reversal," in *Waves Random Media*, vol. 14, no. 3, July 2004, pp. 287 – 302.

[103] A. Giulietti, B. Bougard, and L. V. der Perre, *Turbo Codes - Desirable and Designable*. Kluwer Academic Publishers Group, Massachusetts, USA, 2004.

[104] C. Berrou, R. Pyndiah, P. Adde, C. Douillard, and R. L. Bidan, "An overview of turbo codes and their applications," in *The European Conference on Wireless Technology*, Oct 2005, pp. 1–9.

[105] T. K. Moon, *Error Correction Coding - Mathematical Methods and Algorithms*. John Wiley & Sons, New Jersey, 2005.

[106] D. Laney, G. M. Maggio, F. Lehmann, and L. Larson, "Ber performance and spectral properties of interleaved convolutional time hopping for uwb impulse radio," in *Global Telecommunications Conference*, vol. 4, December 2003, pp. 1994 – 1998.

[107] P. Robertson and T. Worz, "Bandwidth-efficient turbo trellis-coded modulation using punctured component codes," in *IEEE Journal on Selected Areas in Communications*, vol. 16, no. 2, February 1998, pp. 206–218.

[108] S. Lin and J. D. J. Costello, *Error Control Coding*, 2nd ed. Pearson Prentice Hall, New Jersey, 2004.

[109] J. Tan and G. L. Stuber, "A map equivalent sova for non-binary turbo codes," in *IEEE International Conference on Communications*, vol. 2, June 2000, pp. 602–606.

[110] M. Hong, "Analysis of the bit error rate of trellis-coded modulation," Master's thesis, Chalmers University of Technology, December 2002.

[111] C. Berrou, M. Jezequel, C. Douillard, and S. Kerouedan, "The advantages of non-binary turbo codes," in *ITW2001, Cairns, Australia*, September 2001.

[112] L. Cong, W. Xiaofu, and S. Songgeng, "On sova for nonbinary codes," in *Fifth Asia-Pacific Conference on Communications and Fourth Optoelectronics and Communications Conference*, vol. 1, October 1999, pp. 641 – 643.

[113] J. Liu and G. Tu, "Iterative decoding of non-binary turbo codes using symbol based sova algorithm," in *International Conference on Communications, Circuits and Systems*, vol. 2, June 2006, pp. 689–693.

[114] S. W. Kim and W. Stark, "Optimum rate reed-solomon codes for frequency-hopped spread-spectrum multiple-access communication systems," *IEEE Transactions on Communications*, vol. 37, no. 2, pp. 138 – 144, February 1989.

[115] A. V. Jovancevic and E. L. Titlebaum, "New coding schemes for increased number of users or messages in frequency-hopped multilevel fsk," in *46th Vehicular Technology Conference*, vol. 3, April 1996, pp. 1732–1735.

[116] S. V. Maric and E. L. Titlebaum, "Frequency hop multiple access codes based upon the theory of cubic congruences," *IEEE Transactions on Aerospace and Electronic Systems*, vol. 26, no. 6, pp. 1035 – 1039, November 1990.

[117] O. Moreno and S. V. Maric, "A new family of frequency-hop codes," *IEEE Transactions on Communications*, vol. 48, no. 8, pp. 1241 – 1244, August 2000.

[118] P. Fan and M. Darnell, *Sequence Design for Communications Applications*, E. Somerset, Ed. Research Studies Press Ltd, 1996.

[119] Z. Kostic, E. L. Titlebaum, and S. V. Maric, "The design of new optical codes and time-hopping patterns for synchronous spread-spectrum code-division multiple-access communication systems," in *IEEE International Conference on Communications*, vol. 2, June 1991, pp. 585 – 589.

[120] E. L. Titlebaum, S. V. Maric, and J. R. Bellegarda, "Ambiguity properties of quadratic congruential coding," *IEEE Transactions on Aerospace and Electronic Systems*, vol. 27, no. 1, pp. 18 – 29, January 1991.

[121] I. S. Reed and G. Solomon, "Polynomial codes over certain finite fields," in *J Soc. Indust. Appl. Math*, vol. 8, no. 2, June 1960.

[122] A. M. C. Correia, "Design of reed-solomon frequency-time hopping sequences," in *IEEE 5th International Symposium on Spread Spectrum Techniques and Applications*, vol. 3, September 1998, pp. 982 – 986.

[123] R. M. Mersereau and T. S. Seay, "Multiple access frequency hopping patterns with low ambiguity," *IEEE Transactions on Aerospace and Electronic Systems*, vol. 17, no. 4, pp. 571–578, July 1981.

[124] J. Silverman, V. E. Vickers, and J. M. Mooney, "On the number of costas arrays as a function of array size," in *Proceedings of the IEEE*, vol. 76, no. 7, July 1988, pp. 851 – 853.

[125] S. Maric and E. L. Titlebaum, "A class of frequency hop codes with nearly ideal characteristics for use in multiple-access spread-spectrum communications and radar and sonar systems," *IEEE Transactions on Communications*, vol. 40, no. 9, pp. 1442 – 1447, September 1992.

[126] S. V. Maric, I. Seskar, and E. L. Titlebaum, "On cross-ambiguity properties of welch-costas arrays when applied in ss/fh multiuser radar and sonar systems," in *IEEE Third International Symposium on Spread Spectrum Techniques and Applications*, vol. 2, July 1994, pp. 489 – 493.

[127] P. V. Kumar, "On the existence of square dot-matrix patterns having a specific three-valued periodic-correlation function," *IEEE Transactions on Information Theory*, vol. 34, no. 2, pp. 271 – 277, March 1988.

[128] J. E. H. Elliott and A. T. Butson, "Relative difference sets," in *Illinois Journal of Mathematics*, vol. 10, 1966, pp. 517–531.

[129] T. Kirimoto and O.-H. Yoshimasa, "Orthogonal periodic sequences derived from m-sequences on gf(q)," *IEEE Transactions on Information Theory*, vol. 40, no. 2, pp. 526 – 532, March 1994.

[130] J. J. Komo and M. S. Lam, "Primitive polynomials and m-sequences over gf(q^m)," *IEEE Transactions on Information Theory*, vol. 39, no. 2, pp. 643–647, March 1993.

[131] S.-C. Liu and J. J. Komo, "Nonbinary kasami sequences over gf(p)," *IEEE Transactions on Information Theory*, vol. 38, no. 4, pp. 1409–1412, July 1992.

[132] M. Welborn, "Proposal comparison summary," IEEE P802.15 Working Group for Wireless Personal Area Networks (WPANs), May 2004.

[133] M. M. Pietrzyk and J. H. Weber, "Performance of uwb-ir with polarity randomization and interleaved coding-modulation on multipath fading channels," in *in Proc. IEEE Vehicular Technology Conf. (VTC05)*, May 2005.

[134] K. Li, X. Wang, G. Yue, and L. Ping, "A low-rate code-spread and chip-interleaved time-hopping uwb system," *IEEE Journal on Selected Areas in Communications*, vol. 24, no. 4, pp. 864 – 870, April 2006, part 1.

[135] A.-L. Deleuze, P. Ciblat, and C. J. Martret, "Inter-symbol/inter-frame interference in time-hopping ultra wideband impulse radio system," in *IEEE International Conference on Ultra-Wideband*, September 2005, pp. 396–401.

[136] L. Piazzo and F. Ameli, "On the inter-symbol-interference in several ultra wideband systems," in *2nd International Symposium on Wireless Communication Systems*, September 2005, pp. 259 – 262.

[137] M. G. D. Benedetto, "Mac for uwb," 2002, networking with UWB Seminar - UWB Group at University of Rome. [Online]. Available: http://www.icsl.ucla.edu/~spapl/seminar/uwb2.pdf

[138] E. W. Weisstein, "Shah function," MathWorld. [Online]. Available: http://mathworld.wolfram.com/ShahFunction.html

[139] K. Witrisal, "Ofdm air-interface design for multimedia communications," Ph.D. dissertation, Delft University of Technology, Delft, The Netherlands, April 2002. [Online]. Available: http://spsc.inw.tugraz.at/klaus/Thesis.pdf

[140] V. Lakkundi and R. Marsalek, "Novel fec schemes for uwb: Design, modelling and performance analysis," in *Engineering and Technology Forum on Waveform Diversity and Design in Communications, Radar and Sonar*, November 2006, pp. 83–90.

[141] F. Chen, S. Li, and Y. Wang, "A new wireless access scheme: Novel punctured ldpc coded ultra-wideband system," in *Vehicular Technology Conference Spring*, 2007, pp. 3011–3015.

[142] T. Tan and K. Lin, "Performance of space-time block coded mb-ofdm uwb systems," in *4th Annual Communication Networks and Services Research Conference*, May 2006.

[143] S. Vafi, "On the design of turbo codes with convolutional interleavers," Ph.D. dissertation, University of Wollongong, 2005.

[144] A. C. Reid, D. P. Taylor, and T. A. Gulliver, "Non-binary turbo codes," in *IEEE International Symposium on Information Theory*, 2002, p. 57.

[145] Y. Wu, "Matlab code for experiment on turbo codes," MPRG lab, Virginia Tech, 1998. [Online]. Available: http://www.ee.vt.edu/~yufei/turbo.html